NEA/NSC/DOC(93)17
INDC(Ger)-037/LN
Jül-2803

PROGRESS REPORT ON NUCLEAR DATA RESEARCH IN THE FEDERAL REPUBLIC OF GERMANY

for the Period April 1, 1992 to March 31, 1993

July 1993

Edited by
S. M. Qaim
Forschungszentrum Jülich GmbH
Institut für Nuklearchemie
Jülich, Federal Republic of Germany

Dedicated to

Siegfried Cierjacks

who nurtured this series of Progress Reports
for many years.

FOREWORD

This report has been prepared to promote the exchange of nuclear data research information between the Federal Republic of Germany and other member states of OECD/NEA and IAEA. It covers progress reports from KfK Karlsruhe, KFA Jülich, the universities of Dresden, Hannover, Köln, Mainz, Marburg as well as from PTB Braunschweig and FIZ Karlsruhe. The emphasis in the work reported here is on measurement, compilation and evaluation of nuclear data for pure and applied science programmes, such as those relevant to fission- and fusion-reactor technology, radioactive waste management, accelerator shielding and development, astrophysics research, cosmogenic and meteoritic investigations, production of medically important radioisotopes, etc.

Each contribution is presented under the laboratory heading from where the work is reported. The names of other participating laboratories are also mentioned. When the work is relevant to the World Request List for Nuclear Data, WRENDA 87/88 (INDC(SEC)-095/URSF), the corresponding identification numbers are given.

Jülich, July 1993 S. M. Qaim

CONTENTS

INSTITUT FÜR KERNPHYSIK
ARBEITSGRUPPE STRAHLUNGSTRANSPORT
FORSCHUNGSZENTRUM JÜLICH

Page

INSTITUT FÜR NUKLEARCHEMIE
FORSCHUNGSZENTRUM JÜLICH

INSTITUT FÜR KERN- UND TEILCHENPHYSIK
TECHNISCHE UNIVERSITÄT DRESDEN

KERNFORSCHUNGSZENTRUM KARLSRUHE
INSTITUT FÜR KERNPHYSIK

1. STELLAR (n,γ) CROSS SECTIONS OF THE TIN ISOTOPES

K. Wisshak, F. Käppeler, L. Kazakov*, N. Kornilov*, Ch. Theis, F. Voß

The origin of the tin isotopes is of particular interest because all three different nucleosynthetic processes, the s-, r-, and p-process, contribute in a complicated way to the observed abundances in the Cd - In - Sn region. Most important in this mass range is the s-process, where the neutron capture chain follows in general the valley of beta stability. Between ^{112}Cd and ^{116}Sn, however, the s-process flow exhibits minor branchings at ^{113}Cd, ^{115}Cd, and ^{115}In which may result in small s-process contributions to the rare tin isotopes 114 and 115. Furthermore, ^{116}Sn is a pure s-process nucleus, and therefore of relevance as a normalization point for s-process calculations and for the tin abundance in the solar system. All these s-process aspects can only be discussed quantitatively, if an accurate set of stellar (n,γ) cross sections is available. Then, the abundance contributions from the other processes can be deduced and the corresponding implications can be investigated in detail.

In collaboration with the Institute of Physics and Power Engineering, Obninsk, the neutron capture cross sections of ^{114}Sn, ^{115}Sn, ^{116}Sn, ^{117}Sn, ^{118}Sn, and ^{120}Sn have been measured with the Karlsruhe 4π BaF_2 detector in the neutron energy range from 5 to 220 keV. Neutrons were produced via the ^{7}Li(p,n)^{7}Be reaction and the time-of-flight technique was used for neutron energy determination. In total, 3 runs were performed covering different energy regions in order to study systematic uncertainties due to background subtraction and due to scattered neutrons.

By now, the measurements are completed and data analysis will start in early fall. One aspect of this experiment appears quite promising: Despite the small cross sections of the investigated isotopes and the comparably low sample masses, a satisfactory signal-to-background ratio could be achieved for the entire energy range. This good sensitivity of the experimental setup has been achieved by replacing the 6 BaF_2 crystals

*Institute of Physics and Power Engineering, Obninsk

with the largest radium impurities, thus lowering the intrinsic detector background. This means that the 4π BaF_2 detector can now also be used for measuring relatively small cross sections.

2. THE s-PROCESS BRANCHINGS AT A = 133, 134, 135 AND THE ISOTOPIC Ba CROSS SECTIONS

F. Voß, K. Wisshak, F. Käppeler

The branchings of the s-process path at ^{133}Xe, ^{134}Cs, and ^{135}Cs are important because the beta decay rate of ^{134}Cs exhibits a strong dependence on temperature. This means that the resulting s-process abundances of the barium isotopes are determined by the temperature during the s-process. The s-process abundances of the barium isotopes are also needed for the interpretation of isotopic anomalies discovered in meteorites as well as for the barium abundances in the atmosheres of red giant stars.

The strength of these branchings - and hence an estimate for the temperature - can be deduced via the s-only isotopes ^{134}Ba and ^{136}Ba. As can be seen from Fig. 1, ^{134}Ba is partly bypassed by the s-process flow (solid lines) while ^{136}Ba is exposed to the total flow. This difference can be expressed by the branching ratio $f_- \approx \sigma N(^{134}Ba)/\sigma N(^{136}Ba)$. Because the isotopic abundance ratio is known to ± 0.1%, the branching analysis is completely determined by the cross section uncertainties.

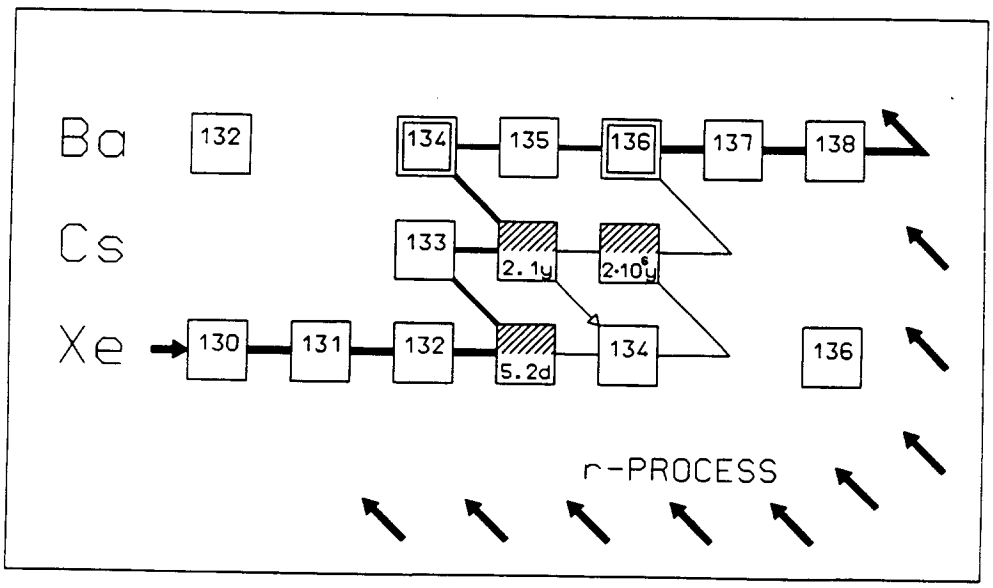

Fig. 1 The s-process neutron capture flow in the mass region 130 < A < 138. The branchings at ^{133}Xe, ^{134}Cs, and ^{135}Cs can be characterized by the s-only isotopes ^{134}Ba and ^{136}Ba.

The cross section information available from literature was too uncertain so that a meaningful analysis of the branching ratio was not possible. Therefore, the neutron capture cross sections of ^{134}Ba, ^{135}Ba, ^{136}Ba, and ^{137}Ba have been measured with the Karlsruhe 4π BaF_2 detector in the neutron energy range from 5 to 220 keV. Neutrons were produced via the $^{7}Li(p,n)^{7}Be$ reaction and the time-of-flight technique was used for neutron energy determination. These measurements were difficult for several reasons: In order to be sure about the stoichiometry, barium carbonate samples had to be used with a very unfavorable capture/scattering ratio per molecule. The large fraction of scattered neutrons gave rise to a large correction for scattered neutrons that are eventually captured by the barium of the scintillator crystals. By definition, this scattering background was almost undistinguishable from the true capture events in the sample.

In view of these problems, the measurement was not only subdivided in 3 runs covering different energy regions in order to study these uncertainties in detail, but measuring times were extended by a factor three compared to previous experiments with the 4π BaF_2 detector for obtaining sufficiently good statistics. Figure 2 shows the

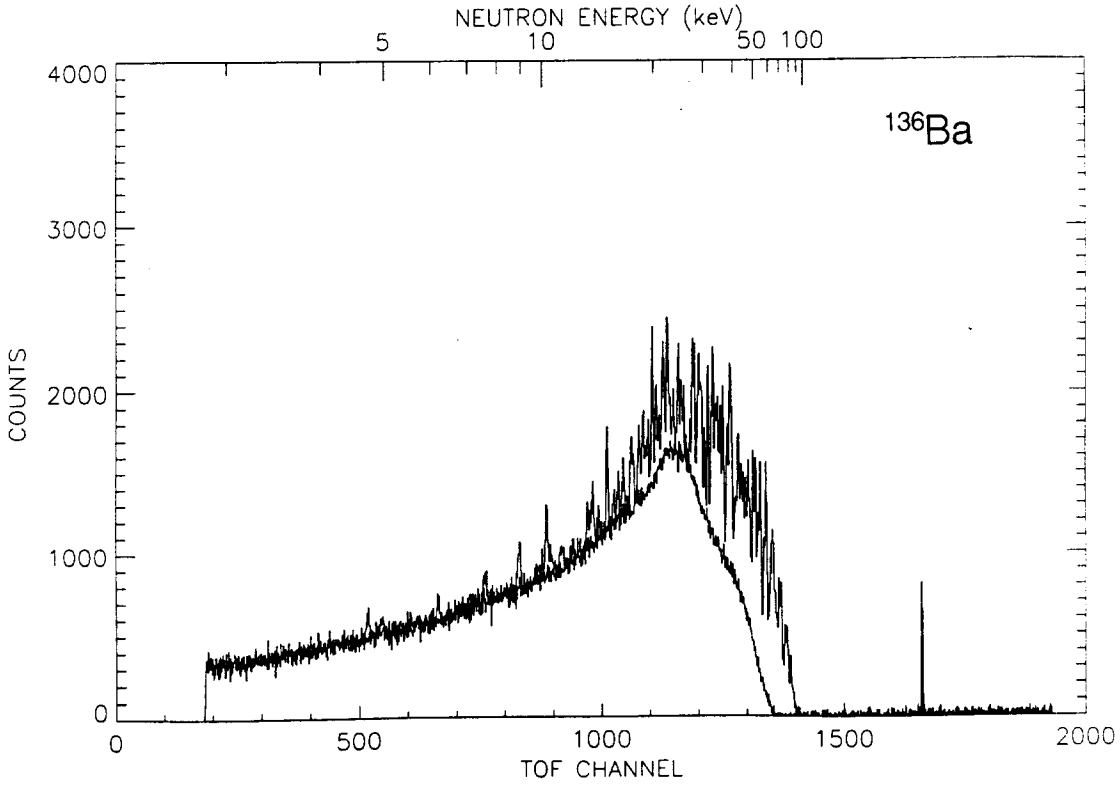

Fig. 2 The time-of-flight spectrum obtained with the ^{136}Ba sample, showing resolved resonances in a wide energy range. Note the large background due to scattered neutrons.

example of the time- of-flight spectrum of ^{136}Ba, where the background due to scattered neutrons is particularly large. Since these barium isotopes are close to magic neutron number N=82, the cross section is dominated by isolated resonances.

At present, data analysis is partly finished. The preliminary cross sections for the example of ^{136}Ba are compared with the previous data in Figure 3. One finds that the large scattering background causes the uncertainties to exceed 5% at energies below 12 keV. Accordingly, the stellar cross sections at typical s-process temperatures exhibit uncertainties of ~2%, twice as large as was obtained for the previously measured Te and Sm cross sections.

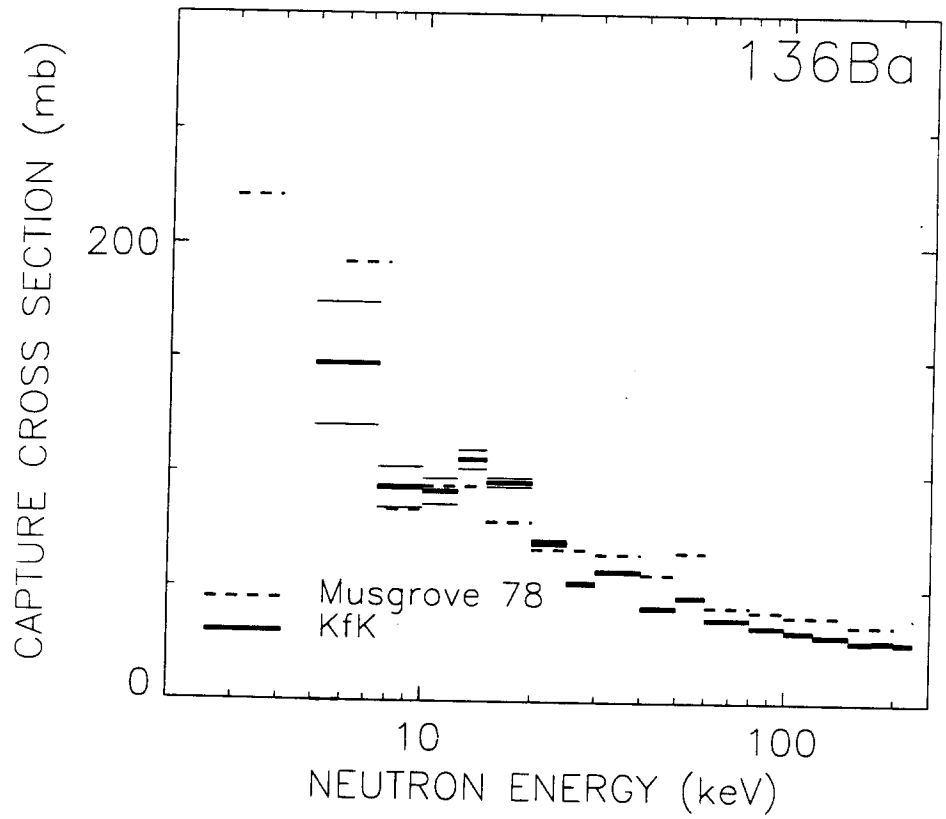

Fig. 3 The preliminary capture cross section of ^{136}Ba averaged over a grid of energy bins suitable for determination of the stellar average. The present results are compared with previous values [1].

[1] Musgrove, A. R. de L., Allen, B. J., Boldeman, J. W., and Macklin, R. L. 1978, in *Neutron Physics and Nuclear Data for Reactors and Other Applied Purposes*, Harwell (Paris: OECD) p. 449.

3. THE STELLAR NEUTRON CAPTURE RATE OF ^{138}Ba

H. Beer, F. Corvi*, A. Mauri*, K. Athanassopulos*, and M. C. Moxon**

High resolution time-of-flight measurements of ^{138}Ba were carried out at the pulsed electron linac GELINA in the energy range 0.5 - 300 keV. The accelerator was operated at a repetition rate of 800 Hz with a pulse width of 1 ns. The measurements were performed at flight paths of 30 and 60 m using a pair of C_6D_6 liquid scintillators to detect the capture events. The relative neutron flux was simultaneously registered by a ^{10}B ionization chamber. In additional calibration runs with a repetition rate of 100 Hz the capture in the first ^{138}Ba resonance at 648 eV was compared to black resonances in ^{197}Au at 4.906 eV and ^{109}Ag at 5.19 eV. The data were analyzed with the R-matrix shape fitting codes FANAC [1] and REFIT [2]. The stellar capture rate is determined

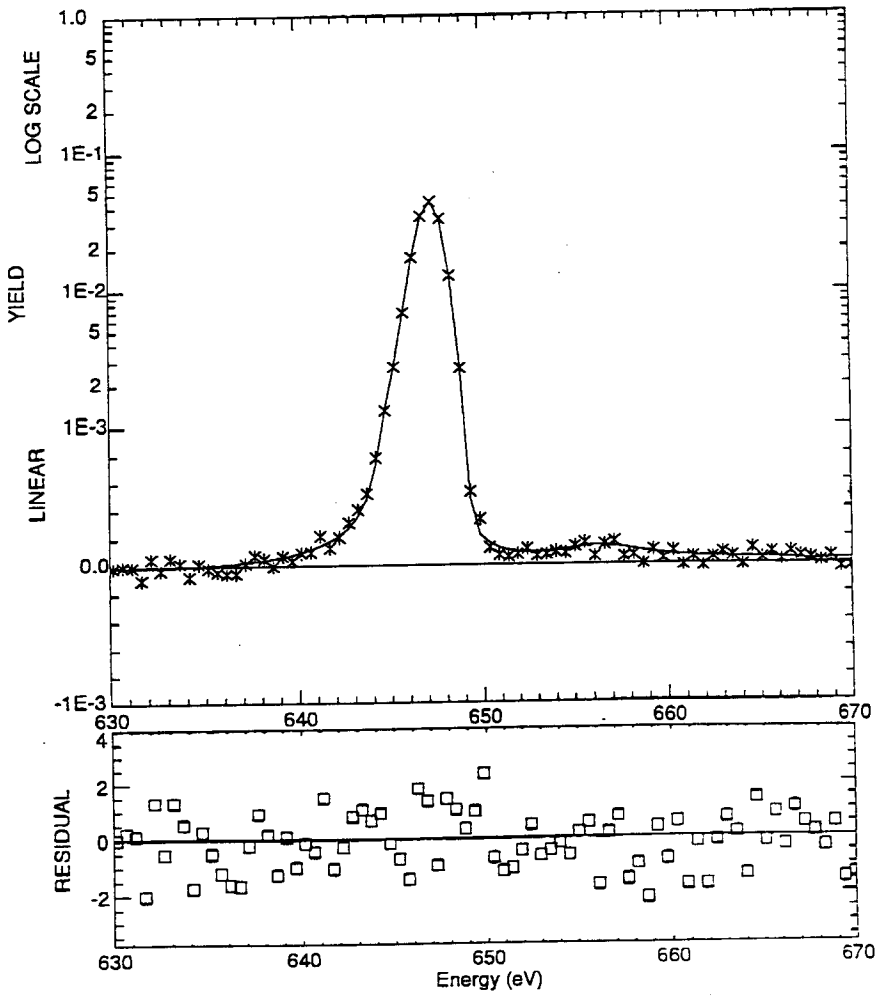

Fig. 1 The ^{138}Ba resonance at 648 eV. The solid line represents the fit by the R-matrix program REFIT. The bump around 657 eV is due to multiple neutron scattering.

from the resonance parameters. As an example, Fig. 1 shows the fit of the first ^{138}Ba resonance at 648 eV. Using REFIT, the quality of the data allowed for a determination of the neutron width, Γ_n = 5.55 meV, and of the radiation width, Γ_γ = 70 meV.

*CEC, JRC, Institute for Reference Materials and Measurements, B-2440 Geel, Belgium
**Harwell Laboratory, UKAEA, Oxon, UK

[1] Fröhner, F. H. 1976, report KfK-2145, Kernforschungszentrum Karlsruhe
[2] Moxon, M. C., and Brisland, J. B. 1991, report AEA-InTec-0630, Harwell Laboratory

4. RADIOACTIVE SAMPLES FOR THE MEASUREMENT OF keV NEUTRON CAPTURE CROSS SECTIONS

S. Jaag, F. Käppeler, M. Wiescher*, P. E. Koehler**, H. Ravn***

It has been pointed out above that the investigation of s-process branchings yields relevant information with respect to the physical conditions of the stellar site. In addition to the s-only isotopes which are characterizing the branchings, the radioactive branch point nuclei are also important. These isotopes are comparably short-lived, with half-lives of typically a few years. Accordingly, sample masses of about 1 g as required by common techniques for the determination of (n,γ) cross sections in the keV range gave rise to very large activities. This means that sample induced backgrounds would become prohibitive even where the radiation hazard could be accepted.

Therefore, techniques must be found where sample masses of a few mg or even less can be used. Capture cross section measurements with samples of a few mg have been performed recently at the Karlsruhe Van de Graaff using a setup of Moxon-Rae detectors in combination with flight paths of only a few cm. This technique has been shown to be well suited for measurements on unstable samples provided that the γ-activity of the sample is restricted to the energy range below about 400 keV. By a first measurement with a sample of 3 mg ^{147}Pm ($t_{1/2}$=2.6 yr), it could be demonstrated that this

*University of Notre Dame, Indiana, USA
**Los Alamos National Laboratory, New Mexico, USA
***CERN, Geneva, Switzerland

method is quite promising.

An alternative to the short flight paths in Van de Graaff experiments is the high neutron flux available at spallation neutron sources. Estimates for the beam line available at the LANSCE facility at LAMPF have shown that the sensitivity could be improved by about two orders of magnitude compared to the Moxon-Rae setup at the Van de Graaff.

A further improvement of the sensitivity can be achieved via the activation technique. However, this method can only be applied when the induced activity is easily distinguishable from the activity of the sample. This means that the half-life of the product nucleus should be much shorter and the radiation associated with its decay should be much harder than that of the sample. Since these criteria are satisfied by a number of important branch point nuclei, a program has been started at Karlsruhe for investigating

Table 1 The most important branching points: feasibility of cross section measurements and relevance for s-process studies.

Isotope	Half-life	Feasibility	Relevance
^{79}Se	$< 6 \cdot 10^4$ yr	yes	temperature
^{85}Kr	10.7 yr	(yes)	neutron density
^{134}Cs	2.06 yr	-	
^{135}Cs	$2 \cdot 10^6$ yr	yes	temperature
^{137}Cs	30 yr	yes	
^{147}Nd	11.0 d	-	
^{147}Pm	2.62 yr	yes	neutron density
^{148}Pm	5.4 d	-	
^{151}Sm	93 yr	yes	
^{152}Eu	13.3 yr	-	
^{154}Eu	8.8 yr	-	temperature
^{155}Eu	4.96 yr	yes	
^{153}Gd	242 d	yes	
^{163}Ho	4570 yr	yes	mass density
^{169}Er	9.4 d	yes	
^{170}Tm	128.6 d	yes	temperature
^{171}Tm	1.9 yr	yes	
^{179}Ta	1.7 yr	yes	mass density
^{185}W	75.1 d	yes	temperature
^{186}Re	3.8 d	-	
^{191}Os	15.4 d	yes	neutron density
^{192}Ir	74.2 d	-	

these cases experimentally. The main advantage of this approach is that measurements can be performed with samples of about 10^{14} to 10^{15} atoms only. This implies not only a small sample activity but allows also to produce these samples with high purity using mass separators. The relevant nuclei being close to stability means that they can be obtained with sufficient intensity from on-line separators like ISOLDE at CERN.

The most important branching point isotopes are compiled in Table 1. The third column indicates which of these can be experimentally studied with the above techniques, provided that a suited sample is available. One finds that most of these data can indeed be measured, to < 10 %, leading to a substantial improvement compared to the ±25 % uncertainty of the statistical model calculations. The relevance of the respective branchings with respect to the parameters of the stellar site is indicated in the last column, respectively.

As far as the experimental studies are concerned, work has been started on four isotopes:

(i) An activation measurement has been performed on ^{147}Pm. The sample was commercially available but contained a significant impurity of ^{146}Pm. The reported cross section is still preliminary until problems with the sample impurity and backgrounds, are fully understood.

(ii) A ^{163}Ho sample could be obtained from the ISOLDE group that had been prepared for an improved half-life determination. The activation measurements are completed by now. Presently, the sample is being analyzed for its composition and mass.

(iii) A ^{155}Eu sample was prepared by irradiation of an isotopically pure ^{154}Sm sample in a reactor and by subsequent chemical separation of the Eu fraction. The macro-micro separation was performed by the carrier-free anion exchange technique using an aqueous methanol solution of ammonium nitrate as eluent. The crucial point in this procedure was to avoid any contamination with ^{154}Eu, since the decay of this isotope would completely cover the induced activity of ^{156}Eu.

(iv) There are plans to produce suited samples of ^{135}Cs and ^{137}Cs at ISOLDE, taking advantage of the high resolution of the on-line separator. This procedure follows the experience from a previous attempt [1].

[1] Naumann, R. A., Burke, D., Ravn, H. L., Hlawatsch, G., von Egidy, T., and de Boer, J. 1980, Nucl. Instr. Meth. *B26*, 59.

KERNFORSCHUNGSZENTRUM KARLSRUHE
INSTITUT FÜR MATERIALFORSCHUNG I

1. Activation Calculations for Single Elements and Alloys Including Sequential (x,n) Reactions

S. Cierjacks†, P. Obložinský[1], S. Kelzenberg, K. Ehrlich

The influence of sequential (x,n) reactions on activation under fusion-like conditions was investigated systematically for all stable elements up to bismuth ($Z \leq 83$) [1]. Inventories were calculated with the European reference code FISPACT making use of the novel algorithm (KfK code PCROSS, improved version, unreleased). For the neutron-induced reactions we used the library EAF-2, while recently developed libraries KFKSPEC and KFKXN [2] were used to handle sequential (x,n) reactions. Their newest, unreleased version is adapted to EAF-2. We found increase in activities due to sequential (x,n) reactions in almost 34 of all 81 single element cases (Tc and Pm have no stable isotopes). In the following 17 cases the effect was greater than one order of magnitude:

Li, N, O, F, Ne, Na, Mg, V, Cr, Mn, As, Y, Xe, Cs, Pt, Au, Tl

Further improvements are necessary for reactions with light nuclei. Additional decay data for 213 isotopes, kinematically allowed by sequential (x,n) reactions have to be included into FISPACT.

As a next step we performed inventory calculations for several alloys. The results recently achieved indicate that the question of impurities is of great importance and has to be discussed further in more detail.

2. Code Development for a General Comparison of Accelerator-based Intense Neutron Sources

S. Cierjacks† E. Daum

In order to compare different accelerator based neutron sources [3-6], the Code Intense Neutron Source (INS) is now finally developed at KfK [7]. This code provides a comparison between the t – H_2O and d-Li concepts for important source parameters like

†Dr. S. Cierjacks passed away in October 1992

[1]Institute of Physics, Slovak Academy of Sciences, 842 28 Bratislave, Slovakia

spatial-dependent neutron flux spectra, minimum flux volumes and the produced H-, He- and DPA values for several elements. A data flow chart of the code structure used for treatment of the t – H_2O and d-Li neutron sources is shown in Fig. 1.

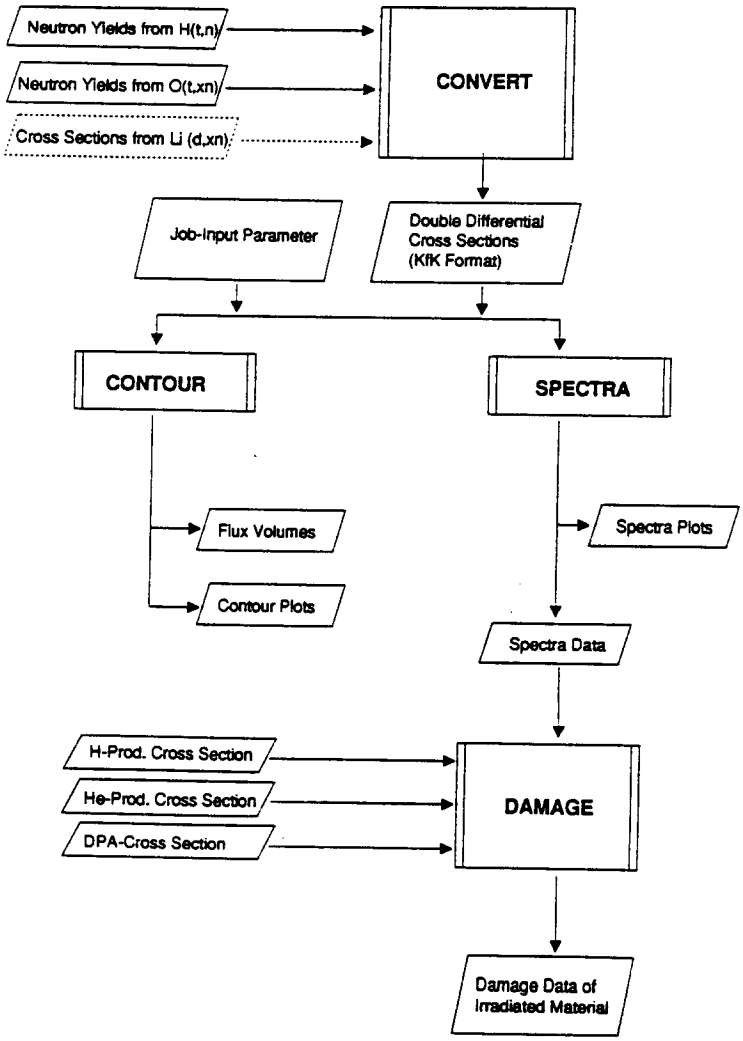

Figure 1: Data flow chart of the INS code calculating the t – H_2O / d-Li - source. The code is separated into four code modules. Module CONVERT for processing the nuclear reaction data, CONTOUR for calculating minimum flux volumes, SPECTRA for calculating the spectral distributions and DAMAGE for calculating the material damage values.

The code was developed to simulate a single source and a double source geometry with variable beam power and target dimensions, target position and target orientation. T – H_2O data [8, 9], d-Li data [10], gas production cross section [11] and damage energy cross section [12] have been used as source data. The calculation of the neutron fluxes in the test cell is performed with high accurancy by using a detailed simulation of the reaction targets. Neutron flux spectra data are the basis for forthcoming flux volume and irradiation

damage calculations. For calculation of minimum flux volumes in the test cell (divided into $\sim 4 * 10^6$ subelements) a CPU-time saving algorithm had to be used, to obtain the results in a reasonable time.

3. Study of High-Intensity, High-Energy Neutron Sources for End-of-Life Fusion Materials Testing

S. Cierjacks†, E. Daum, K. Ehrlich

In continuation of our previous investigations on the KfK proposal for a novel t – H_2O source [3-5], comparative material damage calculations for this and an equivalent d-Li source [6] have been finalized. Uncollided differential space-dependent flux spectra were carried out for two IEA reference designs Fig. 2 as the basis for the displacement and transmutation calculations.

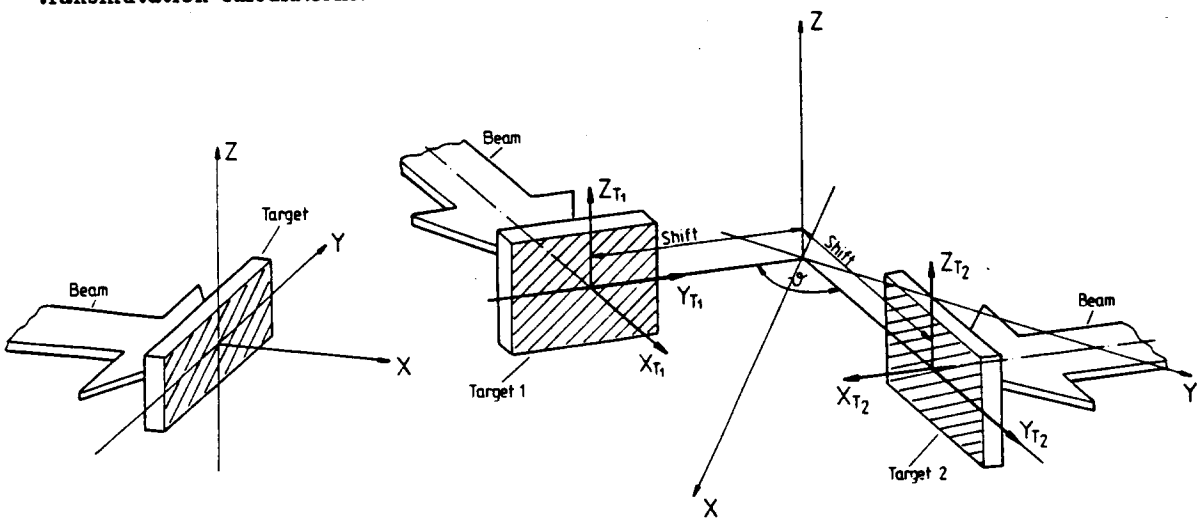

Figure 2: Sketch of the IEA reference designs. Single beam case (1-S): Target rectangular 3 * 1 cm^2, 3.5 MW beam power. Double beam case (2-S): Targets rectangular 7.5 * 2.5 cm^2, shift = 10 cm, ϑ = 90 degree, 17.5 MW total beam power.

The spectra listed in Table 1 are used for the comparison. The coordinates (X,Y,Z) mark the positions of the spectra in the test cell. The total neutron flux and the fraction of neutrons with energies 14 Mev > E_n > 50 MeV is given to qualify the spectra.
The total neutron fluxes at the d-Li concept are by a factor 1.3 - 2.5 higher than the t–H_2O

†Dr. S. Cierjacks passed away in October 1992

Source	Coordinates (cm)			Total flux ($n/s/cm^2$)		Fraction $E_n > 14$ MeV (%)	
	X	Y	Z	$t - H_2O$	d-Li	$t - H_2O$	d-Li
(1-S)	0	0	0	$4.09 * 10^{15}$	$5.25 * 10^{15}$	0.9	19.1
(1-S)	4	0	0	$3.84 * 10^{14}$	$6.57 * 10^{14}$	3.2	34.7
(2-S)	8	0	0	$7.67 * 10^{13}$	$1.89 * 10^{14}$	1.0	6.36
(2-S)	14	0	0	$6.54 * 10^{14}$	$1.19 * 10^{15}$	3.1	34.7
(2-S)	8	8	0	$4.41 * 10^{15}$	$6.84 * 10^{15}$	0.9	15.2

Table 1: Table of neutron flux spectra used as basis for the comparison of material damage values.

concept fluxes. This difference corresponds to the large fraction of neutrons with energies greater 14 MeV for the d-Li concept, which is highly undesireable for fusion material testing, because of not well known inelastic nuclear reactions. The higher neutron flux and also the higher neutron energies, at the d-Li concept, yield higher displacement and transmutation rates than the $t-H_2O$ concept. A typical result from our latest displacement and transmutation calculation for medium weight isotopes is shown in Fig. 3.

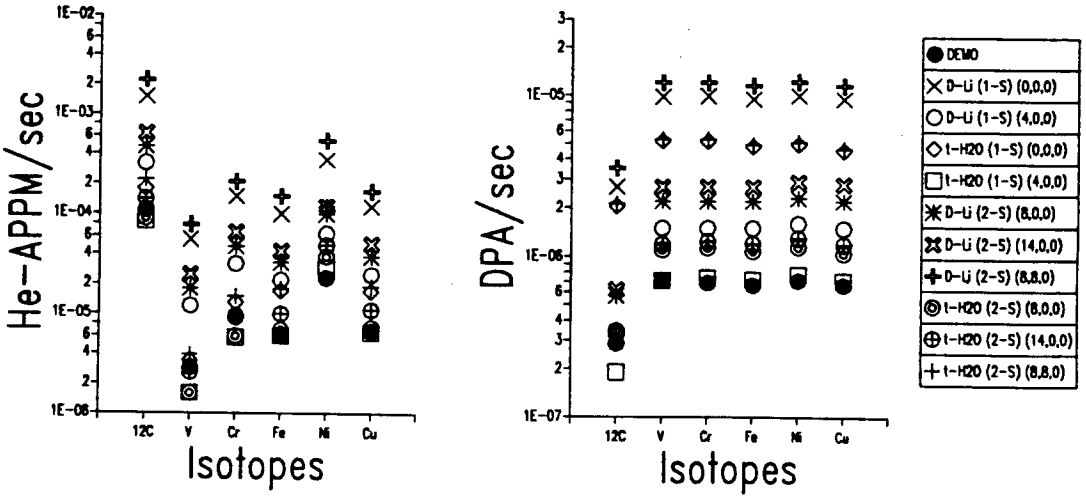

Figure 3: Comparison of the $APPM_{He}/s$ and DPA/s values of several medium weight isotopes produced with the DEMO spectrum [13] and the $t - H_2O$ and d-Li spectra.

The DEMO first wall neutron spectrum is choosen as the reference case. The helium and displacement production rates are, for the d-Li and $t - H_2O$ spectra at positions close to the target, more than one order of magnitude higher than at DEMO. The other positions are always higher or equal to the DEMO values. This shows, that both source concepts are able to test fusion materials with more than DEMO required load for the first wall. However, the d-Li advantage when compared to the $t - H_2O$ source is given by the high energy tail of the neutron flux spectra. Further information will be published in [7, 14].

References

[1] S. Kelzenberg, P. Obložinský: *Influence of sequential (x,n) reactions on production of long-lived radionuclides in fusion reactors*, IAEA Meeting on Activation Cross Sections for the Generation of Long-Lived Radionuclides of Importance in Fusion Reactor Technology, Del Mar near San Diego, California, USA (29-30 April 1993).

[2] S. Cierjacks, P. Obložinský, S. Klelzenberg, B. Rzehorz: *Development of a Novel Algorithm and Production of New Nuclear Data Libraries for the Treatment of Sequential (x,n) Reactions in Fusion Materials Activation Calculations*, Fusion Technology, (November 1993)

[3] S. Cierjacks, Y. Hino and M. Drosg: *Proposal for a High-Intensity 14-MeV Cutoff Neutron Source Based on the* $^1H(t,n)^3He$ *Source Reaction*, Nuclear Science and Engineering **106** ,183-191 (1990)

[4] S. Cierjacks and Y. Hino: *Differential Flux and Spectrum Calculations for a Novel High-Intensity 14-MeV Cutoff Neutron Source Based on the* $^1H(t,n)^3He$ *Source Reaction*, Acta Physica Hungarica **69** (3-4), pp. 285-308 (1991)

[5] S. Cierjacks: *The Intense* $t-H_2O$ *Neutron Source*, IEA Workshop on Intense Neutron Sources, Karlsruhe, September 21-23, 1992, Kernforschungszentrum Karlsruhe, to be published

[6] M.J. Saltmarsh: *The High Intensity d-Li Source*, IEA Workshop on Intense Neutron Sources, Karlsruhe, September 21-23, 1992, Kernforschungszentrum Karlsruhe, to be published

[7] E. Daum: *User and Reference Manual for the KfK Code INS*, Kernforschungszentrum Karlsruhe, KfK-Report, to be published

[8] M. Drosg and O. Schwerer: *Production of Monoenergetic Neutrons between 0.1 and 23 MeV* , Handbook of Nuclear Activation Data, IAEA Report Series No. 273, Vienna, 1987, p. 83

[9] M. Drosg and D.M. Drake: *Fast Neutron Yield from 20-MeV Tritons on Water, Part A: Triton Interaction with Light Water*, Nucl. Instr. and Meth. 73(1993) 387-391, Section B

[10] D.L. Johnson, et. al.: *"Thick Target Neutron Yields and Spectra from the Li(d,xn) Reaction at 35 MeV", Symposium Neutron Cross Sections from 10 to 50 MeV*, Upton, New York, May 3-5, 1980, Report BNL-NCS-51245, p. 99, Brookhaven National Laboratory (1980)

[11] *ENDF/B-V Gas Production file (533), Brookhaven National Laboratory*

[12] L.R. Greenwood and R.K. Smither: *SPECTER: Neutron Damage Calculations for Material Irradiations*, Report ANL/FPP/TM-197, January 1985

[13] L.J. Backer, et al.: *Cullham Report CLM-R-254 (1985).*

[14] D.G. Doran and S. Cierjacks *Some Comparisons of d-Li and t – H_2O Conceptual Neutron Sources*, IEA Working Group on Neutron Sources, to be published

KERNFORSCHUNGSZENTRUM KARLSRUHE
INSTITUT FÜR NEUTRONENPHYSIK UND REAKTORTECHNIK

Nuclear Data Evaluation

1. Uncertainty Assignment for Resonance Parameters of Structural Materials

F.H. Fröhner

The JEF-2/EFF-2 resonance parameter files for ^{58}Ni and ^{60}Ni are being updated with new resonance analysis results from IRMM Geel [1] and supplemented with covariance files. As in the case of the iron isotopes [2] the combination of resonance parameters from different authors and different experiments is based on the thin-sample transmission dip areas, $A = g\Gamma_n$, and capture peak areas, $A_\gamma = g\Gamma_n\Gamma_\gamma/(\Gamma_n + \Gamma_\gamma)$. As these quantities are insensitive to experimental details such as Doppler and resolution broadening they enable the evaluator to combine resonance analysis results obtained by different authors from different transmission and capture data sets taken under widely differing conditions. From the evaluated values, A and A_γ, and their standard deviations, ΔA and ΔA_γ, one gets the evaluated resonance parameters, their uncertainties and covariances as

$$\Gamma_n = \frac{A}{g} \qquad (1) \qquad \Gamma_\gamma = \frac{1}{g}\left(\frac{1}{A_\gamma} + \frac{1}{A}\right)^{-1} \qquad (2)$$

$$\frac{\Delta\Gamma_n}{\Gamma_n} \simeq \frac{\Delta A}{A} \qquad (3) \qquad \frac{\Delta\Gamma_\gamma}{\Gamma_\gamma} \simeq g\Gamma_\gamma\sqrt{\left(\frac{\Delta A_\gamma}{A_\gamma^2}\right)^2 + \left(\frac{\Delta A}{A^2}\right)^2} \qquad (4)$$

$$\mathrm{cov}(\Gamma_n, \Gamma_\gamma) \simeq -\left(g\Gamma_\gamma\frac{\Delta A}{A}\right)^2 . \qquad (5)$$

Data combination is thus performed for each resonance separately, with neglect of level-level interference effects. Long-range correlations are taken into account via the uncertainty of the effective nuclear radius. The comparatively tiny and practically uninteresting energy uncertainties are neglected but all the most important uncertainties and correlations are included. This is about the best one can do without detailed covariance information from the various authors' resonance analyses, and ought to be adequate for most error propagation studies, e. g. in shielding or activation work.

2. Cross Section Fluctuation Factors for Natural Iron

F.H. Fröhner

Recent improvements in microscopic neutron data have alerted users of evaluated files that the resonance structure of e. g. structural-material cross sections must be taken into account far beyond the present range of analysed resonances (0 ... 0.85 MeV for Fe56 in ENDF/B-VI and JEF-2/EFF-2). Berthold, Nazareth, Rohr and Weigmann [3] measured the neutron transmission of a natural iron sample of 48 mm thickness at the Geel electron linear accelerator with very high resolution, in order to investigate the cross section fluctuations up to at least 20 MeV. The time resolution of about 2 ns and a flight path of 388 m make the resolution width similar to the Doppler width at 1 MeV, so that all observable structure should be resolved there. Fig. 1 shows the observed frequency distribution of total cross sections in the energy interval 1.0-1.2 MeV together with Monte Carlo results obtained with the SESH code [4]. Although the Monte Carlo distribution is an average over many sampled resonance ladders, whereas the observed distribution represents the one ladder realized in nature, their spread is roughly the same, i. e. the fluctuations are actually well resolved.

The Geel data [3] were smoothed by a simple sliding-window technique so that the relative fluctuations could be extracted. The smoothed cross section, shown in Fig. 2 for the interval 3.0-4.5 MeV, confirms older data measured by Cierjacks et al. with much less time resolution [5], and a recent IRK evaluation by Vonach et al. [6], but is systematically higher than the JEF-2/EFF-2 evaluation below 4.5 MeV. The relative fluctuations about the average extracted from the Geel high-resolution data were superposed on a new evaluation of iron average cross sections for shielding and activation applications.

[1] R. Shelley, A. Brusegan, priv. comm. (Oct. 1992 and April 1993)
[2] F.H. Fröhner, Karlsruhe report KfK 5079 (1992)(= INDC(Ger)-036/L)
[3] H. Weigmann et al., data available from NEA Data Bank (1992)
[4] F.H. Fröhner, General Atomic GA-8380 (1968)
[5] S. Cierjack, P. Forti, D. Kopsch, L. Kropp, J. Nebe, H. Unseld, Karlsruhe report KfK 1000 (1968)
[6] H. Vonach et al., unpublished report, IRK Vienna (1992)

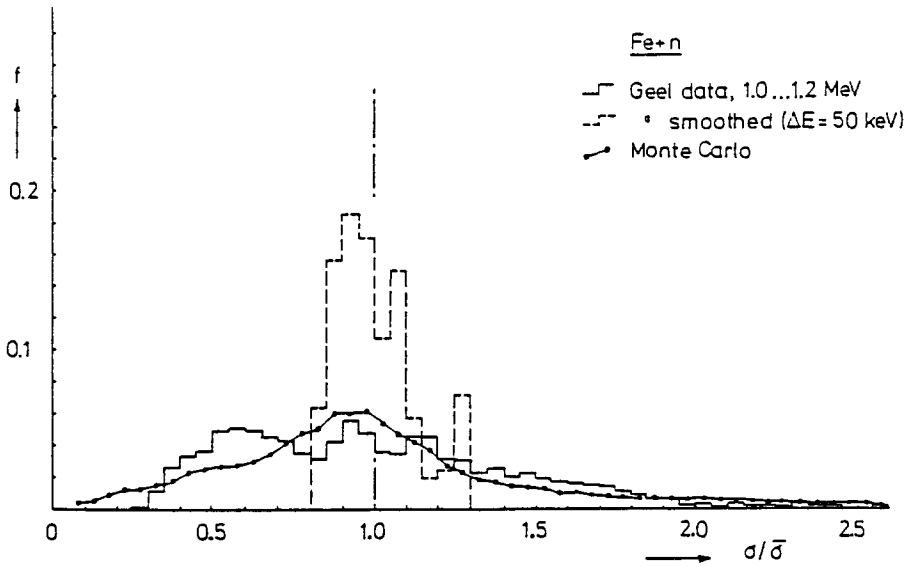

Fig. 1. Relative frequency distributions of total cross section values for natural iron between 1.0 and 1.2 MeV as observed at Geel by Berthold et al. (1992) and as calculated with the Monte Carlo code SESH from strength functions and effective nuclear radii. The effect of smoothing is shown by the dashed histogram.

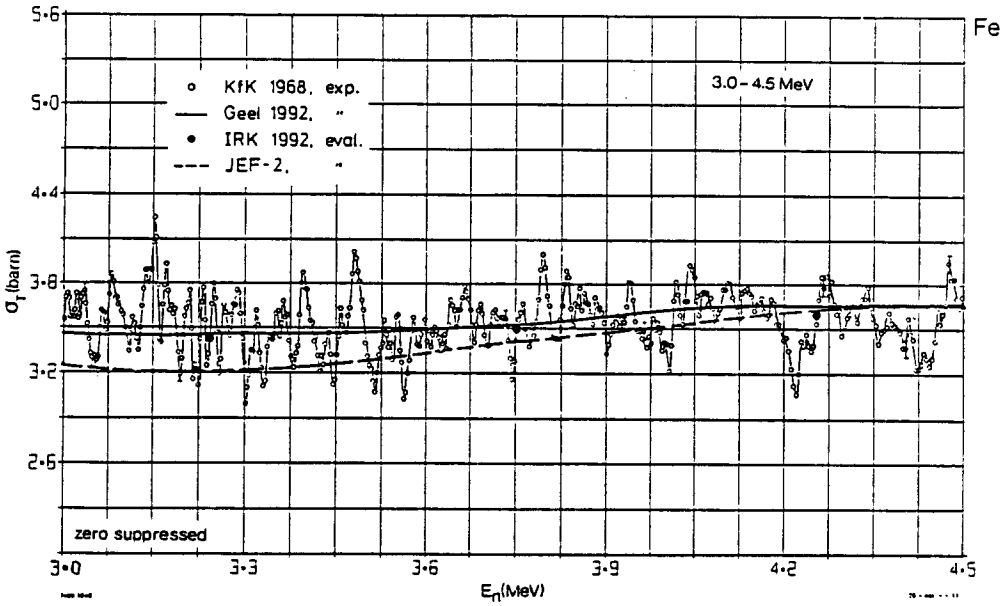

Fig. 2. Smoothed total cross sections obtained with a sliding window (±10% in energy) from the Geel high-resolution data of Berthold et al. (1992) (solid line) and from the JEF-2/EFF-2 evaluation, shown together with the KfK point data of Cierjacks et al. (1968) and the IRK evaluation for ^{56}Fe of Vonach et al. (1992); 3.0-4.5 MeV.

INSTITUT FÜR KERNPHYSIK , ARBEITSGRUPPE STRAHLUNGSTRANSPORT, FORSCHUNGSZENTRUM JÜLICH

The Systematics of Double Differential A(p,xn) Neutron Production by Protons between 100 MeV and 800 MeV on Targets with 12 < A < 238

P. Cloth, V. Drüke and D. Filges

INTRODUCTION

There is still considerable interest in medium energy proton reaction data because of applications in astrophysics, neutron sources, materials research, accelerator technology, space research and high energy physics. Regarding accelerator technology, a new generation of spallation neutron sources has come into operation [1]. The economic design and operation of new high current proton accelerators is strongly dependent on the accurate knowledge of neutron, pion, and radioisotope production, since these reaction products cause the main problem related to shielding, radiation damage, safety, and maintenance aspects. Much of the needed data has to come from nuclear model calculations, mainly above 20 MeV. Such calculations require computer codes capable of multi-particle emission and pre-equilibrium treatment [2-4].

Some basic features of these models, however, can be tested and validated in relatively simple experiments showing clearly defined boundary conditions and excluding any contributions of secondary particle induced reactions. Experiments of this kind are called code validation experiments.

Earlier secondary neutron measurements at incident proton energies above 100 MeV are rather scarce and cover only a few points in the double differential scale [5-9].

Systematics studies and measurements were started as part of a study project for a new spallation source [10] by S. Cierjacks and co-workers [11] in 1981. The publication and the discussion of those measurements (see Refs. 12-15) led then to a collaborative effort between LANL - Los Alamos and KFA Jülich to measure double differential neutron production cross sections at the LAMPF-WNR facility in 1984-1990.

The measurements and validations have been published in several conference proceedings and journals [16-22]. After more than one decade of these measurements based on S. Cierjacks' measurements at the PSI proton cyclotron beam, a complete list of the status of the thin target (p,xn) measurements may be found in Table 1.

Table 1: Thin Target (p,xn) Measurements

Energy (MeV)	Target Materials	Angle (degree)
113	Be,C,O,Al,Fe,W,Pb,U	7.5,30,60,150
256	Be,C,O,Al,Fe,Pb,U	7.5,30,60,150
318	C,Al,Ni,Ta,W,Pb,U	7.5,30
597	Be,B,C,N,O,Al,Fe,Pb,U	30,60,120,150
800	Be,B,C,N,O,Al,Cd,Fe,W,Pb,U	30,60,120,150
800	C,Al,Ni,Ta,W,Pb,U	7.5,30
160(a)	Al,Zr,Pb	0,11....145
597(b)	C,Al,Fe,Nb,In,Ta,Pb,U	30,90,150
800(c)	Al,Cu,In,Pb,U	0,30,45,112

(a) Scobel et al. [23], (b) Cierjacks et al. [13], (c) Howe [6]

MEASUREMENTS

Measurements of neutron spectra were performed via the time-of-flight technique utilizing the unique conditions for this type of experiment at the Los Alamos WNR facility. The flight path lengths were between 30 m and 60 m at several distinct angles. The time resolution was 200 ps, mainly due to the favourable pulse structure of the proton beam, and at a reasonable intensity of about 10^8 protons per micropulse. Other sources of time uncertainty could not be determined. But it is probable that they exist and reduce the accuracy, which can be estimated with the above machine parameters. Fig. 1 gives the theoretically calculated energy resolution in percent for a 30 m flight path versus energy with time resolution as parameter. From Fig. 1 it follows that the worst energy resolution is less than 1%.

Another source of uncertainty, which has to be considered in neutron time-of-flight measurements, is the energy dependent efficiency of the neutron detector. Several efficiency curves for scintillator materials exist, which differ considerably at energies above 400 MeV (see Refs. 20 and 22).

Details about the experimental arrangement and the analysis procedure are given in Refs. 16-18.

MONTE CARLO SIMULATIONS

The present calculations are based on the intranuclear cascade-evaporation model originally developed by Bertini [24], and implemented in the high-energy nucleon-meson transport code [25] developed at Oak Ridge National Laboratory (ORNL). This Monte Carlo code for particle production and radiation transport has been modified several times in the past. Various code modifications of HETC have been made at the Forschungszentrum Jülich (KFA). All the modifications relevant to the included nuclear model refer to the evaporation model, which involves the Ewing-Weisskopf formalism [26] without a contribution from preequilibrium processes. The changes contain an update of the atomic masses using the 1977 Atomic Mass Evaluation values of Wapstra and Bos [27]. The range of possible residual nuclei was extended by implementing the semi-empirical mass formula of Cameron [28] in case of masses not covered by those tables. Furthermore, the parameter B_0 in the formula of the level density is allowed to vary with A, using data compiled by Baba [29]. A new kinematic calculation involving the recoil momentum of the residual nucleus allows non isotropic evaporation. At last the high energy fission model (RAL-model [30]) has been included in the evaporation model based on the statistical model of Fong [31]. In the actual update this modified HETC has been implemented into the framework of the HERMES code system [2], resulting in the actual version HETC/KFA-2.

The calculational predictions of proton induced neutron emission presented were made by using the so-called "thin target"-setup of HETC/KFA-2. In this setup only the included nuclear models of HETC are taken into account. Starting an on-line analysis of emitted nucleons directly after their emission from the nucleus, time consuming extranuclear transport algorithm are switched off. This procedure is somewhat different from previous published calculations [14] avoiding the writing of large event histories on computer storage devices. Physically this setup can be understood as an ideal thin target consisting of only one nucleus. This method is valid because the "geometrical" cross section of the bombarded nucleus is known by the code [2]. This method results in significantly shorter computing times than another method simulating the geometry of a real thin target used in experiments. For U and Pb targets the RAL fission model [30] with a constant value of B_0=8 MeV and isotropic emission of secondary particles during evaporation in the laboratory system were used. For all other target nuclei the fission model was excluded and the variable B_0-option was selected, while non-isotropic emission of evaporation particles was allowed.

To achieve optimum comparison, identical energy intervals as used in the experimental analysis were provided in the HETC calculations. Depending on target material, emission angle and incident proton energy, the number of spallation events varied from $2.5 \cdot 10^5$ to $6.0 \cdot 10^5$ to achieve reasonable statistics in the calculations.

EXPERIMENTAL RESULTS AND COMPARISON WITH MONTE CARLO SIMULATIONS

The predictions of the HETC-INCE model were compared to the experimental data. The total uncertainties of the experimental results (combining statistical and systematic errors) were determined as 10-15%, and thus are of the order of the data point sizes. Theoretical cross sections were calculated with typical statistical uncertainties between 1% and 5% (one standard deviation), except for a few of the highest energy groups.

Some examples of the measurements given in Table 1 were simulated and are partly given in Figs. 2-5 as examples of the (p,xn) cross sections of the following materials. Comparisons of calculated and experimental cross sections are commonly displayed in a double logarithmic scale using units of barns/(MeV·sr). The kind of presentation (per unit of lethargy) was chosen here to pronounce discrepancies between experimental and simulated curves. The respective conversion is given by the relation:

$$\frac{d\sigma_i}{d\Omega \cdot dU} = \frac{d\sigma_i}{d\Omega \cdot dE} = \frac{E_{i+1}-E_i}{\log E_{i+1} - \log E_i}$$

where $d\sigma_i/d\Omega dE$ is the double differential cross section in the energy interval $[E_i, E_{i+1}]$. For this purpose in Fig. 2 and 3 an illustrative example is given.

Measurements of proton induced neutron production cross sections are available now for a wide range of target masses, incident energies and neutron emision angles. Discrepancies between earlier measurements and INCE simulations are considerably smaller with the latest measurements. A detailed analysis of the state-of-the-art of accuracy of neutron cross section measurements and validation simulation will be published in Ref. [32].

REFERENCES

[1] Proc. of ICANS-XI, 1990 KEK Tsukuba, Japan, Report KEK 90-25 (1991)

[2] P.Cloth, D. Filges, R.D. Neef, G. Sterzenbach, Ch. Reul, T.W. Armstrong, B.L. Colborn, B. Anders, H. Brückmann, KFA-Report Jül-2203 (1988)

[3] V.S. Barashenkov, et al., Atomnaya Energiya 32 (1972) 217

[4] E.H. Auerbach, Computer Physics Comm. 15 (1978) 165

[5] J.W. Wachter, W.A. Gibson, W.R. Burrus, Phys. Rev. C6 (1972) 1496

[6] S.D. Howe, Ph.D. thesis, Kansas State University (1980)

[7] R. Madney, F.M. Waterman, Phys. Rev. C8 (1973) 2414

[8] C.G. Cassapakis, H.C. Bryant, B.D. Dieterle et al., Phys. Lett. 64B (1976) 35

[9] B.E. Bonner, J.E. Simmons, C.R. Newsom et al., Phys. Rev. C18 (1978) 1418

[10] G.S. Bauer, et al., Joint KFA-Jülich and KFK-Karlsruhe Report Jül-Spez-113/KfK 3175 (1981)

[11] S. Cierjacks et al., Proc. of the ICANS-V. Editors G.S. Bauer and D. Filges, Jül-Conf-45 (1981)

[12] S. Cierjacks et al., Progress Reports on Nuclear Data Research in the Federal Republic of Germany
NEANDC(E) - 232 U Vol.V (1982)
" - 242 U Vol.V (1983)
" - 252 U Vol.V (1984)
" - 262 U Vol.V (1985)
" - 272 U Vol.V (1986)
" - 282 U Vol.V (1987)

[13] S. Cierjacks et al., Physical Review C36 (1987) 1976

[14] D. Filges et al., Physical Review C36 (1987) 1988

[15] D. Filges, S. Cierjacks and P. Cloth, Joint KFA-Jülich and KFA-Karlsruhe Report Jül-1960/KFA-3779 (1984)

[16] M.M. Meier, D.B. Holtkamp, G.L. Morgan, H. Robinson, G.J. Russell, E.R. Whitaker, W. Amian, N. Paul, Radiation Effects 96 (1986) 73

[17] M.M. Meier, D.A. Clark, C.A. Goulding, J.B. McClelland, G.L. Morgan, C.E. Moss, Nucl. Sci. and Eng. 102 (1989) 310

[18] M.M. Meier, W.B. Amian, C.A. Goulding, G.L. Morgan, C.E. Moss, Report LA-11518-MS (1989)

[19] P. Cloth, P. Dragovitsch, D. Filges, Ch. Reul, W.B. Amian, M.M. Meier, Report Jül-2295 (1989)

[20] W. Amian, P. Cloth, P. Dragovitsch, V. Drüke, D. Filges, M.M. Meier, Int. Conf. on Nuclear Data of Science and Technology, KFA Jülich, 1991, (S.M. Qaim, Editor) Springer Verlag, Berlin/Heidelberg, 1992, p. 696

[21] P. Cloth, V. Drüke, D. Filges, XXI. Int. Symp. on Nuclear Physics, Castle Gaussig, Germany, Nov. 1991, (D. Seeliger, Editor) ISBN 981-02-1013-2

[22] M.M. Meier et al., Nucl. Sci. Eng. 110 (1992) .....
W.B. Amian et al., Nucl. Sci. Eng. 112 (1992) .....

[23] W. Scobel et al., Phys. Rev. C41 (1990) 2010

[24] H.W. Bertini, Phys. Rev. 188 (1969) 1711

[25] T.W. Armstrong, K.C. Chandler, Nucl. Sci. Eng. 49 (1972) 110

[26] V.F. Weisskopf, Phys. Rev. 52 (1937) 295; V.F. Weisskopf and H.D. Ewing, ibid 50 (1940) 475

[27] A.H. Wapstra, K. Bos, At. Data Nucl. Data Tables 19 (1977) 175

[28] A.G. Cameron, Can. J. Phys. 35 (1957) 1021; 36 (1958) 1043

[29] H. Baba, Nucl. Phys. A159 (1970) 625

[30] F. Atchison, Meeting on Targets for Neutron Beam Spallation Sources, KFA Jülich, Report Jül-Conf-34, 17 (1980)

[31] P. Fong, Statistical Theory of Nuclear Fission, Gordon and Breach Science Publishers, New York (1969)

[32] KFA Jül-Report to be published

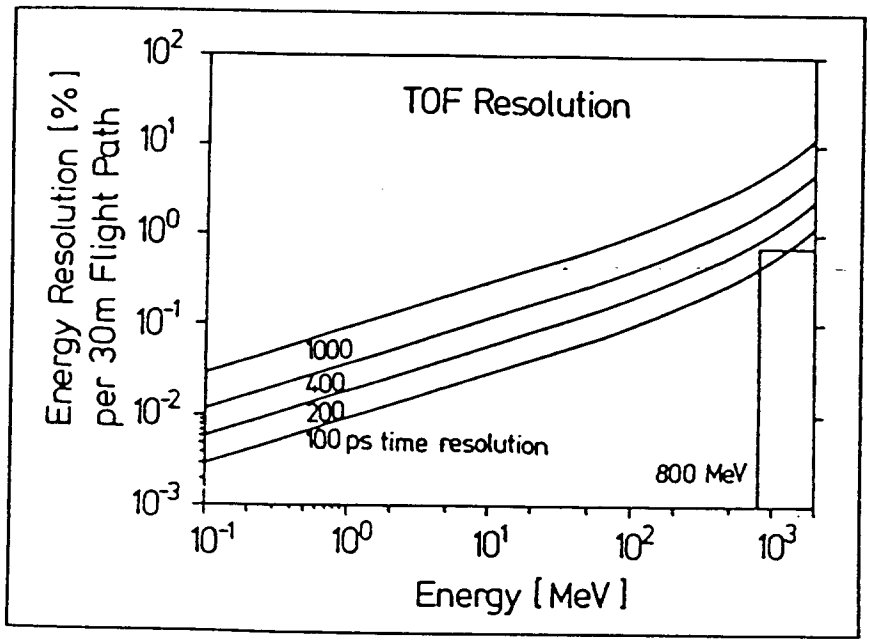

Fig. 1: The neutron energy resolution of the time-of-flight method at the WNR for a 30 m flight path. Time resolution is introduced as parameter. The uncertainty in the flight path length is assumed to be zero. Note, however, that the thickness of the neutron detector corresponds to such an uncertainty.

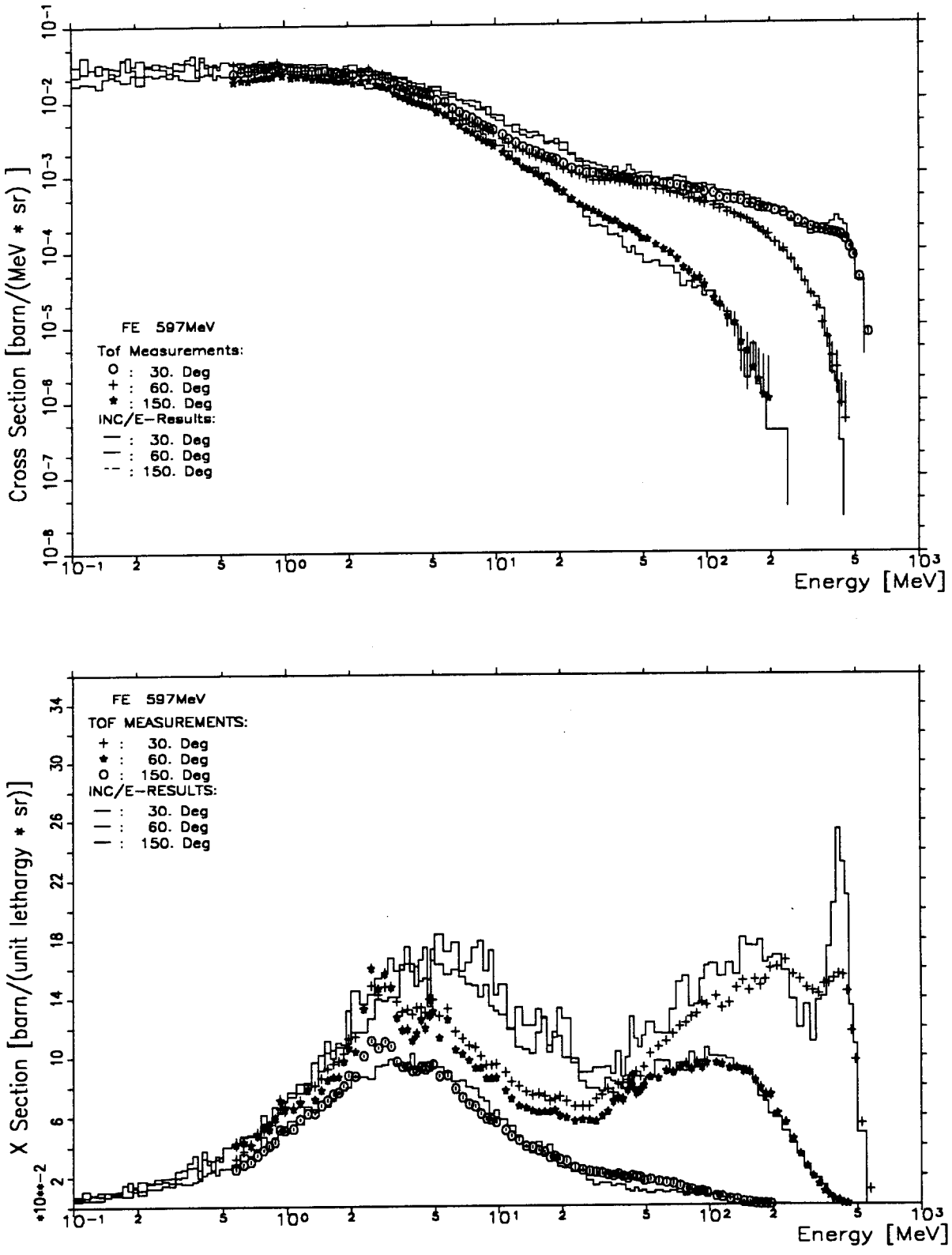

Fig. 2 Example for the presentation of double differential cross sections of neutrons from 597 MeV protons on iron (above: double logarithmic scale [barns * sr^{-1} * Mev^{-1}]; below: linear-logarithmic scale [barns * sr^{-1} per unit lethargy])

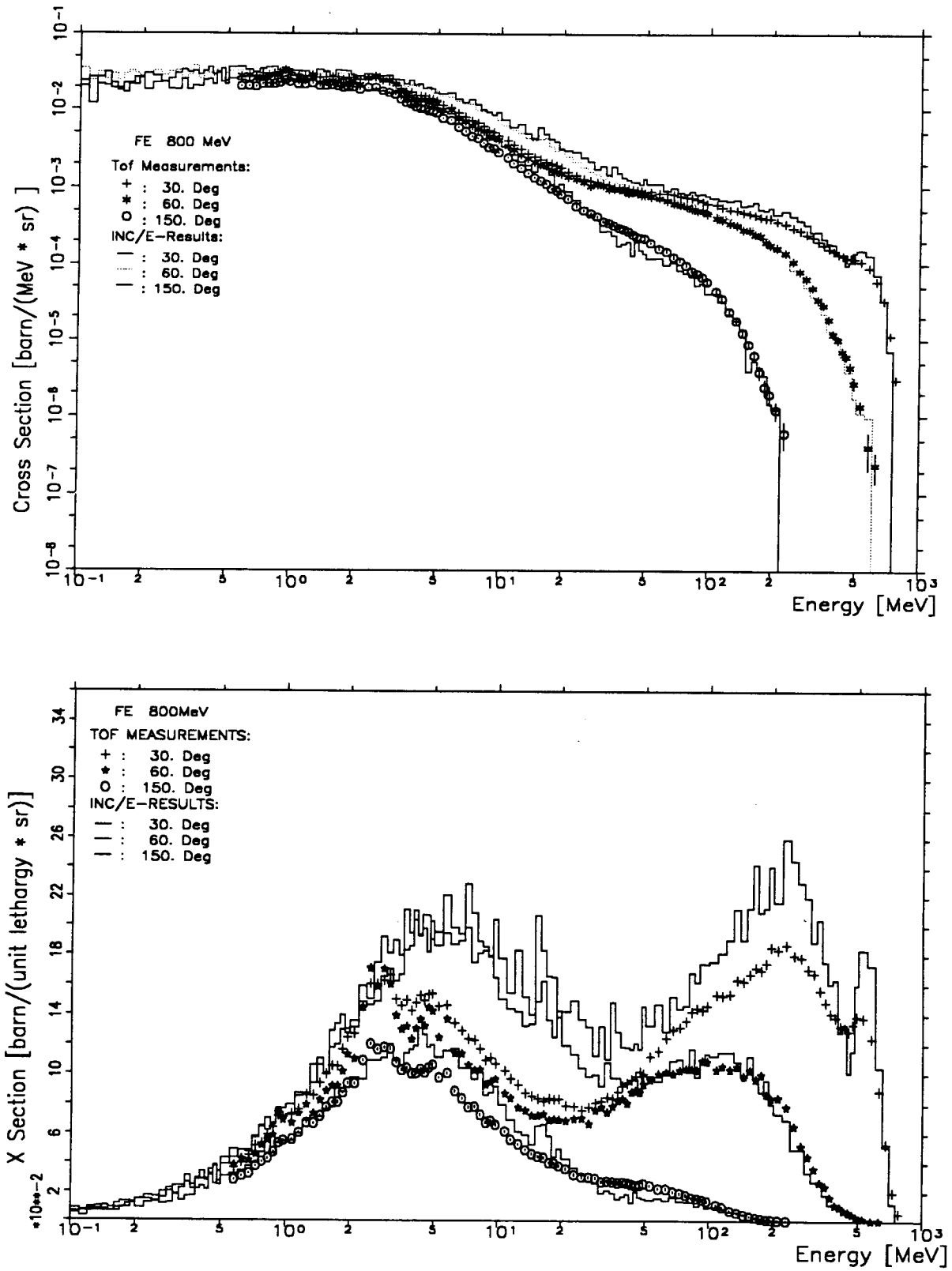

Fig. 3 Example for the presentation of double differential cross sections of neutrons from 800 MeV protons on iron (above: double logarithmic scale [barns * sr^{-1} * Mev^{-1}]; below: linear-logarithmic scale [barns * sr^{-1} per unit lethargy])

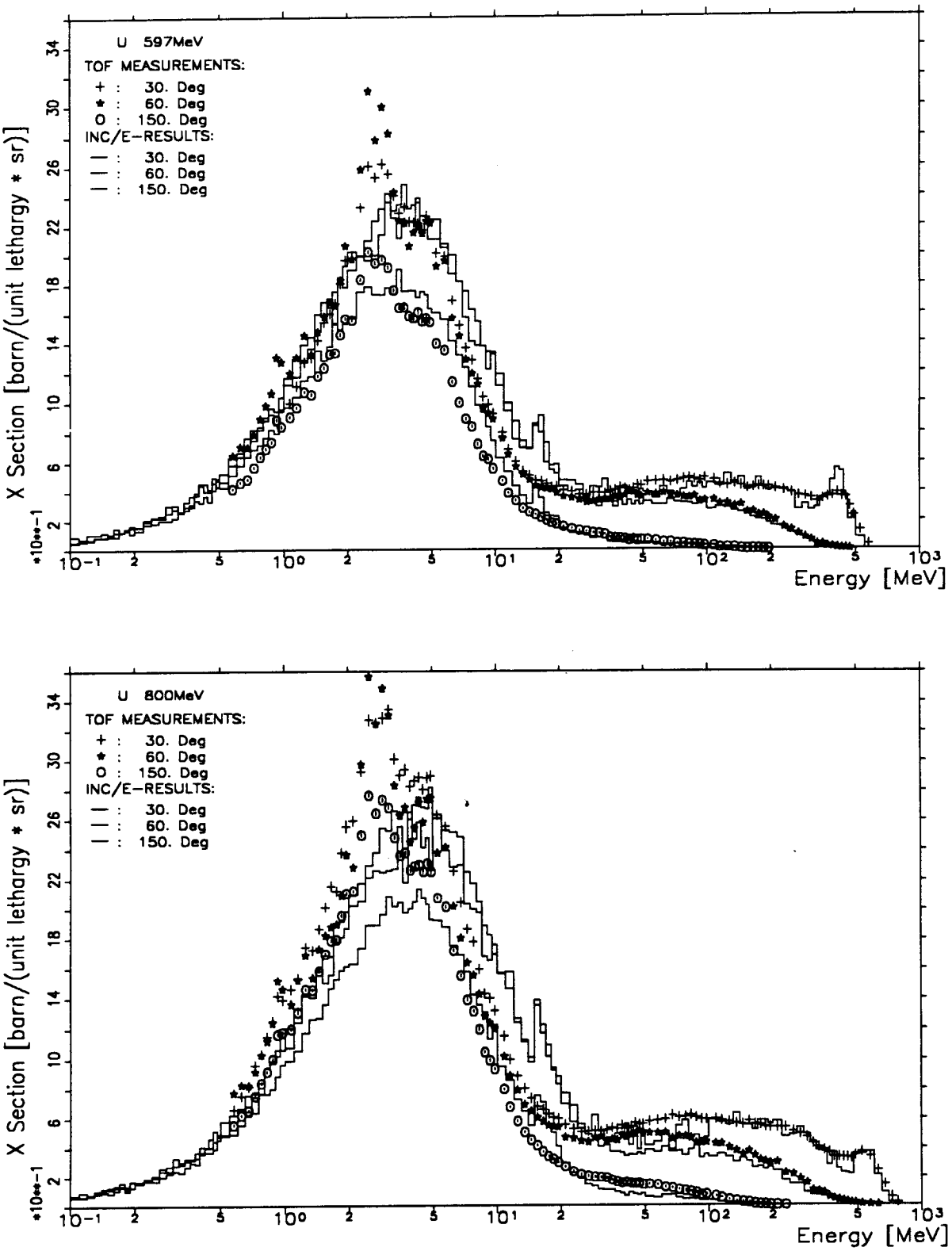

Fig. 4 and 5: Neutrons from 597 MeV protons (above) and 800 MeV protons (below) on uranium

INSTITUT FÜR NUKLEARCHEMIE
FORSCHUNGSZENTRUM JÜLICH

1. Complex Particle Emission Reactions

B. Scholten, B. Neumaier, S.M. Qaim, G. Stöcklin

In continuation of our fundamental studies on neutron and charged particle induced nuclear reactions involving complex particle emission [cf. 1 - 3, and previous Progress Reports] the excitation function of the $^{209}Bi(p,^{7}Be)^{203}Hg$ reaction was investigated in detail. The high cross section for this reaction reported earlier [2] was now found to be due to the disturbing $^{16}O(p,^{7}Be)$-process on the oxygen impurity present in the Bi target. Presently experiments are underway using higher purity Bi as target material. Besides ^{7}Be, the product nucleus ^{203}Hg is also separated radiochemically. Low-level β^- and γ-counting are in progress. The results should give some information on the relative competition between ^{7}Be and (4p3n) emission.

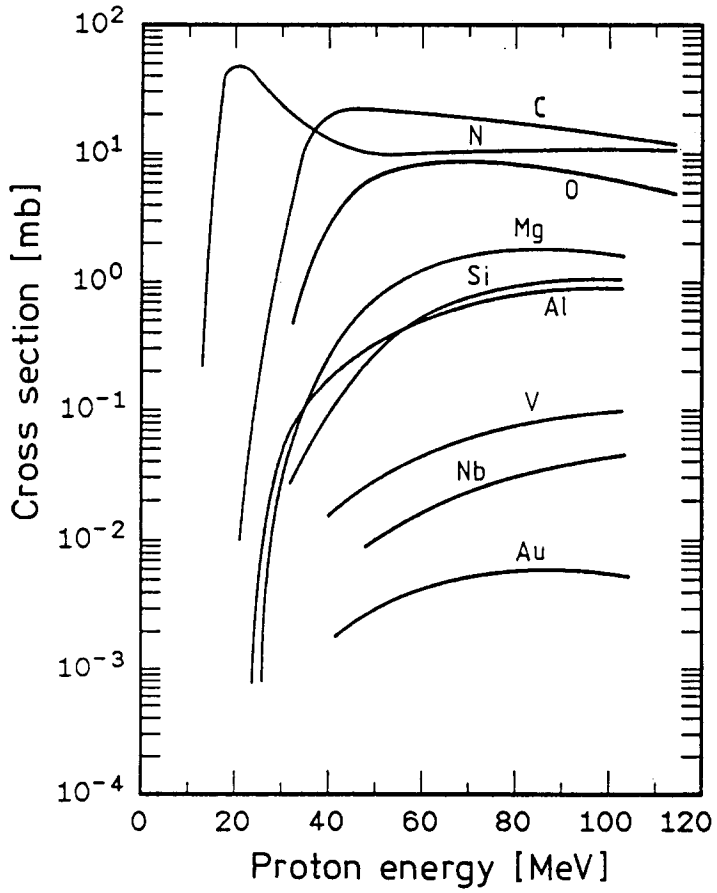

Fig. 1 Systematics of $(p,^{7}Be)$ excitation functions on target nuclides of elements C to Au.

Our on-going studies on (p,^{7}Be) reaction on Al, V, Nb and Au were completed. Some systematic trends in the excitation functions measured in our laboratory as well as those reported in the literature were analysed. A summary of the data is given in Fig. 1. The (p,^{7}Be) cross sections for the light elements C, N and O are rather high, presumably due to both ^{7}Be-emission and ^{7}Be product nucleus formation. In the medium and heavy mass regions the (p,^{7}Be) cross section decreases with the increasing Z of the target nucleus.

2. Isomeric Cross Section Ratios

I. Birn, S. Sudár, F. Rösch, S.M. Qaim

Continuing our studies on isomeric cross section ratios, we investigated the following isomeric pairs:

a) ^{75m,g}Se in (n,p), (n,α) and (n,2n) reactions in collaboration with the Technical University, Dresden. The data analysis of the measurements done at Jülich in the neutron energy range of 5 to 12 MeV was completed. Measurements at 14.7 MeV were done at Dresden. Nuclear model calculations using the code EXIFON have also been performed at Dresden. More refined calculations are in progress.

b) ^{58m,g}Co in several reactions like (n,2n), (p,n), (d,n), (α,n) and (p,α). This work is proceeding in collaboration with the Kossuth University, Debrecen, Hungary. The data analysis is nearing completion. Nuclear model calculations using the code STAPRE are in progress. The calculated isomer ratio appears to depend strongly on the input level scheme of the product nucleus.

c) ^{86m,g}Y in ^{86}Sr(p,n)- and ^{85}Rb(^{3}He,2n)-processes; ^{94m,g}Tc in ^{94}Mo(p,n)-reaction. The measured isomer ratios were interpreted only qualitatively. The ratio depends strongly on the energy of the projectile.

3. Fast Neutron Induced Reaction Cross Sections

I. Birn, M. Bostan, A. Grallert, J. Csikai, S.M. Qaim
(Relevant to request identification numbers: 742117R, 742129R, 761055R, 861120F, 861129F, 861184F)

The aim of these investigations was twofold: a) to test nuclear models, b) to obtain data of some interest in fusion reactor technology.

Excitation function measurements on the reactions $^{45}Sc(n,p)^{45}Ca$, $^{45}Sc(n,\alpha)^{42}K$, $^{45}Sc(n,2n)^{44m,g}Sc$, $^{55}Mn(n,p)^{55}Cr$, $^{55}Mn(n,\alpha)^{52}V$ and $^{55}Mn(n,2n)^{54}Mn$ from threshold to 12 MeV were completed. Of special interest is the $^{45}Sc(n,p)^{45}Ca$ reaction which leads to soft β^-emitting long-lived ^{45}Ca as product. Using radiochemical separations and low-level β^-counting it was possible to measure the data for this reaction for the first time. Nuclear model calculations using the code STAPRE were performed. The experimental excitation functions are reproduced well by the calculation except for the (n,α) reaction on ^{45}Sc target, where, presumably, strong direct interactions are involved.

Systematic experimental and theoretical studies on several neutron threshold reactions were continued in collaboration with the Technical University, Dresden [cf. 4]. Measurements were completed on $^{75}As(n,p)^{75}Ge$, $^{75}As(n,\alpha)^{72}Ga$, $^{75}As(n,2n)^{74}As$, $^{74,76,78}Se(n,p)^{74,76,78}As$, $^{78,80}Se(n,\alpha)^{75,77}Ge$, $^{72,73,74}Ge(n,p)^{72,73,74}Ga$ and $^{70,76}Ge(n,2n)^{69,75}Ge$ reactions over the neutron energy range of 6 to 12 MeV at Jülich, and at 14.7 MeV at Dresden. Nuclear model calculations using the code EXIFON were done at Dresden. In general, the experimental excitation functions are reproduced well by the model calculations. A typical (n,α) excitation function is given in Fig. 2. Above 12 MeV several

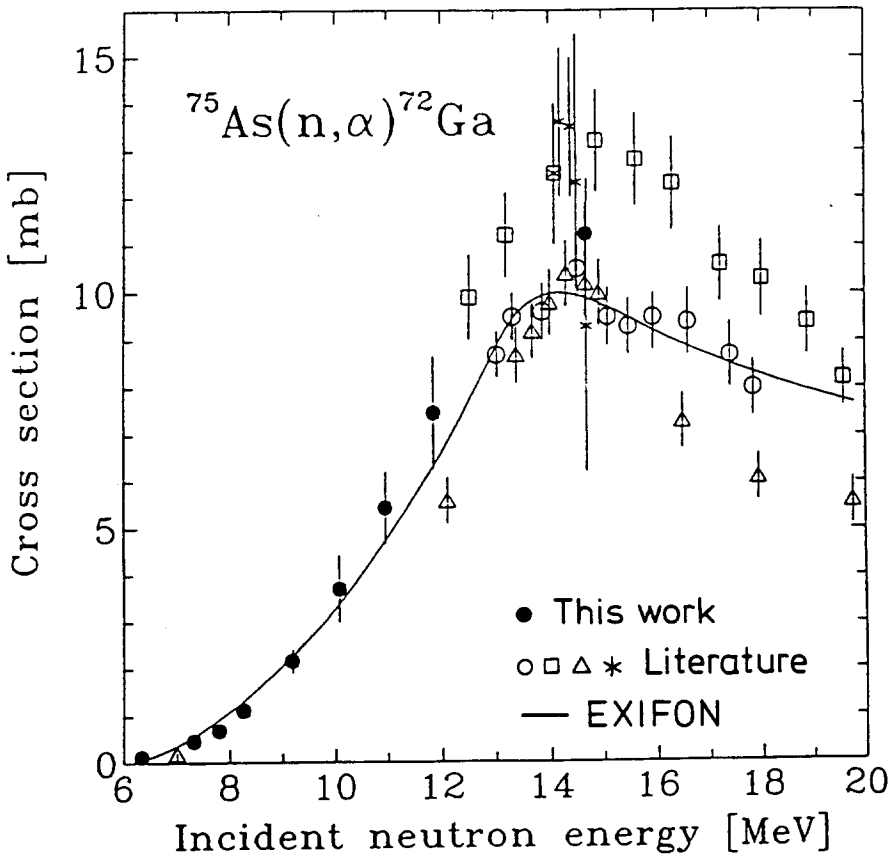

Fig. 2 Excitation function of the $^{75}As(n,\alpha)^{72}Ga$ reaction.

reports exist but the data are discrepant; below 12 MeV the data base was very weak. Our studies furnish new data and thereby allow an investigation of some systematic trends in the excitation functions.

Continuing our studies on fusion related activation products [cf. 5], we measured several (n,p) and (n,α) reaction cross sections on isotopes of zirconium in the neutron energy range of 10 to 12 MeV in cooperation with the Kossuth University, Debrecen, Hungary. Measurements on the $^{63}Cu(n,p)^{63}Ni$ process are in progress. Thick copper samples irradiated with 7, 8, 9, 10 and 14.5 MeV neutrons have been processed chemically and the soft β^- emitter ^{63}Ni($T_{½}$=100y; E_{β^-}=66 keV) has been separated. Its activity is being measured via low-level β^- counting.

4. Excitation Functions Relevant to Radioisotope Production

F. Rösch, F. Tárkányi, Z. Kovács, S.M. Qaim, G. Stöcklin

In continuation of our studies [cf.6 - 8] on the production of medically important short-lived radioisotopes we measured excitation functions of a few reactions relevant to the production of the β^+ emitting radioisotopes ^{86}Y, ^{94m}Tc and ^{75}Br.

The cross section data for the $^{86}Sr(p,n)^{86}Y$ ($T_{½}$ = 14.7 h) reaction were measured using 96 % enriched ^{86}Sr and were reported in the last Progress Report. Further studies included determination of $^{nat}Rb(^3He,xn)^{87,87m,86,86m,85,85m}Y$ excitation functions from threshold to 35 MeV. The optimum energy range for the production of ^{86}Y via this route was found to be $E_{^3He}$ = 24 → 12 MeV, with an expected thick target yield of 190 MBq (5.2mCi)/μAh. From a comparison of the two investigated routes for the production of ^{86}Y, viz. $^{86}Sr(p,n)^{86}Y$ and $^{nat}Rb(^3He,xn)^{86}Y$, the former process is recommended since it leads to higher purity product and a small-sized cyclotron is adequate [9].

The β^+ emitting radioisotope ^{94m}Tc ($T_{½}$ = 52 min) is a potentially useful radioisotope for quantifying biodistribution of Tc-radiopharmaceuticals in humans via Positron Emission Tomagraphy (PET). It can be produced via several nuclear reactions. The cross section data for the $^{94}Mo(p,n)^{94m}Tc$ reaction were measured using 94 % enriched ^{94}Mo. The results are shown in Fig. 3. The optimum energy range for the production of ^{94m}Tc is E_p = 13 → 7 MeV; the thick target yield of ^{94m}Tc amounts to 2GBq (54 mCi)/μAh and the level of the ground state isomer (^{94g}Tc) is 5.5 %. The $^{94}Mo(p,n)$-process is thus ideally suited for the production of ^{94m}Tc at a small-sized cyclotron [10].

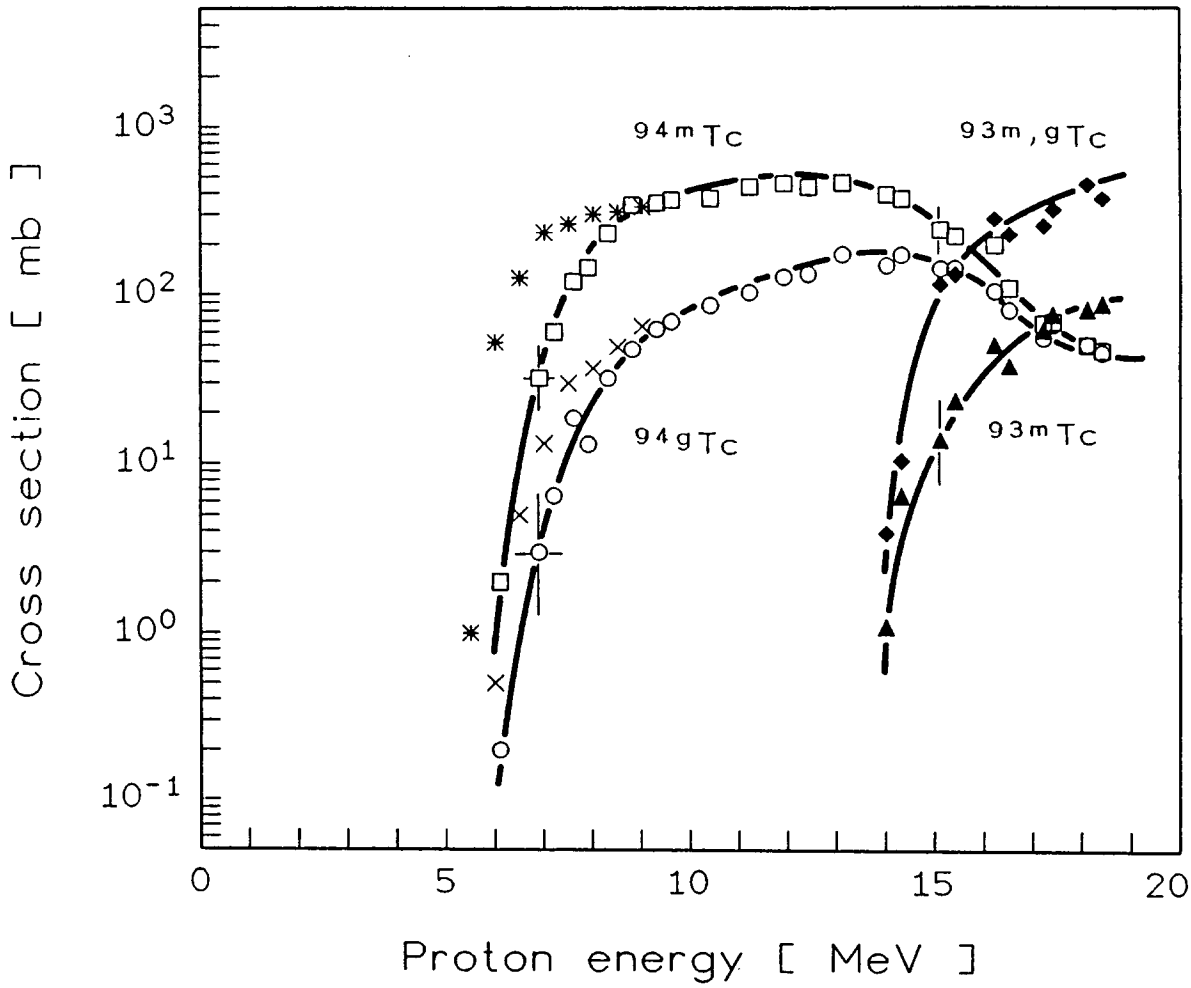

Fig. 3 Excitation functions of ^{94}Mo(p,xn)-processes leading to the formation of ^{94m}Tc, ^{94g}Tc, ^{93m}Tc and ^{93m,g}Tc. Some literature data (*,x) are also shown.

Cross section measurements relevant to the production of ^{75}Br ($T_{1/2}$ = 1.6 h) at a small-sized cyclotron included investigations of ^{78}Kr(p,α)- and ^{74}Se(d,n)-processes [11, 12]. The ^{78}Kr(p,α)-reaction was studied in cooperation with ATOMKI, Debrecen, Hungary, using 99.4 % enriched ^{78}Kr. The proton energy range covered was 12 to 20 MeV. The ^{74}Se(d,n)-process had been investigated at Jülich earlier using 31.4 % enriched ^{74}Se. The data have been now completely analysed. The thick target yields of ^{75}Br calculated from the excitation functions of the two investigated processes are shown in Fig. 4 for comparison. Evidently, the (d,n) reaction gives higher ^{75}Br-yield than the (p,α) reaction. The expected ^{75}Br-yields via the two processes at a baby cyclotron(E_p = 17 MeV; E_d = 10 MeV) amount to 70 MBq (1.9 mCi)/μAh and 228 MBq (6.16mCi)/μAh, respectively. The achievable batch yields of ^{75}Br at a small cyclotron via both the processes are thus limited.

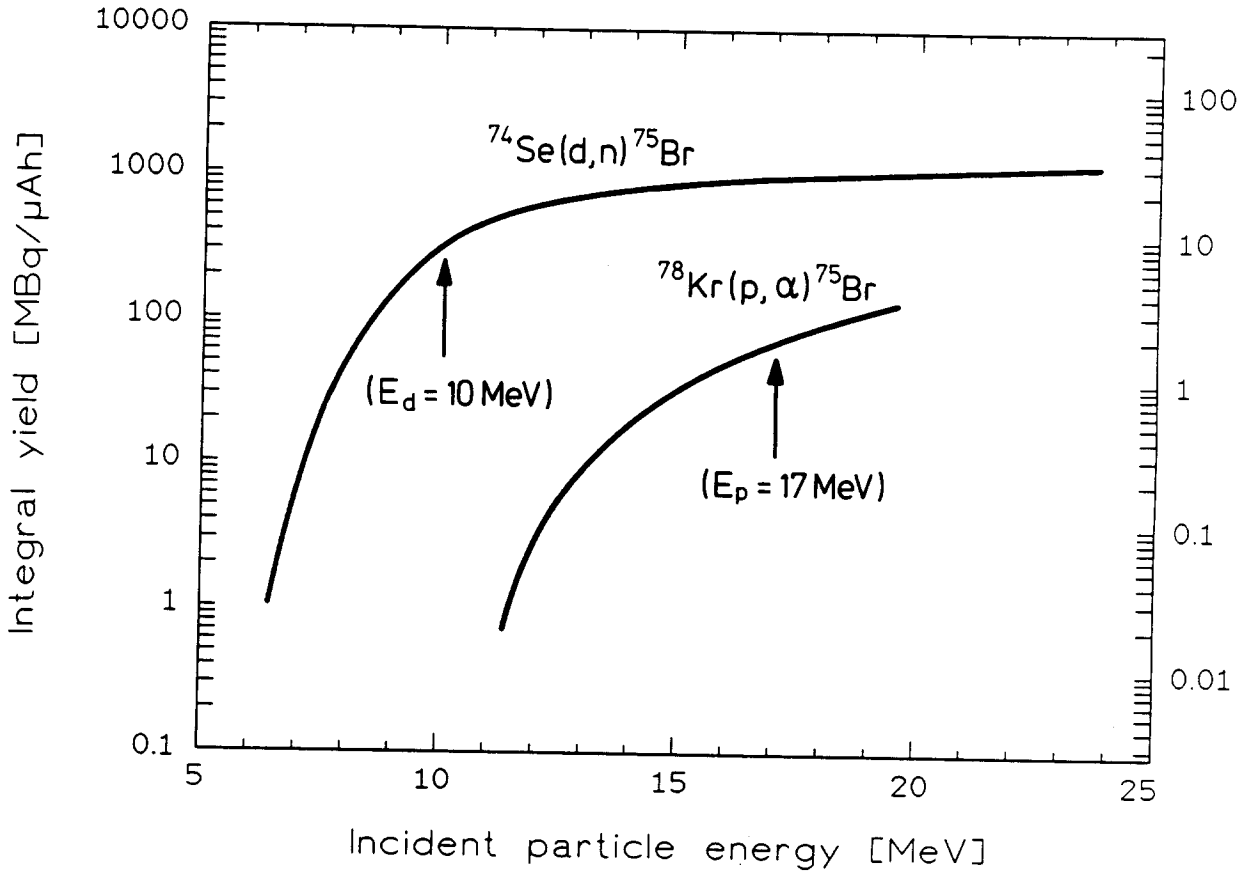

Fig. 4 Thick target yields of ^{75}Br via ^{78}Kr(p,α)- and ^{74}Se(d,n)-processes as a function of incident particle energy. The expected thick target yields at a baby cyclotron (E_p = 17 MeV; E_d = 10 MeV) are indicated.

References

[1] S.M. Qaim, M. Uhl. N.I. Molla, H. Liskien: ^{4}He emission in the interactions of fast neutrons with ^{48}Ti and ^{50}Ti, Phys. Rev. C46 (1992) 1398

[2] B. Scholten, S.M. Qaim, G. Stöcklin: ^{7}Be emission in proton and neutron induced reactions, in Nuclear Data for Science and Technology (S.M. Qaim, Editor), Springer Verlag, Berlin/Heidelberg 1992, p. 711

[3] B. Scholten, S.M. Qaim, G. Stöcklin: A systematic study of (n,^{7}Be) reactions on medium and heavy mass nuclei induced by 53 MeV d(Be)-breakup neutrons, Radiochimica Acta, in press

[4] N.I. Molla, S.M. Qaim, H. Kalka: Excitation functions of $^{46-50}Ti(n,p)^{46-50}Sc$ processes, Phys. Rev. C45 (1992) 3002

[5] S.M. Qaim, F. Cserpák, J. Csikai: Cross sections of $^{151}Eu(n,2n)^{150m}Eu$ and $^{159}Tb(n,2n)^{158}Tb$ reactions near their thresholds, Appl. Radiat. Isotopes 43 (1992) 1065

[6] H. Piel, S.M. Qaim, G. Stöcklin: Excitation functions of (p,xn)-reactions on ^{nat}Ni and highly enriched ^{62}Ni: possibility of production of medically important radioisotope ^{62}Cu at a small cyclotron, Radiochimica Acta 57 (1992) 1

[7] F. Tárkányi, Z. Kovács, S.M. Qaim, G. Stöcklin: Production of ^{38}K via the $^{38}Ar(p,n)$-process at a small cyclotron, Appl. Radiat. Isotopes 43 (1992) 503

[8] F. Szelecsényi, G. Blessing, S.M. Qaim: Excitation functions of proton induced nuclear reactions on enriched ^{61}Ni and ^{64}Ni: possibility of production of no-carrier-added ^{61}Cu and ^{64}Cu at a small cyclotron, Appl. Radiat. Isotopes 44 (1993) 575

[9] F. Rösch, S.M. Qaim, G. Stöcklin: Nuclear data relevant to the production of the positron emitting radioisotope ^{86} via the $^{86}Sr(p,n)$- and $^{nat}Rb(^{3}He,xn)$-processes, Radiochimica Acta, 61 (1993) 1

[10] F. Rösch, S.M. Qaim: Nuclear data relvant to the production of the positron emitting technetium isotope ^{94m}Tc via the $^{94}Mo(p,n)$-reaction, Radiochimica Acta, in press

[11] F. Tárkányi, Z. Kovács, S.M. Qaim: Excitation functions of proton induced nuclear reactions on highly enriched ^{78}Kr: relevance to the production of ^{75}Br and ^{77}Br at a small cyclotron, Appl. Radiat. Isotopes, in press

[12] S.M. Qaim, G. Stöcklin: Excitation functions of $^{74}Se(d,xn)^{75,74m}Br$ reactions: comparative evaluation of possible routes for the production of ^{75}Br at a small cyclotron, Appl. Radiat. Isotopes, in press

References

[1] I. Birn and S. M. Qaim in "Progress Report on Nuclear Data Research in the Federal Republic of Germany for the Period April 1, 1991 to March 31, 1992", S. Cierjacks editor, NEA/NSC/DOC(92)5 (1992).

[2] J. F. Briesmeister (Ed.), "MCNP - A General Monte Carlo Code for Neutron and Photon Transport - Version A", LA-7396, Rev. 2, Los Alamos (1986).

[3] A. Pavlik and G. Winkler, "Calculation of the Energy Spread and the Average Neutron Energy of 14 MeV Neutrons Produced via the T(d,n)^{4}He Reaction in Solid Ti-T Targets", Report INDC(AUS)011 (INT(86)-6), IAEA Nuclear Data Section, Vienna (1986).

[4] M. Wagner, H. Vonach, A. Pavlik, B. Strohmaier, S. Tagesen and J. Martinez-Rico, "Evaluation of Cross Sections for 14 Important Neutron-Dosimetry Reactions", Physics Data 13-5, Fachinformationszentrum Karlsruhe (1990).

[5] I. Birn and S. M. Qaim, "Excitation Functions of Neutron Threshold Reactions on Some Isotopes of Germanium, Arsenic and Selenium in the Energy Range of 6.3 to 14.7 MeV", to be published.

2. Multi- Fold Fragment- Neutron Correlations+

M. Adler, B. Cramer*, I. Düring, U. Jahnke*, H. Märten, A. Ruben

*HMI Berlin

A ^{252}Cf spontaneous-fission correlation experiment combined with a new PC-CAMAC data acquisition system has been performed. Direction-sensitive spectroscopy of fission fragments (twin ionization chamber TIC with Frisch grids) was combined with the measurement of neutron multiplicity distribution P(ν), average total γ-ray energy (2x2π Gd-loaded scintillator) as well as energy and angular distribution of neutrons and γ-rays. Based on the careful account for necessary corrections, scission configurations given by mass asymmetry A_L/A_H, elongation (total kinetic energy TKE of fragments), and shape asymmetry ($\bar{\nu}_L/\bar{\nu}_H$) are studied exclusively in correlation with differential distributions of emission products (neutrons, γ-rays).

In order to determine the neutron multiplicity from *individual* fragments precisely, the counting technique was developed in regard to (i) simultaneous background measurement, (ii) cross talks between signals from the two hemispheres of the neutron tank (25 ns time gate), (iii) pile-up rejection. The $\bar{\nu}_L/\bar{\nu}_H$ separation for given $\bar{\nu}_{tot}$ is done on the basis of a fragment angular cone selection (close to sample plane normal) taking into account the direction correlation between fragments and neutrons. Neutron cross talk rates were simulated on the basis of a Monte-Carlo transport code in combination with a cascade evaporation model describing fission neutron emission as a function of A and TKE in detail. The results agree with measured data. Beside this effect, neutron multiplicity distributions were corrected for counting efficiency (use of a more reliable iteration procedure instead of the inverse response matrix method) and the foreward/backward effect of fragment-neutron correlation derived from the statistical model of fission neutron emission (cf. Fig. 1).

The $\bar{\nu}$(A) curve shown in Fig. 1 is like triple saw-tooth indicating clearly the presence of the super-asymmetric fission mode. Within an energy conservation consistent scission point model [1], the fissioning system at scission point is expected to be cold in the case of very compact, deformed, and shape-asymmetric configurations. In order to prove the latter case, mass yield curves for fixed $\bar{\nu}_L/\bar{\nu}_H$ were deduced. Examples are shown in Fig. 2. The fine-structure for extreme multiplicity ratios due to a pronounced proton odd-even effect is an indication of cold scission configurations. These results confirm some previous observations [2].

The further analysis to be performed in comparison with scission point model and statistical model calculations should provide new information on fission dynamics, e.g. on unusual fission modes, and on the degree of collective vs. intrinsic excitation at scission.

References

[1] H. Märten, Proc. Seminar on Fission, Pont d'Oye II, Oct. 23-25, 1991, ed. by C. Wagemans (1991), p. 15

[2] I.D. Alkhazov et al., Proc. Int. Conf. on 50 th Anniversary of Nuclear Fission, Leningrad, Oct. 16-20, 1989 (at present, only available as report)

+ Supported by BMFT under contract 06 DD 112

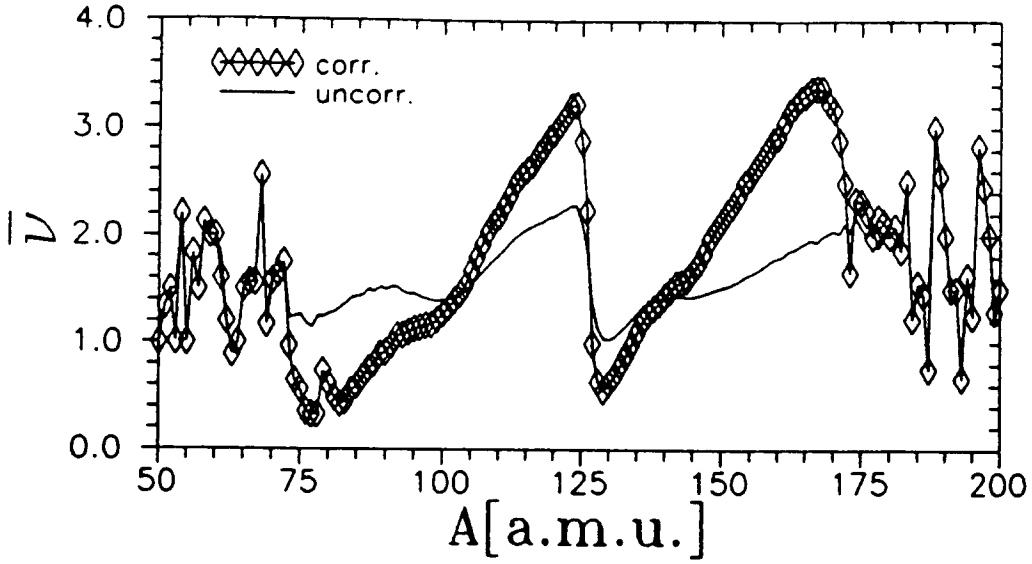

Fig. 1: Average neutron multiplicity vs. mass number

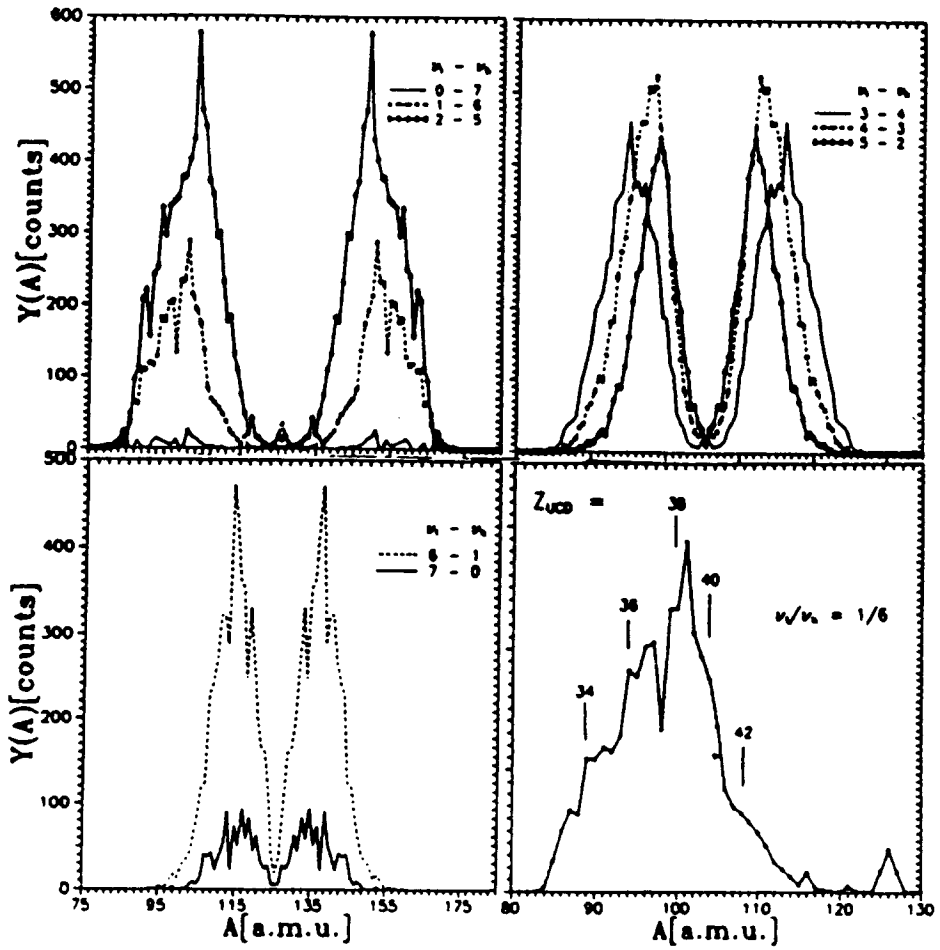

Fig. 2: Fragment mass yield for fixed $\bar{\nu}_L/\bar{\nu}_H$ and $\bar{\nu}_{tot}$ = 7. The (1/6) data structures are compared with the position of even Z according to unchanged charge distribution UCD.

3. CALCULATIONS OF TRANSITION PROBABILITIES IN EXCITED NITROGEN ATOMS AND IONS

I. Reiche, G. Zschornack

In many technical plasmas (flames, nitrification discharges etc.) nitrogen is a very important constituent. Its spectroscopy, therefore, is of interest for the diagnostics of such plasmas. A special case is an ion source for multiply charged ions [1]. Here, abundances of high charged states may be enhanced by adding a light gas – for many heavy gases nitrogen works best as additive [2]. For modelling those discharges insitu measurements of ion densities are necessary because the relation between extracted currents (from ion sources) and ion densities are unclear. Due to electric fields in the presheath ahead of the space charge at the extraction and due to transmission effects of the extraction aperture [3, 4] currents of highly charged ions may be enhanced while electrostatic containment may inhibit extraction of highly charged ions.

Technically the most simple method for density determination is emission spectroscopy. The emitted line intensity is directly proportional to the density of the excited species. For the determination of the ground state density a balancing of excitation and deexcitation in the frame work of a collisional radiative model is necessary [5, 6]. For this balancing one needs to know transition probabilities or oscillator strengths and excitation cross sections mainly for electron impact excitation.

In contrast to the neighbouring elements oxygen and carbon which were thoroughly investigated in fusion research and astronomy very few of these data are known for nitrogen and its ions [7]. In a recent compilation even for N I many transition probabilities even for strong lines are missing [8]. We, therefore, have undertaken calculations of transition probabilities needed for spectroscopic density determinations from absolutely measured line intensities in the VUV-region.

Emission rates of radiative electron transitions were calculated in adiabatic description with the program NONORTHO [9, 10] . The calculations use Multikonfiguration-Dirac-Fock(MCDF) wavefunctions obtained with the program package of Grant et.al., McKenzie et.al.[11, 12].

For the calculation of an emission rate the wavefunctions of the states before and after transition are calculated independent of each other. Since a direct complete optimization on the desired state with all relevant configurations rarely succeeds, several steps are necessary: First of all the occupied orbitals are optimized for the desired configuration and perhaps suitable energetically closely adjacent configurations. In the next step these orbital wavefunctions are frozen and wavefunctions for further orbitals not being occupied in the state of interest are calculated in some separate runs including other configurations. Finally a large scheme of interacting configurations is set up. The Hamilton matrix is calculated using the one electron wavefunctions from the previous runs in the CI scheme. Diagonalizing the Hamilton matrix yields the configuration mixing coefficients.

As an example, the optimization of the wavefunctions for the state $1s^2 2s^2 2p^3\ ^4S^o$ of N I shall be explained: It starts by calculating the orbitals 1s, 2s and 2p optimized on the above state. Holding these orbitals frozen, from the configurations $1s^2 2s^2 2p^2 3p$ and $1s^2 2s^2 2p 3p^2$ one gets a virtual 3p orbital. Another calculation with $1s^2 2s 2p^2 3s$ and $1s^2 2p^3 3s^2$ yields a virtual 3s orbital. Finally a CI calculation is done combining all configurations given above. The table shows our results in the Coulomb gauge. For comparison, available data from model potential calculations of Laughlin [13] and data taken from the compilation of Wiese [8] are included in the table.

	Transition				Wavelength /Å	Emission rate $/s^{-1}$	
N I	$2s^22p^3$	$^4S^o$	$2s^22p^2(^3P)5d$	^4D	885.656	$5.74 \cdot 10^6$	
N I	$2s^22p^2(^3P)3p$	$^4D^o$	$2s^22p^2(^3P)5d$	^4D	5531.8	$6.5 \cdot 10^5$	$5.09 \cdot 10^5$[8]
N I	$2s^22p^2(^3P)3p$	$^4D^o$	$2s^22p^2(^3P)4d$	^4P	6458.9	$1.05 \cdot 10^6$	$5.29 \cdot 10^5$[8]
N II	$2s^22p3s$	$^1P^o$	$2s^22p4p$	^1S	1732.428	$7.96 \cdot 10^6$	
N II	$2s^22p3s$	$^1P^o$	$2s^22p4p$	^1D	1780.51	$1.43 \cdot 10^7$	
N IV	$2s3d$	^3D	$2s4f$	^3Fo	1036.16	$3.8 \cdot 10^9$	$4.13 \cdot 10^9$[13]
N IV	$2s3d$	^1D	$2s4f$	^1Fo	1078.708	$3.5 \cdot 10^9$	$3.25 \cdot 10^9$[13]
N V	$3p$	$^2P^o$	$4d$	^2D	713.75	$4.29 \cdot 10^9$	$4.32 \cdot 10^9$[8]
N V	$3d$	$^2D_{3/2}$	$4f$	$^2F^o_{5/2}$	748.195	$8.05 \cdot 10^9$	
N V	$3d$	$^2D_{5/2}$	$4f$	$^2F^o_{5/2,7/2}$	748.291	$9.2 \cdot 10^9$	
N V	$3d$	$^2D_{5/2}$	$4f$	$^2F^o_{5/2}$		$5.7 \cdot 10^8$	

This work has been supported by BMFT under contract No. 06 DD 111.

References

[1] R. Geller; Z. Phys. D Suppl. 21 (1991) p.117

[2] W. Krauss-Vogt; Untersuchungen zur Ionenproduktion und Strahlformierung bei EZR-Ionenquellen, Dissertation Bonn (1986), Report Jülich 2043, Febr. 1986 KFA Jülich

[3] K.U. Riemann; J. Phys. D: Appl. Phys. 24 (1991) 493

[4] J. Hesse, K. Wiesemann; In T. Takagi (editor); Proc. 8th Symp. on ISIAT84, Kyoto 1984 p. 79-86

[5] R.W.P. McWhirter; in R.H. Huddlestone, S.L. Leonard (editors), Plasma Diagnostic Techniques, Academic Press New York, London 1965 p. 201

[6] M. Jogwich, B.A. Huber, K. Wiesemann; J. Phys. D: Appl. Phys. 24 (1991) 493

[7] K. Berrington; The Belfast Atomic Data Bank and Opacity Project, Daresbury Lab. Information Quaterly for Atomic Pocesses and Applications No. 31 Febr. 1991 p.2

[8] W. Wiese; NIST Washington, private communication (1992), publication forthcoming

[9] I. Reiche und G. Zschornack; EAS 12, Kassel 1990 p.121

[10] I. Reiche; Doctor Thesis, Technische Universität, Fakultät für Naturwissenschaften und Mathematik, Dresden 1992

[11] I.P. Grant, B.J. McKenzie, P.H. Norrington, D.F. Mayers and N.C. Pyper; Comput. Phys. Commun. 21(1980), p.207

[12] B.J. McKenzie, I.P. Grant and P.H. Norrington; Comput. Phys. Commun. 21(1980), p.233

[13] C. Laughlin; Physica Scripta 42 (1990) 551

4. REVISED INTENSITY RATIOS FOR LINES OF THE X-RAY K-SERIES

K.Sieber, I.Reiche, G.Zschornack

X-ray emission rates are not directly observable in experiments, but they are indirectly measured by the determination of relative intensity ratios between individual lines of the characteristic X-ray radiation.

The relative intensity of two emission lines is described by

$$\frac{I_{if}}{I_{ab}} = \frac{\nu_{fi}\, n_i\, \Gamma_{if}^R \left(\Gamma_a^R + \Gamma_a^A\right)}{\nu_{ba}\, n_a\, \Gamma_{ab}^R \left(\Gamma_i^R + \Gamma_i^A\right)}$$

whereby $\nu_{fi} = \frac{1}{\hbar}(E_i - E_f)$ - transition frequency for the transition $i \rightarrow f$; n_i - amount of the atoms, which are ionized in a certain time interval in a subshell i; Γ_i^R, Γ_i^A - energetic widths for the initial state of an X-ray or Auger transition, $\Gamma_i^R = \hbar p_i^R$ and $\Gamma_i^A = \hbar p_i^A$. The p_i^R and p_i^A are the probabilities for an atom to leave the excited initial state by X-ray or radiationless transitions. Further counts Γ_{if}^R - energetic width of a X-ray transition i $\rightarrow$ f.

For the special case, that the initial state is equal for both transitions, yields

$$\frac{I_{if}}{I_{ib}} = \frac{\nu_{fi}\, \Gamma_{if}^R}{\nu_{bi}\, \Gamma_{ib}^R}$$

This is given within an individual X-ray series K, L_1, L_2, ...

Thus the interest of experimental investigations to determine as precise as possible intensity ratios within individual X-ray series, conforms with the results of the theory to arrive at practically relevant values.

To date the most frequently cited, based on the evaluation of experimental data for intensity ratios, is the work of Salem et al. [1] from the year 1974. Considering 238 experimental values of newer date from papers with photo and electron excitation we have undertaken a polynom approximation of the presently available experimental data.

For all dipole lines of the X-ray K-series, which display such an emission intensity, that they are of experimental relevance, new approximations were undertaken for the individual intensity ratios. At this point the example of the K_β/K_α relationship should be given as an overview over the existing situation.

In Fig.1 the course of the K_β/K_α intensity ratio over the entire Z region in comparison with the approximation of Salem et al. is indicated. For reasons of clarity was renounced the indication of experimental errors to the individual values. It is to be considered however, that the reciprocal errors were introduced as weights in the approximation. From Fig.2 it is obvious, that according to the region of atomic numbers deviations to the data of Salem et al. by some percent are observed. A complete discussion of the present results and a comparison with results of different theoretical works will be given in a separate work on the treated problem.

This work was supported by the BMFT (Project No. 06 DD 111).

References

[1] S.I.Salem, S.L.Panossian, R.A.Krause; Atomic Data and Nuclear Data Tables, 14 (1974) 91

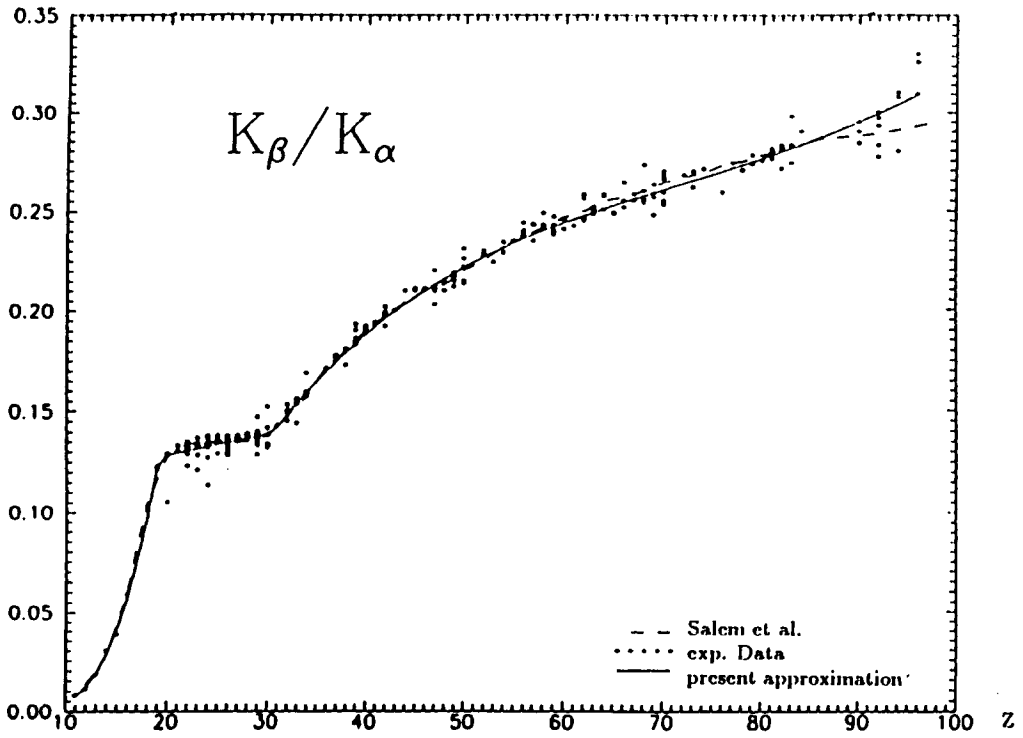

Figure 1: K_β/K_α intensity ratios.

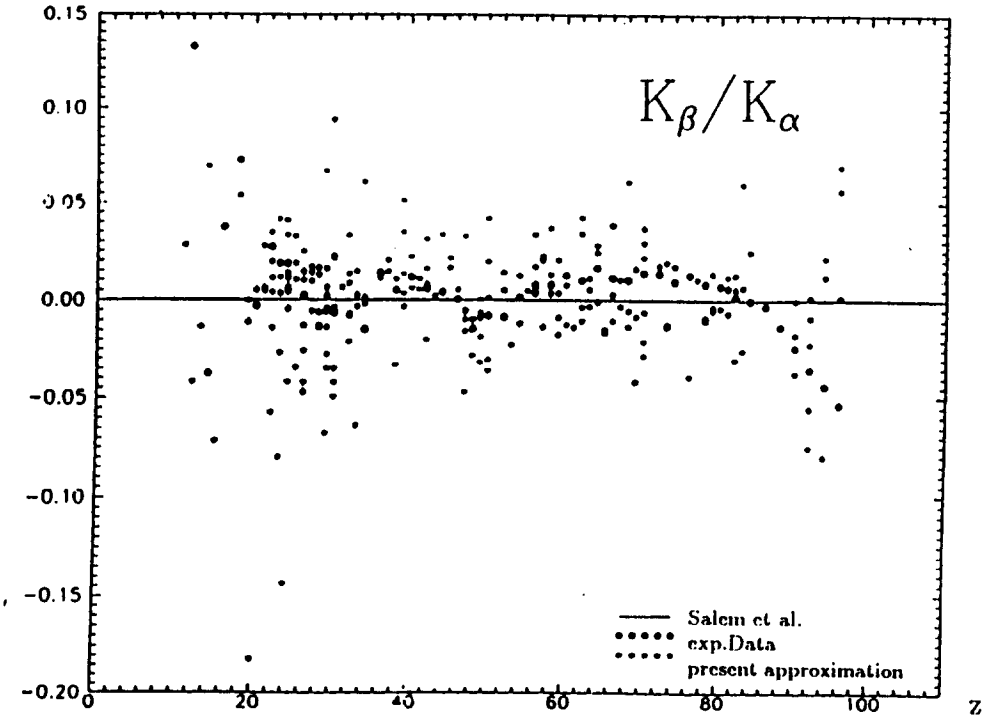

Figure 2: Relative deviations from the approximation of Salem et al. [1]. The deviations of the new experimental data from the current approximation are also given.

5. Measurement of Neutron and Gamma-Ray Spectra of a Shield Penetration Benchmark

T. Elfruth, R. Schwierz, K. Seidel, S. Unholzer

The design of the shielding blankets for fusion reactors as NET/ITER [1] and a detailed uncertainty and sensitivity analysis [2] stressed the need of a benchmark of experimental/calculated neutron and γ-ray flux densities penetrating iron slabs. The optimal geometrical arrangement was found [3] as outlined in Fig. 1. The Fe slab has a thickness of d = 30 cm and is 100 cm x 100 cm (height x width; a = 50 cm). The distance of the 14 MeV neutron source from detector is 349 cm (c = 19 cm, e = 300 cm) The detector (NE 213, 2" x 4" ∅) is sensitive to both, neutron and γ-rays (Fig. 2). The neutron generator is operated in pulsed mode (f.w.h.m. of the pulses 2 ns, frequency 5 MHz or 2.5 MHz) and for each detector event the pulse height and the time-of-arrival are recorded.

Spectra have been taken from the Fe assembly without gap and with gap (x = 20 cm, width b = 5 cm). To treat the background, each measurement is complemented by a run with a thick iron cone in front of the detector (cone geometry, detector collimator etc. are outlined in the contribution below.)

Some of the measured spectra are shown in Fig. 3-4.

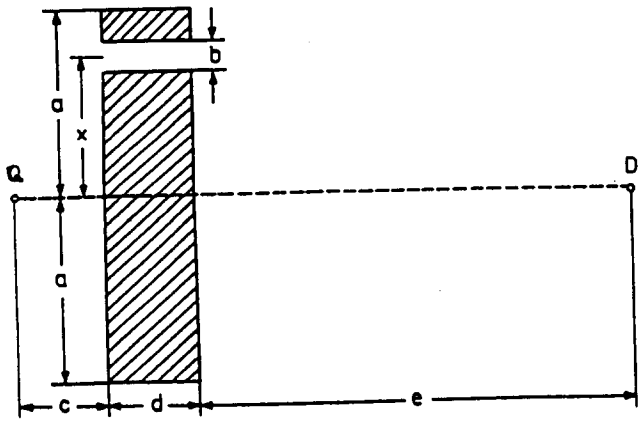

Fig. 1: Horizontal section of the benchmark geometry in the plane of 14 MeV neutron source (Q) and liquid scintillation detector (D)

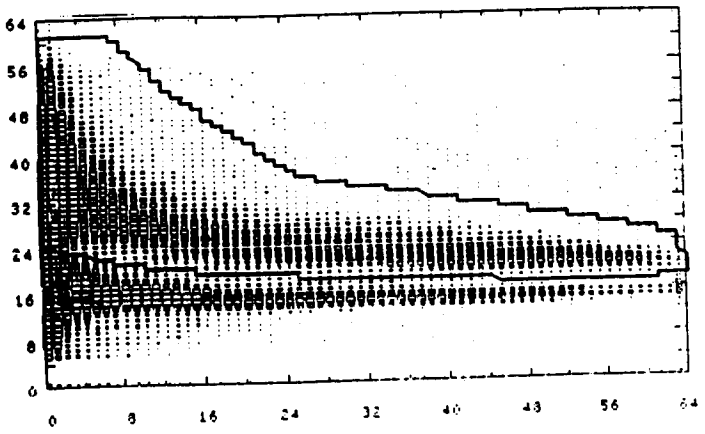

Fig. 2: Contour plot of the neutron-ray distinction (y-identification signal, x-pulse height). Events within the full line are treated as neutrons, the remaining as γ-rays.

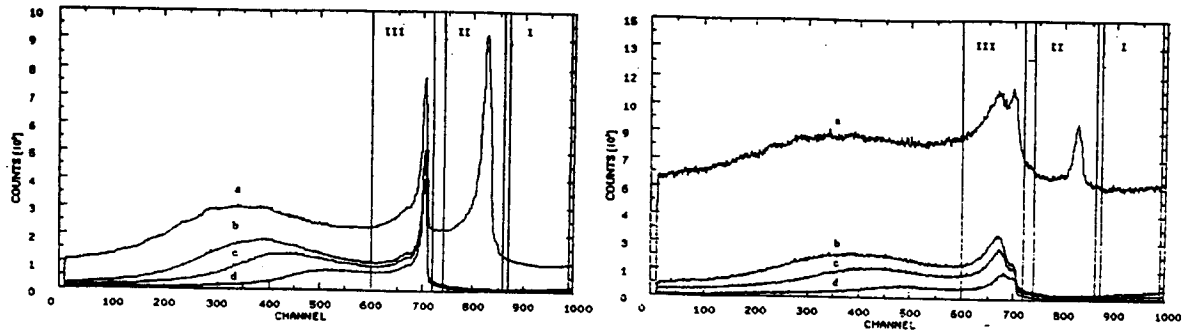

Fig. 3: Time-of-arrival spectra of neutron + γ-ray events (a) from the Fe slab with gap (left hand, in units 10^5) and the same but with the shadow cone added (right hand, in units 10^3). The neutron events are separately presented for detector thresholds corresponding to 0.87 MeV (b), 1.12. MeV (c) and 1.74 MeV (d) neutron energy equivalent.

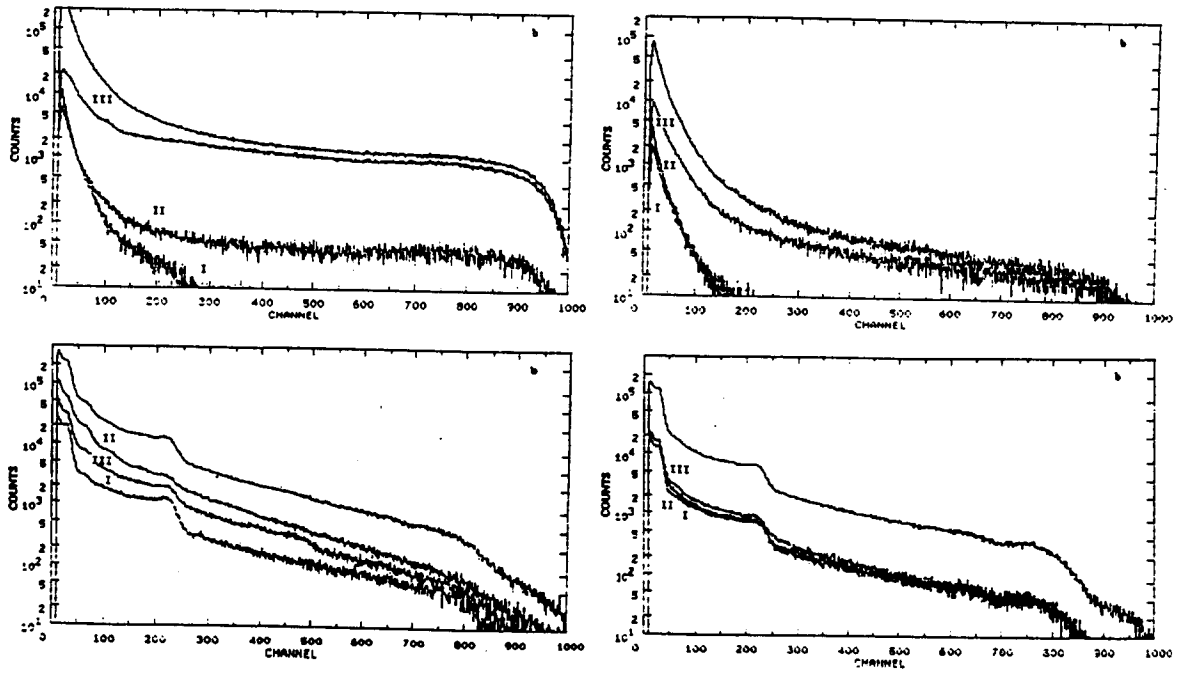

Fig 4: Pulse-height spectra of neutrons (upper part) and γ-rays (lower part) in the time windows indicated in Fig. 3 and for the total time range from the Fe slab with gap (left hand) and the same, but with the shadow cone added (right hand). The detector thresholds are 0.87 MeV neutron energy equivalent and 0.16 MeV electron energy, respectively.

References

[1] W. Daenner, ITER Expert Meeting on Shielding Experiments and Analysis, Garching (FRG) 1980, ITER-IL-5-0-5

[2] T. Parish and A. Santamarina, Sensitivity and Uncertainty Analysis of the NET Magnet Neutronic Design Parameters to Uncertainties in Cross Section Data, CEA 91/333

[3] T. Elfruth, J. Hanke, K. Seidel and S. Unholzer, Shield Penetration Experiments-Specification and optimization of experimental set-up and procedur, Report TU Dresden 1992

6. Low-Energy Neutron Spectra of a Shield Penetration Benchmark

W. Hansen*, D. Richter*, K. Seidel, S. Unholzer, W. Vogel*
*Forschungszentrum Rossendorf, KAI e.V.

In the iron shield penetration benchmark described above for neutron energies E > 0.9 MeV and γ-ray energies $E_\gamma \geq 160$ keV spectra are measured with a liquid scintillation detector. However, a great part of the penetrating neutrons has lower energies. It has been measured between E ≈ 40 keV and 1200 keV with hydrogen-filled spherical proportional counters (pressure/diameter: 1 MPa/4.0 cm, 0.4 MPa/4.0 cm, 0.1 MPa/3.2 cm) [1]. The proton-recoil spectra were unfolded including down-scattering and wall-effect corrections [2]. The results were combined with a neutron flux spectrum measured with an absolutely calibrated stilbene scintillator (∅ 3.0 cm x 2.5 cm)[3] between E = 0.8 MeV and 2.5 MeV and normalized to the total number of 14 MeV source neutrons started in the run.

All detectors had the same position within a collimator as outlined in Fig. 1. A. shadow cone in front of the detector allows the main background components to be treated independently.

For the benchmark experimental/calculated neutron flux the geometry of Fig. 1 completed by the walls of the experimental hall is used in three-dimensional Monte Carlo calculations (code MCNP [4]). The results obtained with the nuclear data of the library EFF-1 are compared in Fig. 2 with the experimental spectrum for the Fe slab without gap. Measurements and calculations with gap in the assembly show in the low-energy neutron region only small differences to the spectra of Fig. 2. The measured spectrum reflects the expected resonance structure but it is significantly higher than the calculated flux for E ≤ 200 keV.

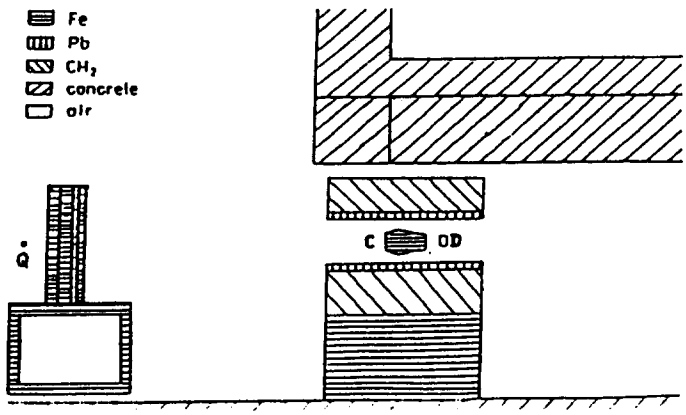

Fig. 1: Vertical section of the benchmark arrangement Q - 14 MeV neutron source, D-detector, C-shadow cone (used for "background" measurements only). The distance QD is 349 cm.

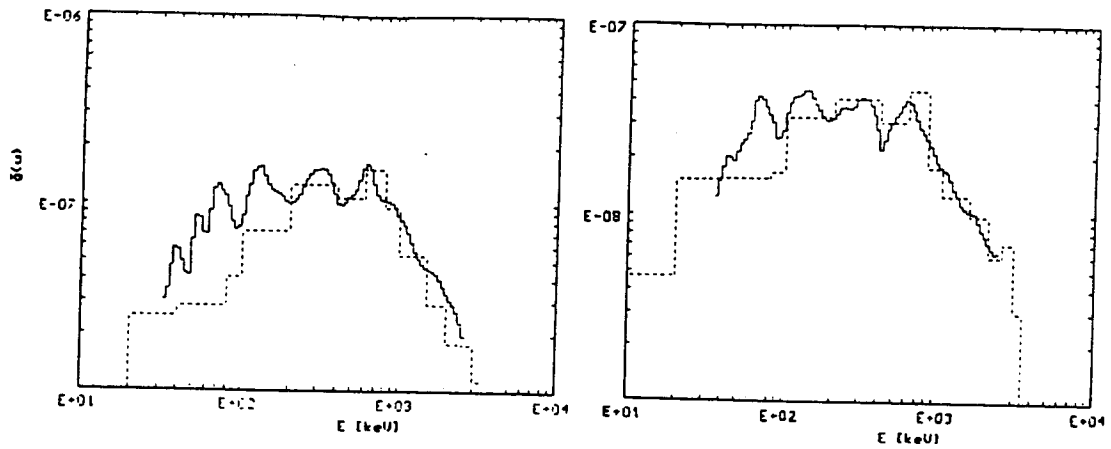

Fig. 2: Neutron flux per source neutron, per cm^2 and per unit of lethargy versus neutron energy for the Fe assembly without gap. Right hand - with additional shadow cone; left hand - without cone. Full line - measurement; dashed line - calculation.

References

[1] D. Albert, W. Hansen, H. Koepernik and W. Vogel., Kernenergie 21(1978)82

[2] D. Albert and W. Hansen, Kernenergie 20(1977)95

[3] D. Albert, U. Brückner, W. Hansen and w. Vogel, Nucl. Instr. Meth. 200(1982)397

[4] J.F. Briesmeister (Editor), MCNP - A General Monte Carlo Code for Neutron and Photon Transport, LA-7396, Los Alamos 1986

ABTEILUNG NUKLEARCHEMIE
UNIVERSITÄT ZU KÖLN
AND
ZENTRALEINRICHTUNG FÜR STRAHLENSCHUTZ
UNIVERSITÄT HANNOVER

1. Production of Residual Nuclei by Proton-Induced Reactions on Carbon, Nitrogen, Oxygen, Magnesium, Aluminum and Silicon

R. Bodemann[1], H.-J. Lange[1], I. Leya[1], R. Michel[1], T. Schiekel[2], R. Rösel[2], U. Herpers[2], H. J. Hofmann[3], B. Dittrich[3], M. Suter[3], W. Wölfli[3], B. Holmqvist[4], H. Condé[5], P. Malmborg[6]

Cross sections for the production of residual nuclides by p-induced reactions are the basic nuclear quantities for an accurate modelling of the interaction of solar cosmic protons with matter. In a series of irradiation experiments at the cyclotron of the Svedberg Laboratory/ University of Uppsala sixteen different target elements were investigated for proton energies up to 100 MeV in order to determine thin-target excitation functions.

Here, we report on the production of radionuclides from the light target elements C, N, O, Mg, Al, and Si (Tables 1-7). Conventional gamma-spectrometry was used to investigate ^{7}Be, ^{22}Na, ^{24}Na, and ^{28}Mg. The long-lived radionuclides ^{10}Be ($T_{1/2}$ = 1.51 Ma [1]) and ^{26}Al ($T_{1/2}$ = 716 ka [2]) were measured by accelerator mass spectrometry (AMS). In the case of ^{10}Be and ^{26}Al from aluminum we also include new cross sections for p-energies between 100 MeV and 200 MeV (table 3). The latter data were derived from targets irradiated earlier at the IPN Orsay.

1 Zentraleinrichtung für Strahlenschutz, Universität Hannover, F.R.G.
2 Abteilung Nuklearchemie, Universität zu Köln, F.R.G.
3 Institut für Mittelenergiephysik, ETH Hönggerberg, Zürich, Switzerland
4 The Studsvik Neutron Research Laboratory, University of Uppsala, Sweden
5 Department of Neutron Research, University of Uppsala, Sweden
6 The Svedberg Laboratory, University of Uppsala, Sweden

This study is part of a larger project to measure cosmochemically relevant thin-target cross sections for p- and ^{4}He-induced reactions for 18 target elements ($6 \leq Z \leq 79$). It extends earlier cross section measurements of our group for protons up to 200 MeV, which up to now covered the target elements Ti, V, Mn, Fe, Co, Ni and Ba [3-9]. A detailed discussion and analysis of the experimental data in the framework of the hybrid model of preequilibrium reactions, investigating several options with respect to the choice of nuclear masses, including also corrections for shell effects of nuclear masses and level densities, will be published elsewhere [10].

Acknowledgement: The authors thank the staff of Svedberg Laboratory/University of Uppsala for their kind cooperation. The AMS measurements were supported financially and personally by the Paul Scherrer Institute/Villigen. This work was supported in part by the Deutsche Forschungsgemeinschaft, Bonn, by the Swedish Natural Science Research Council, Stockholm, and by the Swiss National Science Foundation, Bern.

2. Proton-Induced Spallation at 1600 MeV

M. Lüpke[1], H.-J. Lange[1], M. Schnatz-Büttgen[1], R. Michel[1], R. Rösel[2], U. Herpers[2], P. Cloth[3], D. Filges[3]

During recent years our collaboration made comprehensive investigations of residual nuclide production by p-induced reactions for energies between 600 MeV and 2.6 GeV [13-20]. These investigations were aimed at a better understanding of medium energy reactions and to improve the cross section data base needed for model calculations of the production of cosmogenic nuclides in terrestrial and extraterrestrial matter [21]. During the last years this work was continued by measurements of spallation cross sections for an energy of 1.6 GeV. Thin stacks of pure element foils, technical alloys and suitable chemical compounds were irradiated with 1.6 GeV protons at the Saturne accelerator of the Laboratoire National Saturne, Saclay/France.

The target elements cover C, N, O, Mg, Al, Si, Ca, Ti, Mn, Fe, Co, Ni, Cu, Rb, Sr, Y, Zr, Rh, Ba, and Au. The produced radionuclides were measured by gamma-

1 Zentraleinrichtung für Strahlenschutz, Universität Hannover, F.R.G.
2 Abteilung Nuklearchemie, Universität zu Köln, F.R.G.
3 Arbeitsgruppe Strahlungstransport, IKP/KFA Jülich, F.R.G.

spectrometry. Gamma-energies, branching ratios and half-lives of the radionuclides, which were used for the calculation of cross sections, were taken from [22,23]. The proton fluxes were determined on the basis of the cross sections for the reaction $^{27}Al(p,3p3n)^{22}Na$ as recommended by Tobailem and de Lassus St. Genies [12]. The actual cross section adopted for this reaction was 13.22 mb. A detailed discussion of all experimental results obtained so far for gamma-emitting radionuclides is given elsewhere [24,25]. A comprehensive publication of cross sections for more than 600 target/product combinations for energies from 800 to 2600 MeV, including also cross sections for the production of long-lived radionuclides measured by AMS and of stable rare gas isotopes, is in preparation. Here, we present (Table 8) cross sections for the production of residual nuclides at E_p = 1.6 GeV. These data should have already appeared in the last Progress Report [20], but were left out in the printing process.

Acknowledgement: The authors thank the staff of the Laboratoire National Saturne for their kind cooperation. This work was supported in part by the Deutsche Forschungsgemeinschaft, Bonn.

References

[1] H.J. Hofmann, J. Beer, G. Bonani, H.R. von Gunten, S. Raman, M. Suter, R.L. Walker, W. Wölfli, D. Zimmermann, Nucl. Instr. Meth. Phys. Res. B29 (1987) 32

[2] E.A. Samworth, K. Warburton, G.A. Engelbartinko, Phys. Rev. C5 (1972) 138

[3] R. Michel, G. Brinkmann, H. Weigel, W. Herr, J. Inorg. Nucl. Chem. 40 (1978) 1845

[4] R. Michel, G. Brinkmann, H. Weigel, W. Herr, Nucl. Phys. A322 (1979) 40

[5] R. Michel, H. Weigel, W. Herr, Z. Physik A286 (1978) 393

[6] R. Michel, R. Stueck, J. Geophys. Res. B673 (1984) 89

[7] R. Michel, G. Brinkmann, W. Herr, Progress Report on Nuclear Data Research in the Federal Republic of Germany for the Period April 1, 1978 to March 31, 1979, NEANDC(E)-202U Vol. V, INDC(Ger)-21/L+ Special (1979) 68

[8] R. Michel, F. Peiffer, R. Stueck, Nucl. Phys. A441 (1985) 617

[9] K. Prescher, F. Peiffer, R. Stueck, R. Michel, R. Bodemann, M.N. Rao, K.J.Mathew, Nucl. Inst. Meth. Phys. Res. B53 (1991) 105

[10] R. Bodemann, H.-J. Lange, I. Leya, R. Michel, T. Schiekel, R. Rösel, U. Herpers, H. J. Hofmann, B. Dittrich, M. Suter, W. Wölfli, B. Holmqvist, H. Condé, P. Malmborg, Nucl. Instr. Meth. Phys. Res. B (1993) in press

[11] B. Dittrich, U. Herpers, H.J. Hofmann, W. Wölfli, R. Bodemann, M. Lüpke, R. Michel, P. Dragovitsch, D. Filges, Nucl. Inst. Meth. Phys. Res. B52 (1990) 588

[12] J. Tobailem, C.H. de Lassus St. Genies, Additif No. 2 a la CEA-N-1466(1) (1975), CEA-N-1466(5) (1981)

[13] R. Michel, P. Dragovitsch, K. Prescher, M.N. Rao, J. Methew, in: Progress Report on Nuclear Data Research in the Federal Republic of Germany for the Period April 1, 1987 to March 31, 1988, NEANDC(E)-292 U Vol. V INDC(Ger)-32/LN+Special, 1988, 25

[14] R. Michel, B. Dittrich, U. Herpers, T.Schiffmann, P. Cloth, P. Dragovitsch, D. Filges, The Analyst 114 (1989) 287

[15] B. Dittrich, U. Herpers, M. Lüpke, R. Michel, in: Progress Report on Nuclear Data Research in the Federal Republic of Germany for the Period April 1, 1988 to March 31, 1989, NEANDC(E)-292 U Vol. V INDC(Ger)-34/LN+Special (1989) 31

[16] B. Dittrich, U. Herpers, M. Lüpke, R. Michel, H.J. Hofmann, W. Wölfli, Radiochimica Acta 50 (1990) 11

[17] B. Dittrich, U. Herpers, H.J. Hofmann, W. Wölfli, R. Bodemann, M. Lüpke, R. Michel, P. Dragovitsch, D. Filges, Nucl. Instr. Meth. Phys. Res. B52 (1990) 588

[18] B. Dittrich, U. Herpers, R. Bodemann, M. Lüpke, R. Michel, P. Signer, R. Wieler, H.J. Hofmann, W. Wölfli, in: Progress Report on Nuclear Data Research in the Federal Republic of Germany for the Period April 1, 1989 to March 31, 1990, NEANDC(E)-312-U Vol. V INDC(Ger)-35/LN + Special, 1990, 45

[19] M. Lüpke, R. Michel, B. Dittrich, U. Herpers,P. Dragovitsch, D. Filges, H.J. Hofmann, W. Wölfli, Proc. Int. Conf. "Nuclear Data for Science and Technology", Jülich May 1991, (S.M. Qaim, Editor), Springer Verlag,

Berlin/Heidelberg, 1992, 702

[20] M. Lüpke, H.-J. Lange, M. Schnatz-Büttgen, R. Michel, R. Rösel, U. Herpers, P. Cloth, D. Filges, Progress Report on Nuclear Data Research in the Federal Republic of Germany for the Period April 1, 1991 to March 31, 1992, NEA/NSC/DOC(92)5, INDC(Ger)-036/L, KFK 5079, 1992, 51

[21] R. Michel, in: N.P. Kocherov, Intermediate Energy Nuclear Data for Applications, INDC(NDS)-245, IAEA, Vienna (1991) 17

[22] W. Seelmann-Eggebert, G. Pfennig, H. Muenzel, H. Kleve-Nebenius, Chart of the Nuclides, 5th Edition, Kommunalschriften-Verlag Jehle, Muenchen (1981)

[23] U. Reuss, W. Westmeier, Atomic Data Nucl. Data Tables 29 (1983) 1 and ibid. 193

[24] M. Lüpke (1993) Untersuchungen zur Wechselwirkung galaktischer Protonen mit Meteoroiden - Dicktarget-Simulationsexperimente und Messung von Dünntarget-Wirkungsquerschnitten -, Ph.D. Thesis, University of Hannover

[25] R. Bodemann (1993) Zur Wechselwirkung der solaren kosmischen Strahlung mit extraterrestrischer Materie - Messung von Wirkungsquerschnitten und Modellrechnungen -, Ph.D. Thesis, University of Hannover

Table 1: Experimental cross sections for the production of ^{7}Be and ^{10}Be from carbon, nitrogen and oxygen

target: carbon			target: nitrogen			target: oxygen		
E [MeV]	Be-7 [mb]	Be-10 [mb]	E [MeV]	Be-7 [mb]	Be-10 [mb]	E [MeV]	Be-7 [mb]	Be-10 [mb]
96.3 ± 0.4	15.6 ± 1.6	0.939 ± 0.072	97.9 ± 1.0	10.6 ± 0.8		98.2 ± 0.9	6.93 ± 0.58	
93.5 ± 0.5	16.2 ± 1.7		96.2 ± 1.1	10.8 ± 0.8	0.489 ± 0.051	96.6 ± 1.0	7.06 ± 0.59	
90.6 ± 0.5	16.4 ± 1.7	0.904 ± 0.070	94.4 ± 1.1	10.8 ± 0.9		94.9 ± 1.0		0.505 ± 0.041
87.7 ± 0.5	16.1 ± 1.6		92.6 ± 1.2	11.2 ± 0.9		93.2 ± 1.1	7.20 ± 0.59	
84.7 ± 0.6	16.8 ± 1.7	0.850 ± 0.067	90.8 ± 1.2	11.1 ± 0.9	0.481 ± 0.050	91.5 ± 1.1		0.495 ± 0.040
81.6 ± 0.6	17.2 ± 1.8		88.9 ± 1.2	11.4 ± 0.9		91.3 ± 2.5	7.75 ± 0.56	
78.4 ± 0.6	19.3 ± 2.0	0.846 ± 0.066	87.0 ± 1.3	11.0 ± 0.8		89.8 ± 1.2	7.29 ± 0.59	
75.2 ± 0.7	18.7 ± 1.9		85.1 ± 1.3	11.1 ± 0.9		88.1 ± 1.2	7.30 ± 0.59	
71.8 ± 0.7	19.3 ± 2.0	0.756 ± 0.061	83.1 ± 1.4	11.0 ± 0.9	0.424 ± 0.044	86.3 ± 1.2		0.475 ± 0.038
68.3 ± 0.7	21.1 ± 2.2		81.1 ± 1.4	11.3 ± 0.9		82.8 ± 1.2	7.47 ± 0.61	
64.6 ± 0.8	21.8 ± 2.2	0.719 ± 0.054	79.1 ± 1.4	11.3 ± 0.9		79.2 ± 1.3		0.445 ± 0.036
60.8 ± 0.8	20.5 ± 2.1	0.569 ± 0.045	77.0 ± 1.5	11.2 ± 0.9	0.386 ± 0.040	77.4 ± 1.3	7.75 ± 0.63	
56.7 ± 0.8	23.3 ± 2.4	0.522 ± 0.042	74.9 ± 1.5	11.4 ± 1.0		71.6 ± 1.5	7.81 ± 0.64	
52.5 ± 0.8	22.4 ± 2.5	0.408 ± 0.035	72.7 ± 1.6	11.1 ± 0.9	0.358 ± 0.037	69.6 ± 1.5		0.372 ± 0.030
48.5 ± 0.9	23.7 ± 2.4		70.5 ± 1.6	11.4 ± 0.9		67.4 ± 1.6	8.03 ± 0.66	
48.0 ± 0.9	21.2 ± 2.3	0.241 ± 0.019	68.3 ± 1.7	11.4 ± 0.9	0.300 ± 0.034	63.1 ± 1.7	8.05 ± 0.66	
44.5 ± 0.9	27.1 ± 2.7		65.9 ± 1.7	11.4 ± 0.9	0.290 ± 0.030	61.0 ± 3.7	8.69 ± 0.62	

Table 1 (continued): Experimental cross sections for the production of ^{7}Be and ^{10}Be from carbon, nitrogen and oxygen

target: carbon			target: nitrogen			target: oxygen		
E [MeV]	Be-7 [mb]	Be-10 [mb]	E [MeV]	Be-7 [mb]	Be-10 [mb]	E [MeV]	Be-7 [mb]	Be-10 [mb]
40.3 ± 0.9	27.7 ± 2.8	0.138 ± 0.013	63.5 ± 1.7	11.4 ± 0.9		60.8 ± 1.6		0.241 ± 0.020
35.7 ± 0.9	22.4 ± 2.4	0.0382 ± 0.0030	61.1 ± 1.8	11.0 ± 0.8	0.219 ± 0.024	58.6 ± 1.7	8.26 ± 0.68	
30.5 ± 1.0	12.1 ± 1.2	0.0045 ± 0.0016	58.5 ± 1.9	10.9 ± 0.8		54.0 ± 1.8		0.111 ± 0.009
24.6 ± 1.0	0.567 ± 0.064		55.9 1.9	10.9 ± 0.8		51.5 ± 1.8	7.21 ± 0.59	
			53.2 ± 2.0	10.7 ± 0.8	0.137 ± 0.016	49.0 ± 1.9	6.68 ± 0.54	0.0390 ± 0.0029
			50.4 ± 2.0	10.6 ± 0.8		46.4 ± 2.0	5.38 ± 0.49	
			46.5 ± 2.1	10.1 ± 0.8	0.0689 ± 0.0088	43.5 ± 2.1		0.0113 ± 0.0009
			42.5 ± 2.3	9.89 ± 0.77	0.0370 ± 0.0059	40.4 ± 2.2	2.80 ± 0.22	
			38.0 ± 2.4	10.6 ± 0.8	0.0225 ± 0.0044	33.5 ± 2.4	0.987 ± 0.079	
			33.2 ± 2.6	13.8 ± 1.2	0.0100 ± 0.0035			
			27.6 ± 2.9	24.6 ± 2.1				
			21.0 ± 3.4	39.6 ± 3.1				
			11.5 ± 5.0	10.2 ± 0.8				

Table 2: Experimental cross sections for the proton-induced production of ^{7}Be, ^{22}Na and ^{24}Na from magnesium and aluminum. For ^{10}Be from Mg, in addition, one cross section, 0.099 ± 0.010 mb at E = 98.0 ± 0.3 MeV, was measured.

target: magnesium				target: aluminum			
E [MeV]	Be-7 [mb]	Na-22 [mb]	Na-24 [mb]	E [MeV]	Be-7 [mb]	Na-22 [mb]	Na-24 [mb]
98.0 ± 0.3	1.87 ± 0.20	48.1 ± 4.9	6.34 ± 0.65	98.5 ± 0.3	0.912 ± 0.098	19.8 ± 2.0	
93.5 ± 0.5	2.05 ± 0.23	52.0 ± 5.4	6.88 ± 0.72	93.9 ± 0.5	0.98 ± 0.12	20.8 ± 2.3	12.0 ± 1.2
85.0 ± 0.6	1.76 ± 0.19	52.2 ± 5.3	7.19 ± 0.74	85.6 ± 0.7	0.829 ± 0.090	20.9 ± 2.1	
70.4 ± 0.9	1.61 ± 0.18	60.3 ± 6.1	7.60 ± 0.78	71.0 ± 0.9	0.692 ± 0.078	22.8 ± 2.3	
62.3 ± 1.1	1.48 ± 0.18	65.4 ± 6.8	9.07 ± 0.94	62.9 ± 1.2	0.629 ± 0.081	26.0 ± 3.0	13.3 ± 1.4
53.2 ± 1.4	1.08 ± 0.13	73. ±11.	8.30 ± 0.85	54.0 ± 1.4	0.521 ± 0.066	33.3 ± 3.4	
30.4 ± 2.5		23.8 ± 2.4	6.40 ± 0.65	31.6 ± 2.5	0.061 ± 0.018	7.24 ± 0.74	

Table 3: Experimental cross sections for the p-induced production of ^{10}Be and ^{26}Al from aluminum

E [MeV]	Be-10 [mb]	Al-26 [mb]	E [MeV]	Be-10 [mb]	Al-26 [mb]
199.5 ± 0.4	0.244 ± 0.020	26.9 ± 2.2	74.9 ± 0.7	0.0395 ± 0.0037	
183.6 ± 0.6	0.203 ± 0.017	27.8 ± 2.1	68.6 ± 0.7	0.0361 ± 0.0042	
172.3 ± 0.9	0.200 ± 0.017	28.2 ± 2.2	66.8 ± 0.7		66.3 ± 5.1
160.6 ± 1.1	0.162 ± 0.014	31.5 ± 3.3	64.3 ± 0.7	0.0179 ± 0.0023	
147.6 ± 0.8	0.150 ± 0.013	32.1 ± 2.5	60.4 ± 0.8		69.1 ± 5.3
132.0 ± 1.0	0.127 ± 0.011	37.8 ± 2.9	57.1 ± 0.8	0.0080 ± 0.0014	
115.0 ± 1.1	0.105 ± 0.009	39.6 ± 3.0	52.1 ± 0.8		78.3 ± 6.0
98.8 ± 0.4		45.5 ± 3.5	47.5 ± 0.8		78.1 ± 6.2
96.6 ± 0.4	0.0747 ± 0.0065		39.8 ± 0.9		96.7 ± 7.1
93.8 ± 0.4		48.6 ± 3.8	35.2 ± 0.9		106. ± 8.
90.9 ± 0.5	0.0571 ± 0.0053		31.1 ± 0.9		135. ± 10.
88.0 ± 0.5		50.0 ± 3.8	29.9 ± 0.9		140. ± 10.
85.0 ± 0.5	0.0571 ± 0.0053		23.8 ± 1.0		181. ± 13.
81.9 ± 0.6		53.6 ± 4.2	18.0 ± 1.0		124. ± 9.
78.7 ± 0.5	0.0422 ± 0.0039		16.1 ± 1.0		78.1 ± 5.6

Table 4: Experimental cross sections for the production of radionuclides from natural silicon determined from pure Si-targets

E MeV]	Be-7 [mb]	Be-10 [mb]	Na-22 [mb]	Na-24 [mb]	Mg-28 [mb]	Al-26 [mb]
97.7 ± 0.6	1.02 ± 0.10	0.0231 ± 0.0021	18.7 ± 1.9	3.35 ± 0.34	0.0269 ± 0.0038	33.1 ± 3.6
97.0 ± 0.6		0.0182 ± 0.0019				32.0 ± 3.5
96.8 ± 0.6	1.07 ± 0.11		20.7 ± 2.1			42.3 ± 5.1
94.9 ± 0.7	0.981 ± 0.102		18.4 ± 1.9	3.27 ± 0.33	0.0262 ± 0.0038	
94.0 ± 0.5	1.05 ± 0.11		21.3 ± 2.1			
92.9 ± 0.6	1.14 ± 0.12		22.7 ± 2.3	3.91 ± 0.41	0.0333 ± 0.0043	46.1 ± 5.1
92.1 ± 0.7	0.963 ± 0.100	0.0193 ± 0.0017	18.9 ± 1.9	3.25 ± 0.33	0.0265 ± 0.0038	37.8 ± 4.5
89.2 ± 0.8	0.930 ± 0.096		19.1 ± 2.0	3.20 ± 0.33	0.0260 ± 0.0038	
86.2 ± 0.8	0.908 ± 0.094	0.0178 ± 0.0017	19.7 ± 2.0	3.08 ± 0.31	0.0256 ± 0.0037	37.1 ± 4.5
83.6 ± 0.9	0.969 ± 0.100		22.5 ± 2.3			
83.2 ± 0.9	0.879 ± 0.091		20.2 ± 2.1	3.02 ± 0.31	0.0259 ± 0.0037	
80.1 ± 0.9	0.853 ± 0.089	0.0092 ± 0.0011	21.0 ± 2.1	2.85 ± 0.29	0.0251 ± 0.0036	36.9 ± 4.2
76.8 ± 1.0	0.803 ± 0.084		21.8 ± 2.2	2.63 ± 0.27	0.0248 ± 0.0035	
73.5 ± 1.0	0.751 ± 0.079	0.0079 ± 0.0010	22.5 ± 2.3	2.34 ± 0.24	0.0245 ± 0.0034	34.4 ± 4.1
70.0 ± 1.1	0.718 ± 0.075	0.00394 ± 0.00045	23.1 ± 2.4	2.00 ± 0.20	0.0247 ± 0.0034	43.6 ± 5.2

Table 4 (continued): Experimental cross sections for the production of radionuclides from natural silicon determined from pure Si-targets

E [MeV]	Be-7 [mb]	Be-10 [mb]	Na-22 [mb]	Na-24 [mb]	Mg-28 [mb]	Al-26 [mb]
68.8 ± 1.3	0.785 ± 0.081		25.7 ± 2.6			53.7 ± 5.9
66.5 ± 1.1	0.645 ± 0.068	0.00221 ± 0.00034	22.7 ± 2.3	1.62 ± 0.17	0.0244 ± 0.0033	
65.5 ± 1.1	0.706 ± 0.073		26.3 ± 2.6			41.6 ± 5.0
62.7 ± 1.2	0.565 ± 0.060	0.00139 ± 0.00045	20.9 ± 2.1	1.28 ± 0.13	0.0242 ± 0.0032	41.3 ± 4.5
61.5 ± 1.2	0.683 ± 0.074		26.6 ± 2.8	1.87 ± 0.20	0.0325 ± 0.0040	
58.8 ± 1.2	0.485 ± 0.052		16.6 ± 1.7	0.98 ± 0.10	0.0240 ± 0.0031	
57.8 ± 1.2		0.00070 ± 0.00035				61.2 ± 6.7
54.6 ± 1.3	0.399 ± 0.043		10.2 ± 1.0	0.724 ± 0.074	0.0227 ± 0.0029	57.9 ± 6.4
51.2 ± 1.7	0.424 ± 0.045		11.6 ± 1.2			74.1 ± 8.2
50.2 ± 1.3	0.307 ± 0.034		4.32 ± 0.44	0.567 ± 0.058	0.0186 ± 0.0024	59.1 ± 6.5
45.6 ± 1.4	0.204 ± 0.023		1.42 ± 0.15	0.384 ± 0.039	0.0101 ± 0.0015	
44.3 ± 1.4						66.0 ± 7.3

Table 5: Experimental cross sections for the production of ^{22}Na, ^{24}Na, and ^{28}Mg from natural silicon determined from Si_3N_4 -targets.

E [MeV]	Na-22 [mb]	Na-24 [mb]	Mg-28 [mb]	E [MeV]	Na-22 [mb]	Na-24 [mb]	Mg-28 [mb]
97.9 ± 1.0	20.4 ± 1.7	3.22 ± 0.23	0.0259 ± 0.0032	70.5 ± 1.6	25.3 ± 2.0	2.31 ± 0.16	0.0256 ± 0.0030
96.2 ± 1.1	20.7 ± 1.6	3.33 ± 0.23	0.0263 ± 0.0033	68.3 ± 1.7	25.6 ± 2.2	2.04 ± 0.14	0.0254 ± 0.0029
94.4 ± 1.1	20.8 ± 1.7	3.24 ± 0.23	0.0257 ± 0.0032	65.9 ± 1.7	25.7 ± 2.1	1.85 ± 0.13	0.0251 ± 0.0029
92.6 ± 1.2	21.3 ± 1.7	3.37 ± 0.24	0.0274 ± 0.0034	63.5 ± 1.7	25.2 ± 2.1	1.61 ± 0.11	0.0247 ± 0.0028
90.8 ± 1.2	21.3 ± 1.8	3.29 ± 0.23	0.0265 ± 0.0033	61.1 ± 1.8	23.5 ± 1.9	1.41 ± 0.10	0.0250 ± 0.0027
88.9 ± 1.2	22.2 ± 1.8	3.40 ± 0.24	0.0276 ± 0.0034	58.5 ± 1.9	20.9 ± 1.7	1.21 ± 0.09	0.0250 ± 0.0027
87.0 ± 1.3	21.6 ± 1.7	3.33 ± 0.23	0.0276 ± 0.0034	55.9 ± 1.9	17.7 ± 1.4	1.01 ± 0.07	0.0245 ± 0.0027
85.1 ± 1.3	22.1 ± 1.8	3.18 ± 0.22	0.0263 ± 0.0033	53.5 ± 2.0	13.5 ± 1.1	0.851 ± 0.060	0.0237 ± 0.0025
83.1 ± 1.4	22.1 ± 1.8	3.02 ± 0.21	0.0259 ± 0.0032	50.4 ± 2.0	9.24 ± 0.75	0.719 ± 0.050	0.0219 ± 0.0023
81.1 ± 1.4	22.9 ± 1.9	3.06 ± 0.22	0.0271 ± 0.0033	46.5 ± 2.1	4.63 ± 0.38	0.552 ± 0.038	0.0170 ± 0.0020
79.1 ± 1.4	23.4 ± 2.0	2.96 ± 0.21	0.0265 ± 0.0032	42.5 ± 2.2	2.15 ± 0.18	0.417 ± 0.029	0.0107 ± 0.0014
77.0 ± 1.5	23.5 ± 1.9	2.85 ± 0.20	0.0266 ± 0.0032	38.0 ± 2.3	1.11 ± 0.10	0.187 ± 0.013	0.00389 ± 0.00083
74.9 ± 1.5	24.5 ± 2.2	2.62 ± 0.18	0.0254 ± 0.0031	33.2 ± 2.6	0.652 ± 0.064	0.0388 ± 0.0027	0.00122 ± 0.00032
72.7 ± 1.6	24.4 ± 2.0	2.44 ± 0.17	0.0264 ± 0.0031	27.6 ± 2.9	0.346 ± 0.044	0.0161 ± 0.0011	

Table 6: Experimental cross sections for the production of ^{28}Mg from natural silicon determined from SiO_2 -targets. In addition, there were two cross sections for the production of ^{22}Na from natural silicon determined from SiO_2 -targets, which are not affected by thermodiffusion: 21.7 ± 1.5 mb at 91.3 ± 2.5 MeV and 26.1 ± 1.9 mb at 61.0 ± 3.7 MeV.

E [MeV]	Mg-28 [mb]	Al-26 [mb]	E [MeV]	Mg-28 [mb]	Al-26 [mb]
98.2 ± 0.9	0.0292 ± 0.0048		60.8 ± 1.5		43.5 ± 4.8
96.6 ± 1.0	0.0291 ± 0.0044		58.6 ± 1.7	0.0268 ± 0.0037	
94.9 ± 1.0		41.9 ± 5.0	56.3 ± 1.7		53.5 ± 5.9
93.2 ± 1.1	0.0276 ± 0.0043		51.5 ± 1.8	0.0257 ± 0.0033	
91.5 ± 1.1		32.5 ± 3.6	46.4 ± 2.0	0.0198 ± 0.0027	78.2 ± 9.4
89.8 ± 1.2	0.0294 ± 0.0045		49.0 ± 1.9	0.0244 ± 0.0032	
88.1 ± 1.2	0.0310 ± 0.0046		46.4 ± 2.0	0.0198 ± 0.0027	
82.8 ± 1.2	0.0281 ± 0.0043		40.4 ± 2.2	0.00903 ± 0.00168	69.9 ± 8.4
79.2 ± 1.1		38.5 ± 4.6	37.1 ± 2.1		63.5 ± 7.6
77.4 ± 1.3	0.0299 ± 0.0044		33.5 ± 2.4	0.00237 ± 0.00066	
73.6 ± 1.5		34.9 ± 4.2	29.8 ± 2.5		17.3 ± 2.0
71.6 ± 1.5	0.0296 ± 0.0043		25.7 ± 2.7		5.58 ± 0.67
67.4 ± 1.6	0.0271 ± 0.0039		21.0 ± 3.0		2.84 ± 0.34
63.1 ± 1.7	0.0275 ± 0.0037				

Table 7: Revision of experimental cross sections for the production of ^{10}Be from various target elements as reported earlier by our group [11]. A recalculation of the p-energies became necessary due to a recalibration of the the initial p-energy of the accelerator. This recalibration changes the values of the monitor cross sections of the reaction $^{27}Al(p,3p3n)^{22}Na$ used [12] and thereby also the experimental cross sections.

Target	$E^{a)}$ old [MeV]	E new [MeV]	Be-10 [mb]	Target	$E^{a)}$ old [MeV]	E new [MeV]	Be-10 [mb]
O	96.7 ± 1.0	96.6 ± 1.0	0.52 ± 0.03	Si	96.9 ± 0.7	96.8 ± 0.7	0.029 ± 0.004
	93.4 ± 1.7	91.3 ± 2.5	0.52 ± 0.03		94.6 ± 0.5	92.9 ± 0.6	0.023 ± 0.002
	68.1 ± 1.6	67.4 ± 1.6	0.34 ± 0.02		68.2 ± 1.2	68.8 ± 1.3	0.020** ± 0.003
	52.6 ± 1.8	51.5 ± 1.8	0.073 ± 0.005		50.0 ± 1.4	51.2 ± 1.7	0.009** ± 0.003
Mg	95.0 ± 0.2	95.0 ± 0.3	0.078 ± 0.009	Mn	93.1 ± 0.5	93.1 ± 0.5	0.045 ± 0.004
	66.0 ± 0.7	62.3 ± 0.8	0.017 ± 0.006		63.5 ± 1.0	59.4 ± 1.0	0.019 ± 0.003
Al	95.5 ± 0.2	94.0 ± 0.4	0.041 ± 0.003	Fe	91.7 ± 0.6	90.1 ± 0.6	0.021 ± 0.011
	66.7 ± 0.8	63.0 ± 0.9	0.015 ± 0.004		61.7 ± 1.1	57.9 ± 1.1	0.008 ± 0.003
				Ni	88.4 ± 0.6	86.9 ± 0.7	0.007 ± 0.002
					57.2 ± 1.1	53.3 ± 1.2	0.003 ± 0.001

a) energies according to ref. 11, tables 1 and 2.

* There are two cross sections for the reaction $^{27}Al(p,pn)^{26}Al$ in ref. [11], which also have to be revised: 77.0 ± 4.3 mb at 63.2 MeV and 56.2 ± 3.1 mb at 94.0 MeV, respectively.

** probably affected by contamination.

Table 8: Cross sections for the production of radionuclides by 1.6 GeV protons from target elements C, N, O, Mg, Al, Si, Ca, Ti, Mn, Fe.

REACTION	CROSS SECTION [mb]	REACTION	CROSS SECTION [mb]
C(p,3pXn)^{7}Be	11.6 ± 0.8	Ti(p,2pXn)^{48}Sc	2.34 ± 0.25
		Ti(p,Xn)^{48}V	0.522 ± 0.072
N(p,4pXn)^{7}Be	13.3 ± 1.3		
		Mn(p,22p27n)^{7}Be	5.85 ± 0.56
O(p,5pXn)^{7}Be	11.2 ± 1.0	Mn(p,15p19n)^{22}Na	1.92 ± 0.18
		Mn(p,15p17n)^{24}Na	3.81 ± 0.32
Mg(p,9pXn)^{7}Be	10.6 ± 0.8	Mn(p,14p14n)^{28}Mg	0.474 ± 0.044
Mg(p,2pXn)^{22}Na	28.9 ± 2.1	Mn(p,7p7n)^{42}K	7.37 ± 0.64
Mg(p,2pXn)^{24}Na	7.94 ± 0.67	Mn(p,7p6n)^{43}K	2.79 ± 0.23
		Mn(p,5p7n)^{44m}Sc	7.80 ± 0.64
Al(p,10p11n)^{7}Be	8.65 ± 0.63	Mn(p,5p5n)^{46}Sc	12.4 ± 1.0
Al(p,3p3n)^{22}Na	13.1 ± 1.0	Mn(p,3p5n)^{48}V	13.1 ± 1.1
Al(p,3pn)^{24}Na	12.3 ± 1.0	Mn(p,2p6n)^{48}Cr	0.338 ± 0.047
		Mn(p,2p3n)^{51}Cr	32.1 ± 2.8
Si(p,11pXn)^{7}Be	10.7 ± 0.8	Mn(p,p3n)^{52}Mn	3.67 ± 0.38
Si(p,4pXn)^{22}Na	16.4 ± 1.2	Mn(p,pn)^{54}Mn	34.0 ± 3.7
Si(p,4pXn)^{24}Na	5.83 ± 0.45		
Si(p,3pXn)^{28}Mg	0.098 ± 0.014	Fe(p,23pXn)^{7}Be	7.22 ± 0.56
		Fe(p,16pXn)^{22}Na	2.24 ± 0.18
Ca(p,10pXn)^{22}Na	8.21 ± 0.62	Fe(p,16pXn)^{24}Na	3.44 ± 0.26
Ca(p,10pXn)^{24}Na	4.71 ± 0.36	Fe(p,15pXn)^{28}Mg	0.326 ± 0.028
Ca(p,9pXn)^{28}Mg	0.170 ± 0.018	Fe(p,8pXn)^{42}K	5.27 ± 0.44
Ca(p,2pXn)^{42}K	0.769 ± 0.105	Fe(p,8pXn)^{43}K	1.59 ± 0.12
Ca(p,2pXn)^{43}K	0.716 ± 0.062	Fe(p,7pXn)^{47}Ca	0.055 ± 0.012
Ca(p,Xn)^{44m}Sc	0.005 ± 0.001	Fe(p,6pXn)^{44m}Sc	8.47 ± 0.65
		Fe(p,6pXn)^{46}Sc	8.81 ± 0.68
Ti(p,19pXn)^{7}Be	6.48 ± 0.50	Fe(p,6pXn)^{47}Sc	3.08 ± 0.24
Ti(p,12pXn)^{22}Na	3.12 ± 0.24	Fe(p,6pXn)^{48}Sc	0.632 ± 0.052
Ti(p,12pXn)^{24}Na	5.68 ± 0.43	Fe(p,4pXn)^{48}V	17.8 ± 1.4
Ti(p,11pXn)^{28}Mg	0.701 ± 0.056	Fe(p,3pXn)^{48}Cr	0.837 ± 0.068
Ti(p,4pXn)^{42}K	11.3 ± 0.9	Fe(p,3pXn)^{51}Cr	37.7 ± 3.1
Ti(p,4pXn)^{43}K	4.63 ± 0.36	Fe(p,2pXn)^{52}Mn	8.77 ± 0.74
Ti(p,3pXn)^{47}Ca	0.335 ± 0.028	Fe(p,2pXn)^{54}Mn	35.9 ± 3.1
Ti(p,2pXn)^{44m}Sc	6.42 ± 0.51	Fe(p,Xn)^{55}Co	0.188 ± 0.031
Ti(p,2pXn)^{46}Sc	29.0 ± 2.4	Fe(p,Xn)^{56}Co	0.416 ± 0.059
Ti(p,2pXn)^{47}Sc	25.2 ± 2.2	Fe(p,Xn)^{57}Co	0.565 ± 0.047

INSTITUT FÜR KERNCHEMIE
UNIVERSITÄT MAINZ

1. Isomeric Yield Ratios and Distribution of Angular Momentum in the Fission of ^{249}Cf by Thermal Neutrons

O. Alhassanieh, H.O. Denschlag, V. Scheuermann, H.R. Faust*

The yields of isomeric states of fission products are of importance for fundamental questions like the understanding of the transfer of angular momentum on fission fragments and for practical questions like decay heat calculations in nuclear reactors. Unfortunately the yield ratios of isomeric pairs are frequently not known and it exists no reliable way to predict these values for different fission reactions. More experimental data are needed for the improvement of existing systematics.

Using the mass separator Lohengrin [1] of the Institut Laue-Langevin in Grenoble we have measured a number of isomeric ratios in the fission of ^{249}Cf by thermal neutrons [2,3]. Lohengrin is a separator for unslowed fission fragments separating the fragments at (nearly) their full kinetic energy of 60 to 110 MeV. At this energy a dynamical equilibrium for the ionic charge distribution of the fragments (ranging from q = 16+ to 30+) is established when the ions pass through the target. The fractions of high spin isomer relative to the sum of both isomers (F_H) obtained for various kinetic energies (E in MeV) and for an ionic charge (q) near the mean ionic charge state are given in Table 1.

In principle, for the technical uses mentioned above and for a comparison with radiochemical measurements the present values of F_H should be integrated over the distributions of ionic charges and kinetic energies. Beam time economy did not allow us to perform the number of measurements required for this purpose.

---

* Institut Laue-Langevin, Grenoble, France

However, the present values near the mean kinetic energies (underlined) represent good approximations of radiochemical values as the dependence on kinetic energy is generally not very pronounced and as they have been measured for the most probable ionic charge state.

Table 1 also gives the "root mean square angular momentum" (J_{rms}) of the fragments calculated using a simple statistical model [4]. It should be pointed out that this model cannot be expected to be valid for very high or very low values of F_H; in consequence values of J_{rms} based on F_H >0.80 or <0.20 are shown in parentheses.

References

[1] Moll, H. Schrader, G. Siegert, H. Hammers, M. Asghar, J. P. Bocquet, P. Armbruster, H. Ewald, H. Wollnik, Kerntechnik 19, 374-381 (1977)

[2] V. Scheuermann, Diplomarbeit, Mainz (1991)

[3] O. Alhassanieh, Dissertation, Mainz in preparation

[4] D. G. Madland and T. R. England, Nucl. Science and Engineering 64, 859 (1977)

Table 1: Fraction of high spin isomer (F_H) formed directly in the thermal neutron induced fission of ^{249}Cf at various kinetic energies of the fragments (E in MeV, not corrected for a small energy loss in target and target cover foil) and at the most probable ionic charge state (q) and "Root mean square angular momentum" (J_{rms} in $\hbar$) calculated according to a simple statistical model [4]. Kinetic energies near the mean value are underlined. J_{rms}-values outside the validity of the model are in parentheses.

E/q	Isomers [Spin]	F_H	J_{rms}
90/22	^{97}Y [1/2],[9/2]	0.801 ± 0.073	(7.25 ± 0.98)
<u>100</u>/22		0.490 ± 0.066	3.90 ± 0.46
110/22		0.517 ± 0.018	4.08 ± 0.12
96/22	^{98}Y [1],[4]	0.041 ± 0.041	(1.60 ± 0.11)
<u>100</u>/22		0.041 ± 0.072	(1.60 ± 1.03)
104/22		0.048 ± 0.117	(1.65 ± 1.16)
108/22		0.054 ± 0.013	(1.70 ± 0.09)
90/22	^{100}Nb [1],[4]	0.795 ± 0.038	7.88 ± 0.87
<u>100</u>/22		0.673 ± 0.039	5.95 ± 0.46
110/22		0.821 ± 0.072	(8.52 ± 2.16)
72/23	^{130}Sn [0],[7]	0.620 ± 0.153	6.84 ± 1.90
<u>82</u>/23		0.700 ± 0.035	7.53 ± 0.54
96/23		0.750 ± 0.170	8.41 ± 4.84
72/23	^{130}Sb [4],[8]	0.630 ± 0.107	12.49 ± 2.4
<u>82</u>/23		0.873 ± 0.026	(23.11 ± 2.6)
96/23		0.711 ± 0.103	14.55 ± 3.36
<u>82</u>/23	^{132}Sb [4],[8]	0.462 ± 0.204	7.91 ± 2.53
<u>87</u>/23		0.447 ± 0.146	7.74 ± 1.68
92/23		0.442 ± 0.125	7.70 ± 1.41
77/23	^{133}Te [1/2],[9/2]	0.722 ± 0.039	13.05 ± 1.10
<u>82</u>/23		0.835 ± 0.055	(17.58 ± 3.46)
87/23		0.880 ± 0.032	(20.90 ± 3.12)
72/23	^{134}I [4],[8]	0.427 ± 0.129	7.53 ± 1.41
74/23		0.463 ± 0.228	7.92 ± 2.90
77/23		0.542 ± 0.130	8.91 ± 1.68
<u>82</u>/23		0.586 ± 0.017	9.55 ± 0.27
87/23		0.553 ± 0.038	9.06 ± 0.54
92/23		0.546 ± 0.102	8.96 ± 1.46
72/23	^{136}I [2],[6]	0.778 ± 0.047	10.01 ± 1.26
<u>80</u>/23		0.878 ± 0.114	(13.95 ± 4.29)
<u>85</u>/23		0.892 ± 0.030	(14.89 ± 2.35)
90/23		0.935 ± 0.060	(19.43 ± 5.66)

INSTITUT FÜR KERNCHEMIE
PHILIPPS-UNIVERSITÄT MARBURG

Measurement of the Intensities of Gamma-Rays Accompanying the Decay of ^{227}Ac in Transient Equilibrium with Its Daughters: A Suggested Long-Lived Multiple-Line Gamma-Ray Calibration Standard §

J. van Aarle, W. Westmeier, R.A. Esterlund and P. Patzelt

Effective gamma-ray spectroscopy/spectrometry demands germanium detectors accurately calibrated in both gamma-ray energy and detection efficiency. Until relatively recently however, available calibration sources usually consisted of single nuclides with only one or two gamma-ray lines of high intensity. Consequently, it has been common to utilize a set of as many as fifteen or so gamma-ray standards in order to properly calibrate a germanium detector. The disadvantages of such a procedure are twofold: 1) it is very time-consuming; and 2) most of the available gamma-ray standards have half-lives of less than one year, necessitating their frequent and often expensive replacement. In recent years however, the use of long-lived multiple-line calibration standards emitting gamma rays over a wide energy range has become an alternative.

The raison d'être of the present work is the investigation of the suitability of ^{227}Ac to serve as yet another long-lived multiple-line gamma-ray efficiency calibration source for germanium detectors. This is achieved via a new high-precision measurement of both gamma-ray and X-ray emission intensities of ^{227}Ac and its daughters in transient equilibrium. The parent nuclide has a suitably long half-life of 21.77 y, and gamma-ray lines (accompanying its and its daughter's decay) in the energy range 20 keV $\leq E_\gamma \leq$ 1110 keV have I_γ values sufficiently large ($I_\gamma > 0.1\%$) so as to be useful for efficiency calibrations. Inasmuch as the longest-lived daughter $t_{1/2}$ is 18.72 d (^{227}Th), a sealed ^{227}Ac sample will achieve transient equilibrium within a few months. With regard to a possible practical advantage to choosing ^{227}Ac as a calibration source over other candidates, it should be noted that, since ^{227}Ac is an α-emitter, it is not even necessary to obtain an absolutely calibrated ^{227}Ac source: instead, it is relatively straightforward for the user himself to assay such a source *directly* for its absolute decay rate via α-spectrometric measurements. Finally, it may be pointed out that, although it is possible to ascertain the relevant I_γ values for the ^{227}Ac gamma-ray and X-ray lines of interest using the existing literature, most of the data are at least a score or more years old, and present-day measuring techniques might be expected to yield I_γ values with greater precision than those that are presently extant. We thus felt that a new series of measurements was justified.

The 26 most intense and therefore most useful gamma-ray lines measured in the present work are summarized in the accompanying table. The energy range of 50 keV $\leq E_\gamma \leq$ 1109 keV is more than adequate for most applications. We believe that this table clearly demonstrates that ^{227}Ac can indeed be a useful long-lived gamma-ray E_γ and I_γ calibration standard for both Li-drifted and high-purity germanium detectors.

Table: Recommended E_γ and I_γ Values For Calibrating a Germanium Detector with an ^{227}Ac Source.

Energy (keV)			Intensity (%)		
50.05	±	0.08	9.37	±	0.37
81.10	±	0.07	13.97	±	0.63
83.82	±	0.07	23.03	±	0.99
94.67	±	0.07	8.95	±	0.49
122.37	±	0.07	1.28	±	0.04
144.32	±	0.07	3.43	±	0.09
154.30	±	0.07	6.02	±	0.18
236.08	±	0.07	12.29	±	0.29
256.35	±	0.07	6.44	±	0.16
269.55	±	0.07	13.12	±	0.32
271.33	±	0.07	10.59	±	0.26
286.18	±	0.08	1.68	±	0.04
300.08	±	0.08	2.06	±	0.05
323.99	±	0.08	3.56	±	0.09
329.89	±	0.08	2.58	±	0.06
338.39	±	0.08	2.54	±	0.06
351.14	±	0.08	13.02	±	0.30
401.90	±	0.08	6.33	±	0.15
404.90	±	0.08	3.87	±	0.09
427.16	±	0.09	1.83	±	0.04
445.06	±	0.09	1.17	±	0.03
704.57	±	0.12	0.497	±	0.016
766.41	±	0.13	0.678	±	0.018
831.90	±	0.14	3.35	±	0.09
897.70	±	0.15	0.272	±	0.009
1109.37	±	0.21	0.114	±	0.006

§ Submitted to Int. J. Appl. Radiat. Isot. **44** (1993).

PHYSIKALISCH TECHNISCHE BUNDESANSTALT BRAUNSCHWEIG

1. Neutron Data

1.1 Differential Neutron Cross Sections from Natural Iron at Incident Energies between 9.4 MeV and 15.2 MeV

D. Schmidt, W. Mannhart, R. Nolte

Neutron scattering measurements on natural iron have been completed in the incident energy region between 9.4 MeV and 15.2 MeV in steps of about 0.5 MeV. First, differential cross sections were deduced for the elastic and the inelastic scattering to the first excited state in ^{56}Fe (Q = -0.847 MeV).

Because the two scattering fractions are separated in the TOF spectra by a 2.4 - 3.0 FWHM, their influence on each other had to be corrected. This correction was carried out in two different ways leading to consistent results. A publication of the detailed correction procedure, and the final results of the cross section determination is under preparation.

Fig. 1a shows the angle-integrated elastic cross sections. The agreement with data from other authors is reasonably well within the uncertainties given. At energies below 11 MeV, the ENDF/B-VI evaluation gives values that are too high (5%), but a more recent evaluation [1] yields values that are too low above 11 MeV.

A comparison of the differential cross sections at incident energies near 14.1 MeV (Fig. 1b) shows that the agreement with three older experiments [3, 4, 7] is very good. However, more recent measurements show systematic deviations ([6]: 20% lower, [8]: 15% higher) or other unsystematic discrepancies ([9]), and ENDF/B-VI shows considerable differences up to a factor two.

A new evaluation of the differential angular distributions, which should also include data measured below 10 MeV at ANL [10], is necessary. A joint analysis with suitable physical models of our data and those from ANL is under study.

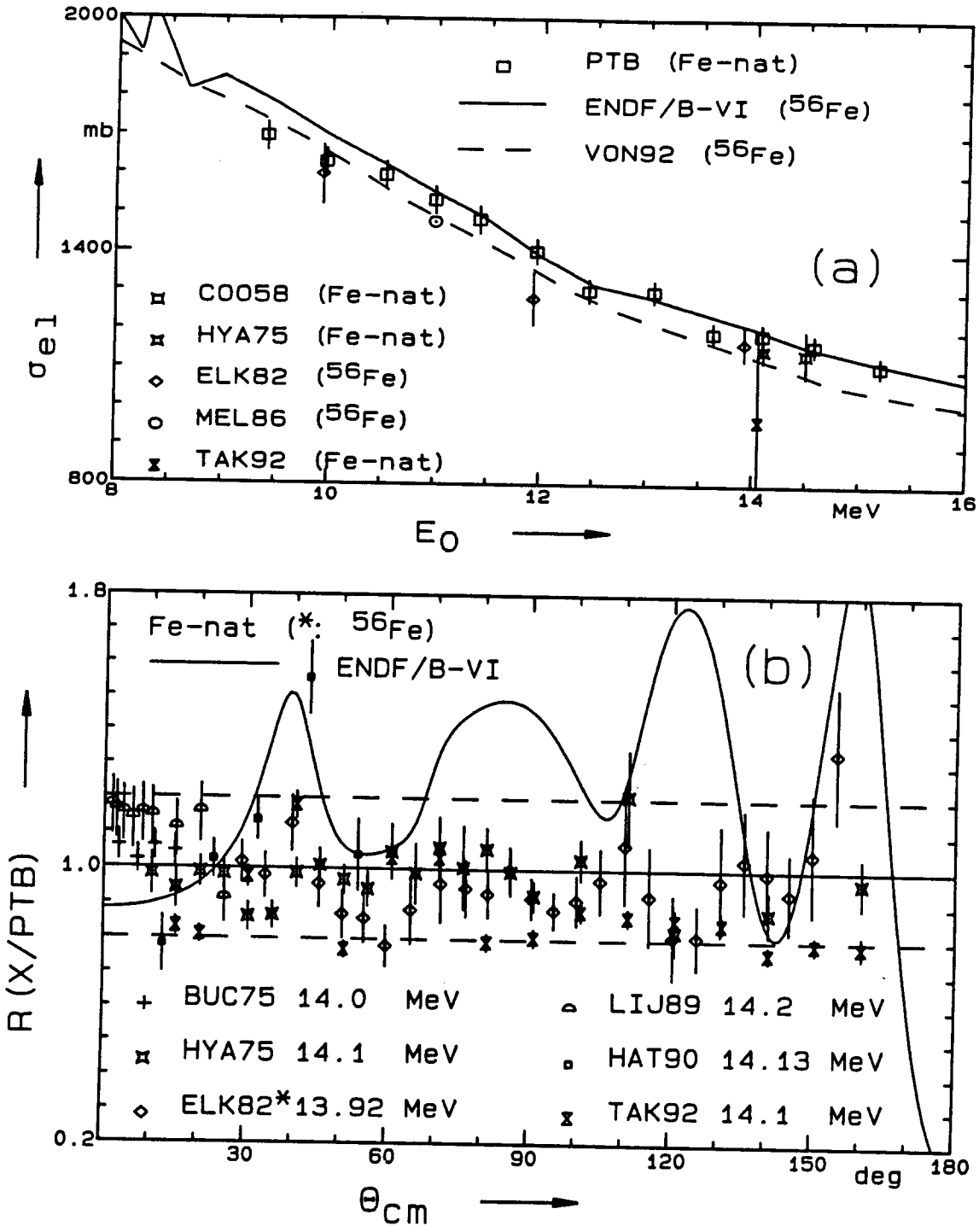

Fig. 1 (a): Angle-integrated elastic neutron cross sections from iron (PTB: this work; evaluations (ENDF/B-VI, VON92 [1]) and data from other authors (COO58 [2], HYA75 [3], ELK82 [4], MEL86 [5] and TAK92 [6]) are included for comparison. (b): Ratio of data to the fitted Legendre polynomial curve of this work (E_0 = 14.09 MeV), taken from other authors (BUC75 [7], LIJ89 [8], HAT90 [9], see also above).

1.2 Inelastic Neutron Emission Cross Sections from Natural Iron

D. Schmidt, W. Mannhart, Nolte

After the determination of the differential elastic (Fe-nat) and the first inelastic (^{56}Fe, Q = -0.847 MeV) scattering cross sections in the incident energy region between 9.4 MeV and 15.2 MeV, in the second step only the inelastic scattering was analyzed up to excitation energies of about 5.5 MeV. At higher excitation energies the TOF spectra of inelastic neutron scattering are contaminated by elastically (and inelastically) scattered breakup neutrons from the DD source used.

For each angle, the TOF spectra were transformed to the energy scale and the elastic scattering fraction was separated for normalization, using the precisely determined elastic cross section including all corrections. The complete inelastic part of the spectra was cut into 0.5 MeV intervals and analyzed like a neutron line (pseudo-level) using an angle-independent correction for multiple scattering.

Figs. 2a,b show angular distributions at one of the incident energies (14.09 MeV). The lowest excitation energy bin almost corresponds to the first level in ^{56}Fe. The scatter of the data seems to be due to the arbitrary energy interval width of 0.5 MeV (mixing of scattering fractions from different levels) and to small cross sections (less than 1 mb/sr). The angle-integrated cross sections were taken from Legendre polynomial fits with ℓ_{max} = 2 (only at the lowest excitation energy: ℓ_{max} = 6).

Fig. 2c shows a comparison of the angle-integrated pseudo-level cross sections with emission energy spectra from other authors. The agreement with the results from ref. [6] is quite good below emission energies of 11 MeV. There are considerable differences above this energy due to the experimental resolution, which was not taken into account in the data analysis [6].

Further analysis of the continuous neutron emission spectra is under study together with a correction of the breakup scattering of the DD neutron source which was successfully applied in the case of neutron scattering on carbon (see section 1.3).

1.3 Partial Cross Section Determination of the ^{12}C(n,n') [Q = -9.641 MeV] Reaction

D. Schmidt, B.R.L. Siebert

Because monoenergetic neutron sources in the energy range between 8 MeV and 13 MeV are not available in practice for scattering experiments, reactions with a breakup component such as the D(d,n)^{3}He reaction are used. In TOF scattering measurements, below a certain

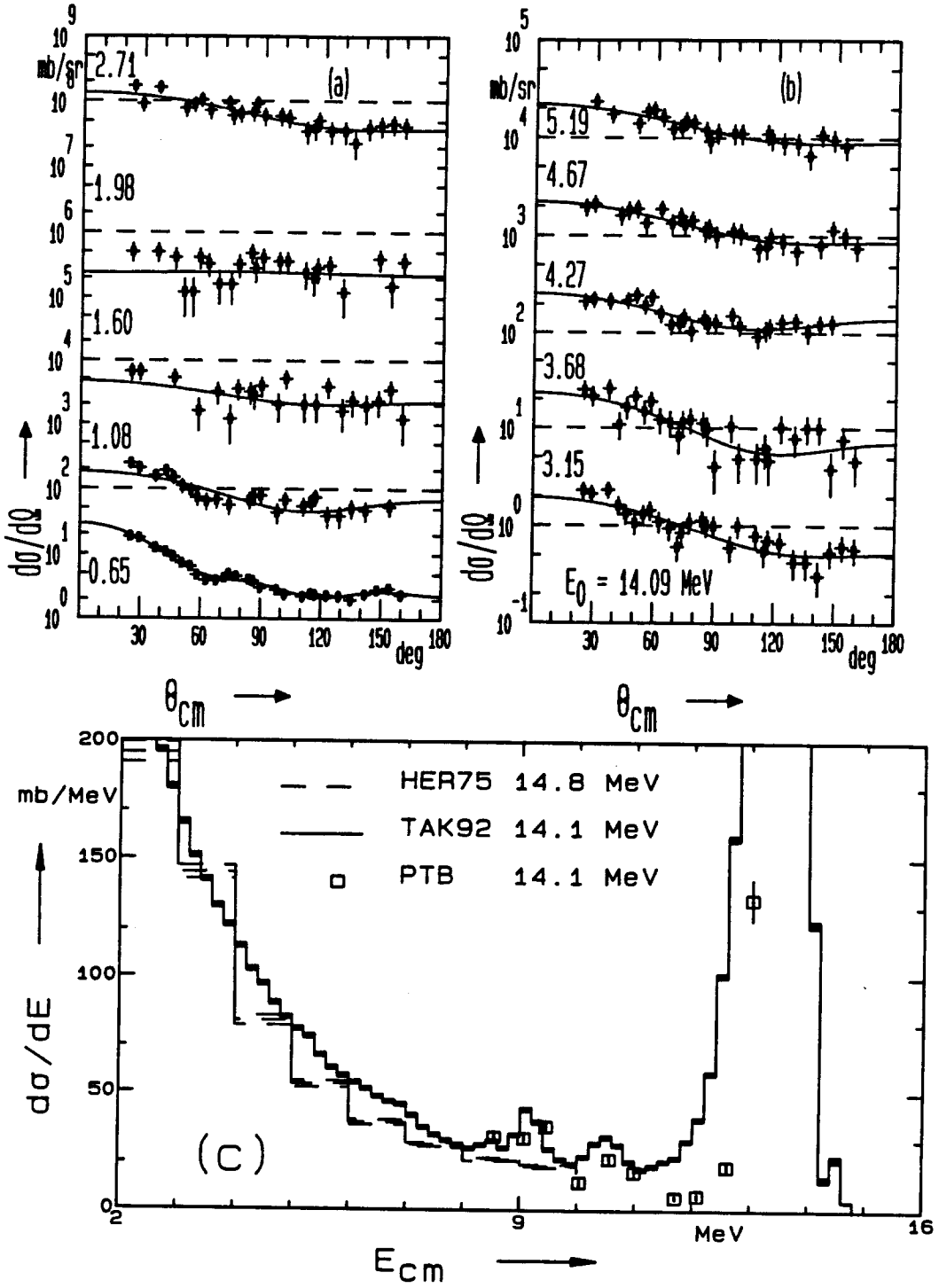

Fig. 2 (a),(b): Pseudo-level differential cross sections from iron at E_0 = 14.09 MeV; the numbers on the left-hand side are average excitation energies in MeV; the dashed lines are the 1 mb/sr levels for the corresponding angular distributions; curves: Legendre polynomial fits.

(c): Angle-integrated emission spectra (HER75 [11], TAK92 [6]) from iron, compared with the angle-integrated pseudo-level cross sections of this work (PTB).

emission energy the inelastic scattered monoenergetic neutrons and the scattered breakup ones are superposed.

The correction of TOF spectra for the scattered breakup component by a complete Monte Carlo simulation was studied. The preparation and test of the input data needed for such simulation is described elsewhere [12].

Fig. 3a shows a comparison of a measured TOF spectrum with a simulated one from scattered breakup neutrons for a carbon sample. The agreement is good, despite the remarkable resonance structure of the carbon cross sections used. The difference in the region near the n_3 line is well visible, but the n_2 line disappears at all angles because of its small cross sections (less than 2 mb/sr). Consequently, the separation of the n_3 line and derivation of differential cross sections were possible. The results are given in Figs. 3b to d, together with data from other authors, this data having been measured using a DT neutron generator (b, c) and a tritium gas target (d). The agreement is in most cases satisfactory.

The results show that the correction for scattered breakup neutrons by means of a complete Monte Carlo simulation works quite well, but its quality depends on the certainty of the evaluated differential cross sections used in the calculation. The method and results of such a correction procedure will be published in detail later.

1.4 Cross Sections for the $^{103}Rh(n,n')^{103}Rh^m$ Reaction

H. Vonach*, M. Miah*, D. Schmidt, W. Mannhart

Measurements of the cross section for the $^{103}Rh(n,n')^{103}Rh^m$ reaction were carried out at 14 neutron energies between 5.69 and 12.00 MeV . The neutrons were produced via the $D(d,n)^3He$ reaction with the PTB compact cyclotron. Metallic rhodium foils 10 mm in diameter and 0.125 mm thick were attached to a low-mass fission chamber with a ^{238}U fission deposit acting as a neutron fluence monitor and were irradiated at a distance of 6 cm from the gas target. Radioactivity counting was done with a Si(Li) detector calibrated with standard sources of ^{109}Cd and $^{93}Nb^m$. Thorough correction procedures are being studied for the absorption of the 20 keV X-ray radiation in the sample and for the large contribution to the radioactivity from breakup neutrons of the D(d,n) reaction.

The aim of the present work was to improve knowledge of this cross section, which shows large uncertainties [16] in this energy region. The data analysis and reduction are in progress.

*Institut für Radiumforschung und Kernphysik, Vienna, Austria

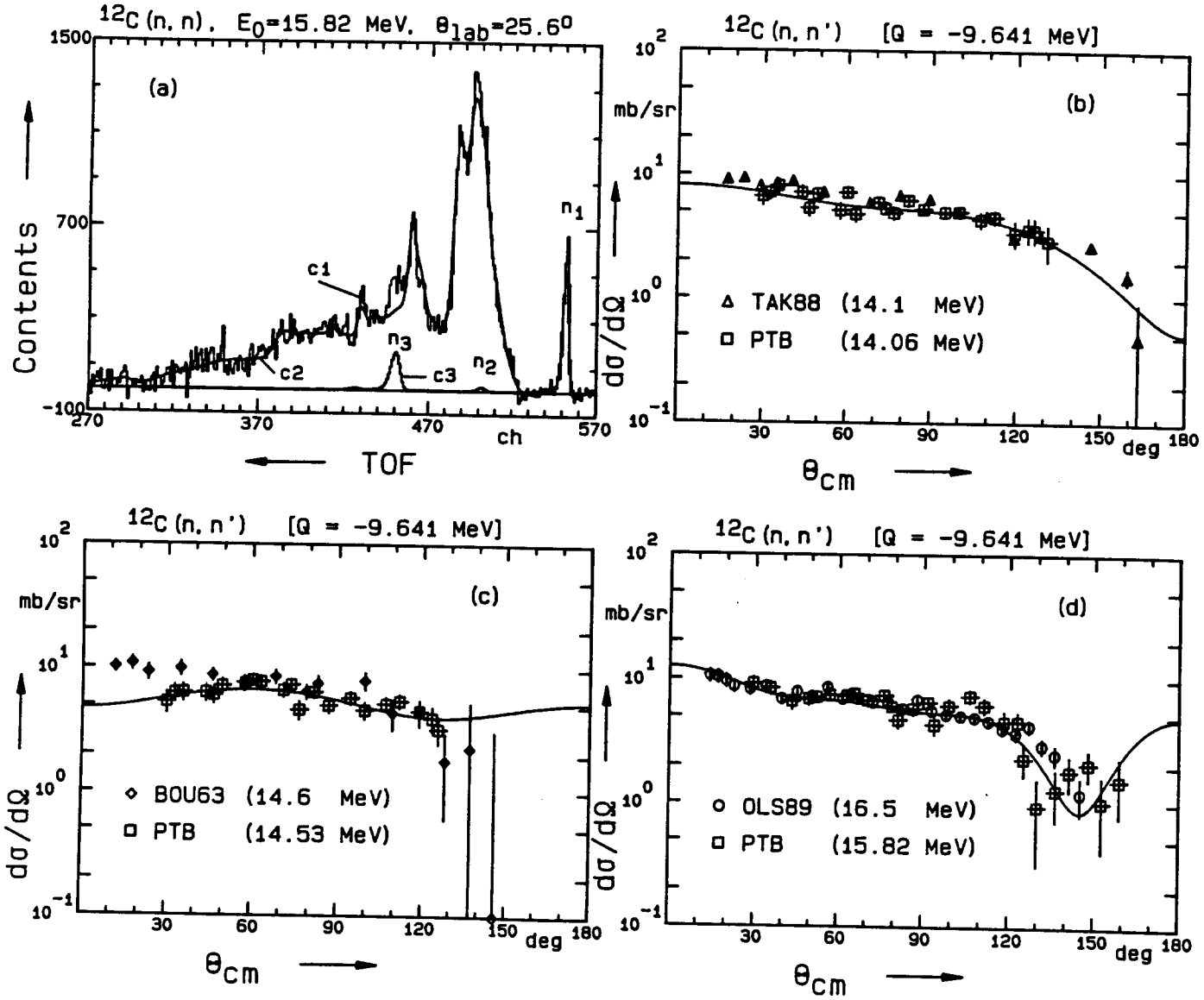

Fig. 3 (a): Experimental TOF spectrum (c1) and calculated ones (c2: only scattered breakup, c3: only inelastic neutron lines n_1 [Q = -4.439 MeV], n_2 [Q = -7.654 MeV], n_3 [Q = -9.641 MeV]).
(b),(c),(d): Angular distributions of the n_3 neutron line at different incident energies (PTB: this work); data from other authors: TAK88 [13], BOU63 [14] and OLS89 [15]; curves: Legendre polynomial fits to the data of this work.

1.5 Update of the Evaluation of the Fission Neutron Spectrum of ^{252}Cf

W. Mannhart

The previous evaluation [17] of the prompt fission neutron spectrum of californium-252 has been updated. Three additional experimental data sets [18,19] mainly investing the high-energy portion of the spectrum have been added to the evaluation. Revised data of two earlier experiments [20,21] have also been included in the evaluation. The evaluation procedure was similar to the previous one and was performed at 70 discrete neutron energies (point data) between 25 keV and 20 MeV. The result is shown in Fig. 4a. The data were smoothed with a spline fit and resulted in a continuous description of the spectrum.

In Fig. 4b, the difference between the old and the new (continuous) evaluation is plotted. The uncertainties stated are for the previous evaluation and show agreement between the old and the new evaluation within these uncertainties. The main modification is above 12 MeV, with reduced uncertainties and numerical values which exceed the previous result by up to 9% at 20 MeV. At the low neutron energies the present result is about 1% lower than before.

During the evaluation process an error was identified in one of the covariance matrices previously used for the individual experiments. The removal of this error reduces the structure of the evaluated point data between 1.0 and 2.5 MeV, as seen in the previous evaluation [17]. The result of the present work will be published elsewhere [22].

2. Radionuclide Data

2.1 Gamma and X-ray Emission Probabilities

U. Schötzig, E. Schönfeld, E. Günther, H. Janßen, R. Klein

Gamma- and X-ray emission probabilities per decay of $^{123}Te^{m}$ [23], ^{141}Ce [24] and ^{186}Re [25] have been derived from emission rates measured with Ge and Si(Li) detectors, and the activity determined by $4\pi\beta$-γ coincidence techniques or liquid scintillation counting. Results are summarized in Table 1; uncertainties (in parentheses in terms of the last digit) correspond to one standard deviation. For the 158.99 keV transition in $^{123}Te^{m}$ and the 145.44 keV transition in ^{141}Ce additionally the total conversion coefficients were determined: $\alpha_T(158.99) = 0.1895(13)$ and $\alpha_T(145.44) = 0.452(8)$.

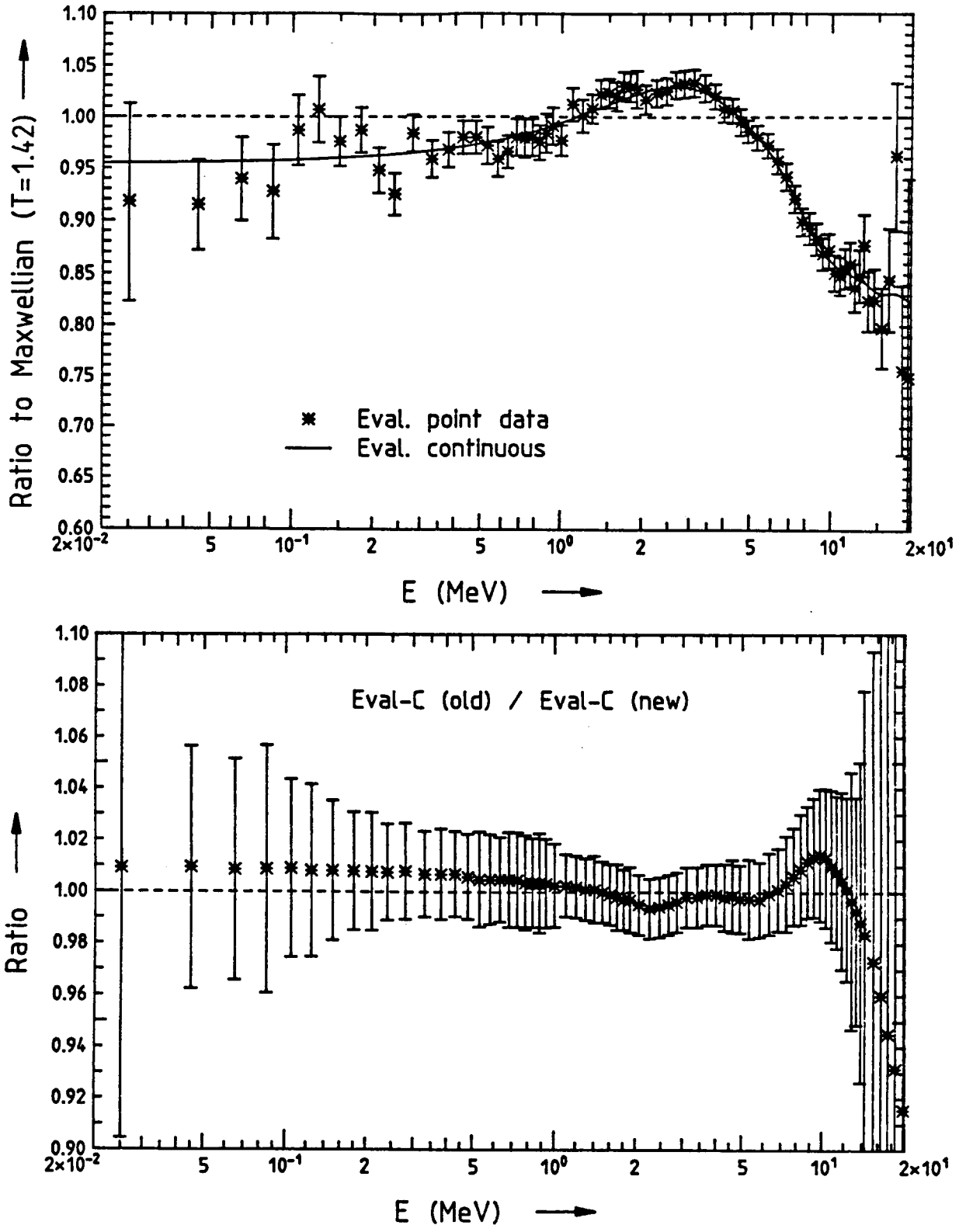

Fig. 4 (a): Updated evaluation of the ^{252}Cf neutron spectrum. The point-wise evaluation performed at 70 discrete energies is smoothed with a weighted spline fit.
(b): Ratio of the previous evaluation to the present one. The error bars are for the result of the previous evaluation.

Table 1: Emission probabilities p

Nuclide	Energy [keV]	Radiation	p
$^{123}Te^{m}$	158.99	γ	0.8407(9)
^{141}Ce	145.44	γ	0.480(5)
^{186}Re	9.3	W-L_ℓ	0.0191(21)
	9.9	Os-L_ℓ	0.031(4)
	57.98	W-$K_{\alpha 2}$	0.0175(4)
	59.33	W-$K_{\alpha 1}$	0.0302(6)
	61.49	Os-$K_{\alpha 2}$	0.0112(3)
	63.00	Os-$K_{\alpha 1}$	0.0195(4)
	67.2	W-$K_{\beta 1}$	0.00986(20)
	69.1	W-$K_{\beta 2}$	0.00268(6)
	71.3	Os-$K_{\beta 1}$	0.00633(14)
	73.4	Os-$K_{\beta 2}$	0.00185(4)
	122.61	γ	0.00603(6)
	137.16	γ	0.0939(9)
	630.33	γ	0.000293(6)
	767.47	γ	0.000327(6)

2.2 Half-Lives

H. Schrader

Half-life values $T_{1/2}$ were determined by following the radioactive decay with an ionization chamber. Recently obtained results are given in Table 2.

Table 2: Half-life measurements

Nuclide	n	$t/T_{1/2}$	$T_{1/2}$	
^{68}Ge	825	0.75	270.82(21)d	preliminary value
$^{108}Ag^{m}$	330	0.03	433(15)a	preliminary value
^{186}Re	329	7.3	3.7183(11)d	

n: Number of measurements

t: Duration of measurements

References

[1] H. Vonach, S. Tagesen, M. Wagner, V. Pronyaev: Physics Data 13-7, KfK Karlsruhe/FRG (1992)

[2] J.H. Coon, R.W. Davis, H.E. Felthauser, D.B. Nicodemus: Phys. Rev. 111 (1958) 250

[3] M. Hyakutake, M. Matoba, T. Tonai: J. Phys. Soc. Japan 38 (1975) 606

[4] S.M. El-Kadi, C.E. Nelson, F.O. Purser, R.L. Walter: Nucl. Phys. A390 (1982) 509

[5] S. Mellema, R.W. Finlay: Phys. Rev. C33 (1986) 481

[6] A. Takahashi, M. Gotoh, Y. Sasaki, H. Sugimoto: report A—92—01, Osaka University/Japan (1992)

[7] W. Bucher, C.E. Hollandsworth: Phys. Lett. 58B (1975) 277

[8] Li Jingde, Wang Shiming, Xie Daquan, Ma Gonggui, Zou Yiming, Chen Shuying: Chinese J. Nucl. Phys. 11 (1989) 19

[9] K. Hata, S. Shirato, Y. Ando: EXFOR 22189, IAEA Vienna (1990)

[10] A.B. Smith, private communication, ANL Argonne/USA (1992)

[11] D. Hermsdorf, A. Meister, S. Sassonoff, D. Seeliger, K. Seidel: report ZfK-277, ZfK Rossendorf/GDR (1975)

[12] D. Schmidt, B.R.L. Siebert: "Monte Carlo Simulation of Fast Neutron Scattering Experiments Including DD-Breakup Neutrons", to be published

[13] A. Takahashi, E. Ichimura, Y. Sasaki, H. Sugimoto: J. Nucl. Sci. Technol. 25 (1988) 215

[14] R. Bouchez, J. Duclos, P. Perrin: Nucl. Phys. 43 (1963) 628

[15] N. Olsson, B. Trostell, E. Ramström: Nucl. Phys. A498 (1989) 505

[16] B. Strohmaier, S. Tagesen, H. Vonach: Physics Data 13-2 (1980)

[17] W. Mannhart: IAEA-TECDOC-410, IAEA, Vienna (1987) 158 and
W. Mannhart: INDC(NDS)-220/L, IAEA, Vienna (1989) 305

[18] H. Märten, D. Richter, D. Seeliger, W.D. Fromm, R. Böttger, H. Klein: Nucl. Sci. Eng. 106 (1990) 353

[19] A. Chalupka, L. Malek, S. Tagesen, R. Böttger: Nucl. Sci. Eng. 106 (1990) 367

[20] R. Böttger, H. Klein, A. Chalupka, B. Strohmaier: Nucl. Sci. Eng. 106 (1990) 377

[21] A. Lajtai, P.P. Dyachenko, E.A. Seregina, V.N. Kononov: Nuclear Data for Science and Technology, ed. S. Igarasi (Saikon, Tokyo) (1988) 737

[22] W. Mannhart: Proc. Symp. on Nuclear Data Evaluation Methodology, Brookhaven National Laboratory, 12 — 16 October 1992 (in press)

[23] H. Janßen, E. Schönfeld, R. Klein: Appl. Radiat. Isot. 43 (1992) 1309

[24] E. Schönfeld, H. Janßen, U. Schötzig: Appl. Radiat. Isot. 43 (1992) 1071

[25] E. Schönfeld, U. Schötzig, E. Günther, H. Schrader: Proc. of ICRM Symp., Teddington, UK (1993) (to be published in Nucl. Instrum. Meth.)

FACHINFORMATIONSZENTRUM KARLSRUHE

STATUS REPORT

H. Behrens, H.-W. Müller

1. Information Systems with Relevance to Nuclear Data

a) Inorganic Crystal Structure Data File (ICSD)

ICSD is a comprehensive compilation of data defining crystal structure of inorganic compounds, based preferentially on X-ray and neutron diffraction studies. It includes the crystal parameters like unit cell, space group, atomic coordinates, thermal parameters etc. and, additionally, experimental methods and bibliographic data. Both investigations of powders and single crystals are covered. Hence ICSD is a useful tool to obtain information about neutron diffraction on inorganic materials.

Data are critically evaluated from journal articles. Presently (Apr. 93), ICSD covers about 35,000 entries. The file is updated twice a year.

ICSD is produced by FIZ KARLSRUHE and the GMELIN Institute, Frankfurt. It can be retrieved online from the STN Host. In-house and CD-ROM versions are also available.

b) The Physics Database (PHYS)

This database covers the world-wide appearing literature on physics, astronomy and related topics since 1979. It appears in printed form as "Physics Briefs" derived from "Physikalische Berichte", an abstracting journal founded in 1845. There is also a good coverage of Eastern European and East Asian literature. Data sources in 1992 were:

- journals (82%)
- books (14%)
- reports (2.0%)
- other non-conventional literature (2.5%)
- conference contributions (32%)

Traditionally, nuclear physics is a major part of the physics database. 152.844 documents since 1979 cover this subject. The numbers of cited nuclear relevant articles and their increases in the last year are (Apr. 93):

470	(+2.6%)	Nuclear physics (general)
30,604	(+7.7%)	Nuclear structure
13,680	(+11.2%)	Radioactivity and electromagnetic transitions
13,064	(+6.2%)	Nuclear reactions and scattering (general)
56,519	(+6.5%)	Nuclear reactions and scattering (specific reactions)
7,785	(+7.1%)	Nuclear engineering and nuclear power studies
54,695	(+6.3%)	Experimental methods and instrumentation for elementary-particle and nuclear physics

The database is updated 24 times annually. PHYS is available online from the Scientific and Technical Information Network (STN). Access is possible via DATEX-P or WIN nets, or, on request, from FIZ KARLSRUHE.

c) Catalog of Gamma Rays and Alpha Particles from Radioactive Decay (GAMCAT)

GAMCAT is a Personal Computer database system comprising 46,950 gamma and 1,904 alpha lines, originating from more than 2,200 radionuclides. It is designed for use in gamma and alpha spectrometry as well as in cross-section measurements, activation analysis, environmental pollution control or waste composition control. GAMCAT runs on an AT-compatible computer and is available on two HD floppy disks.

2. Data Compilations

A further issue containing nuclear data appeared in our series PHYSICS DATA:

Evaluation of the fast neutron cross sections of ^{56}Fe including complete covariance information
H. Vonach, S. Tagesen, M. Wagner and V. Pronyaev
Fachinformationszentrum Karlsruhe, PHYSICS DATA 13-7 (1992)

APPENDIX

Addresses of Contributing Laboratories

Institut für Kernphysik III
Director: Prof. Dr. G. Schatz
Senior reporter: Dr. F. Käppeler
Kernforschungszentrum Karlsruhe
Postfach 36 40
76021 Karlsruhe

Institut für Materialforschung I
Director: Prof. Dr. K.-H. Zum Gahr
Senior reporter: Prof. Dr. K. Ehrlich
Kernforschungszentrum Karlsruhe
Postfach 36 40
76021 Karlsruhe

Institut für Neutronenphysik und Reaktortechnik
Director: Prof. Dr. G. Kessler
Senior reporter: Dr. F. Fröhner
Kernforschungszentrum Karlsruhe
Postfach 36 40
76021 Karlsruhe

Institut für Kernphysik
Arbeitsgruppe Strahlungstransport
Senior reporter: Dr. D. Filges
Forschungszentrum Jülich
Postfach 19 13
52425 Jülich

Institut für Nuklearchemie
Director: Prof. Dr. G. Stöcklin
Senior reporter: Dr. S.M. Qaim
Forschungszentrum Jülich
Postfach 19 13
52425 Jülich

Institut für Kern- und Teilchenphysik
Director: Prof. Dr. H. Freiesleben
Senior reporter: Prof. Dr. K. Seidel
Technische Universität Dresden
Mommsenstr. 13
01062 Dresden

Zentraleinrichtung für Strahlenschutz
Head and senior reporter: Prof. Dr. H. Michel
Universität Hannover
Am Kleinen Felde 30
30167 Hannover

Institut für Kernchemie
Director: Prof. Dr. G. Herrmann
Senior reporter: Prof. Dr. H.O. Denschlag
Universität Mainz
Fritz-Strassmann-Weg 2
55128 Mainz

Abteilung Nuklearchemie
Director: Prof. Dr. G. Stöcklin
Senior reporter: Dr. U. Herpers
Universität zu Köln
Otto-Fischer-Straße 12-14
50674 Köln

Fachbereich Physikalische Chemie
Kernchemie
Senior reporter: Prof. Dr. P. Patzelt
Philipps-Universität Marburg
Lahnberge
35043 Marburg/Lahn

Physikalisch-Technische Bundesanstalt
Abteilung 6, Atomphysik
Director: Prof. Dr. R. Jahr
Senior reporter: Dr. W. Mannhart
Bundesallee 100
38116 Braunschweig

Fachinformationszentrum Energie, Physik, Mathematik
Directors: Dr. W. Rittberger, Dr. E.-O. Schulze
Senior reporters: Dr. H. Behrens, Dr. H.-W. Müller
Kernforschungszentrum
76344 Eggenstein-Leopoldshafen